MULTISCALE FEATURES INCLUDING WATER CONTENT OF POLYMER-INDUCED KAOLINITE FLOC STRUCTURES

by

Sugandha Sharma

A thesis submitted to the faculty of
The University of Utah
in partial fulfillment of the requirements for the degree of

Master of Science

Department of Metallurgical Engineering

The University of Utah

August 2016

The University of Utah Graduate School

STATEMENT OF THESIS APPROVAL

The thesis of **Sugandha Sharma**

has been approved by the following supervisory committee members:

Jan D. Miller	, Chair	**05/12/2016** Date Approved
Michael L. Free	, Member	**05/12/2016** Date Approved
Chen-Luh Lin	, Member	**05/12/2016** Date Approved

and by **Sivaraman Guruswamy** , Chair/Dean of

the Department/College/School of **Metallurgical Engineering**

and by David B. Kieda, Dean of The Graduate School.

ABSTRACT

Despite their many uses, fine clay particles such as kaolinite are a nuisance in management of tailings in various industries such as the oil sands and phosphate processing industry. The effective flocculation, sedimentation, and consolidation of these fine particles are a major challenge. In industries, polymers are added to tailings suspension to facilitate formation and eventual sedimentation of flocs. The structure of floc and the water entrapped within the floc determine floc behavior and settling characteristics. The quantification of water entrapped within the kaolinite flocs has not been reported before. The information on kaolinite floc size and shape is also limited due to the challenges in experimental procedures for these delicate structures.

In this thesis research, operating conditions for kaolinite flocculation were determined and a suitable polymer was chosen by settling experiments. Further investigation of the floc formed was done in suspended state as well as in sedimented state. The flocs were analyzed for their size, shape, water content, and microstructure. A pool of analytical techniques like the Particle Vision & Measurement (PVM), Dynamic Image Analysis (DIA), Scanning Electron Microscopy (SEM), High Resolution X-ray Microtomography (HRXMT), and image processing software like Fiji, Medical Image Processing Analysis & Visualization (MIPAV), and Drishti were used. The analysis of suspended flocs by PVM and DIA revealed a mean floc size of about 225 μm for high molecular weight, 5% anionic polyacrylamide-

induced flocs. The low molecular weight, 70% cationic polymer-induced flocs were found to be smaller in size (145 μm). DIA was used to analyze the flocs at different solid concentration. It was found that the increase in solid concentration leads to increase in floc size. Floc circularity was also analyzed by using both these methods. Most flocs were irregular in shape with circularity ranging between 0.2-0.3. However, the circularity results from both these methods do not agree well due to the difference in methods of detection and different definitions used for circularity/sphericity.

Major contribution of this thesis work includes development of a new technique for water content and size analysis of sedimented kaolinite flocs. The sediment bed was segmented into about 13 thousand individual flocs and each floc was analyzed for its size and water content. The results suggest a normal distribution of water content for these flocs, with mean water content of 53.9% and standard deviation of 11.8%. About 98% of the flocs have water content in the range 30-80%. The size analysis revealed that about 90% of the flocs are less than 1.5 mm in size. The water content was found to decrease with increase in size of the floc. The flocs were found to be fairly irregular, with sphericity values around 0.1. The floc shape analysis was also done but limited to 10 flocs.

In addition to macroscopic analysis of individual flocs, flocs were also analyzed for their microstructure. Visualization of floc microstructure and polymer chain was done with the help of SEM. Microstructures of up to 10 μm in size were revealed along with the web formed by polymer chain.

TABLE OF CONTENTS

LIST OF TABLES

Table Page

ACKNOWLEDGEMENTS

I would like to express my heartfelt gratitude to my advisor, Professor Jan D. Miller, for all his help, support, guidance and encouragement during my thesis research. The time spent with him has been a great learning experience for me and I have always been inspired by his dedication for research. He always motivated me to keep going in difficult times and appreciated my efforts. He really brings out the best in each one of his students.

I would also like to express my sincerest thanks and gratitude to members of my supervisory committee, Dr. Michael L. Free and Dr. Chen-Luh Lin, for their valuable input, suggestions and for their precious time reviewing my thesis. Special thanks to Dr. Lin for helping me design the experiments and being there to help me at every step. Without his help and guidance, this thesis would not be accomplished.

Thanks are also extended to previous graduate students who worked with kaolinite and 3D particle segmentation for paving the way for my research. Heartfelt thanks to Dr. Vishal Gupta, Dr. Xuihi Yin, Dr. Jing Liu, Dr. Alvaro Videla and Dr. Yan Wang. I would also like to thank my research group members for their help in times of need. Special thanks are extended to to Dr. Yan Wang for her help with CT imaging. I would also like to thank Dr. Shoeleh Assemi for teaching me the basics and motivating me towards research during my internship. I have always enjoyed discussions with her during my thesis research.

Thanks are also extended to Dorrie Spurlock for her help and kind words of

encouragement during these two years.

Finally, I would like to thank my family and friends for always being there for me. Special thanks to my friends in Salt Lake City, Manas Pathak, Pankaj Kumar and Ankit Jha, for helping and supporting me during my stay here.

Last but not the least, I would like to thank the Department of Metallurgical Engineering for giving me the wonderful opportunity to work, learn and grow here. I will leave this place as a better professional and as a better person.

CHAPTER 1

INTRODUCTION

1.1 Kaolinite Structure and Surface Charge

Kaolinite belongs to the phyllosilicate family of clay minerals. It is one of the most important clay minerals and has wide-ranging applications. In the paper industry, kaolinite is used both as filler and as a coating for paper sheet. Other industries where kaolinite is widely used include the ceramic industry, sanitary ware, insulators and refractories (Grim, 1953; Lagaly and Bergaya, 2013; Murray, 1991, 2000; Van Olphen, 1977). On calcination of kaolinite, special products are produced with excellent dielectric properties, which are used as a filler in electrical wire coatings. Economic lightweight ceramic proppants (additives for drilling fluids and products for oil well cementing) have been produced from calcined kaolin clay used for increased gas and oil production (Lemieux and Rumpf, 1991). Despite its many uses, kaolinite clay is a nuisance in the process of tailings management of oil sands, phosphate rocks and other mineral resources.

Kaolinite primary particles are white or nearly white, soft, platy and chemically inert. They are almost hexagonal in shape and less than a μm in size. Figure 1.1 shows a Transmission Electron Microscopy image of a 600 nm kaolinite primary particle taken at the Nanofab facility, University of Utah. Kaolinite has a low swelling capacity and low cation exchange capacity (1-15 meq/100g). (Lyklema, 1995; Olphen, 1963).

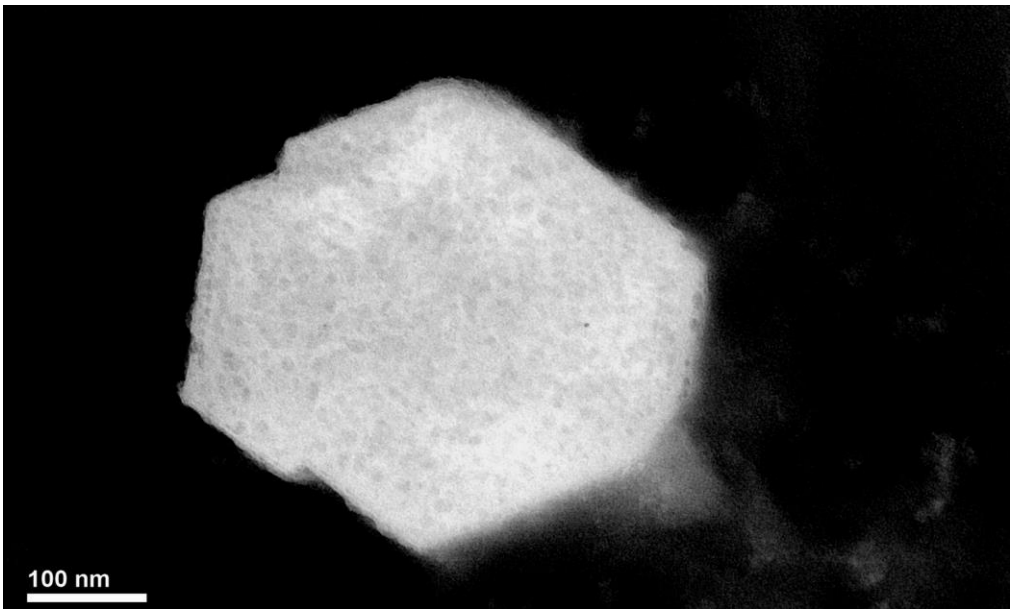

Figure 1.1: TEM image of kaolinite primary particle, about 600 nm in size. As is evident, most of these particles have a hexagonal shape.

Phyllosilicate minerals are composed of two types of sheets, namely a silica tetrahedral sheet and an alumina or magnesia octahedral sheet. The phyllosilicates can be classified as bilayer phyllosilicates (1:1 type) or trilayer phyllosilicates (2:1 type) depending on the ratio of silica and alumina/magnesia sheets. The crystal structure of these two types of phyllosilicates is illustrated in Figure 1.2. The kaolin group belongs to the bilayer or 1:1 type phyllosilicates (see Figure 1.2 A) and consists of alternating layers on silica tetrahedral and alumina octahedral. The spacing between two repeating kaolinite bilayers is about 0.72 nm. The double sheets are bonded to each other by hydrogen bonds (involving OH of the octahedral sheet and oxygens of the adjacent silica sheet) and van der Waal forces. The solution kaolinite has a rigid crystal structure that cannot be swollen by changing pH or ionic strength. Trilayer (2:1) phyllosilicates include the groups of talc, illite, muscovite, smectite, and

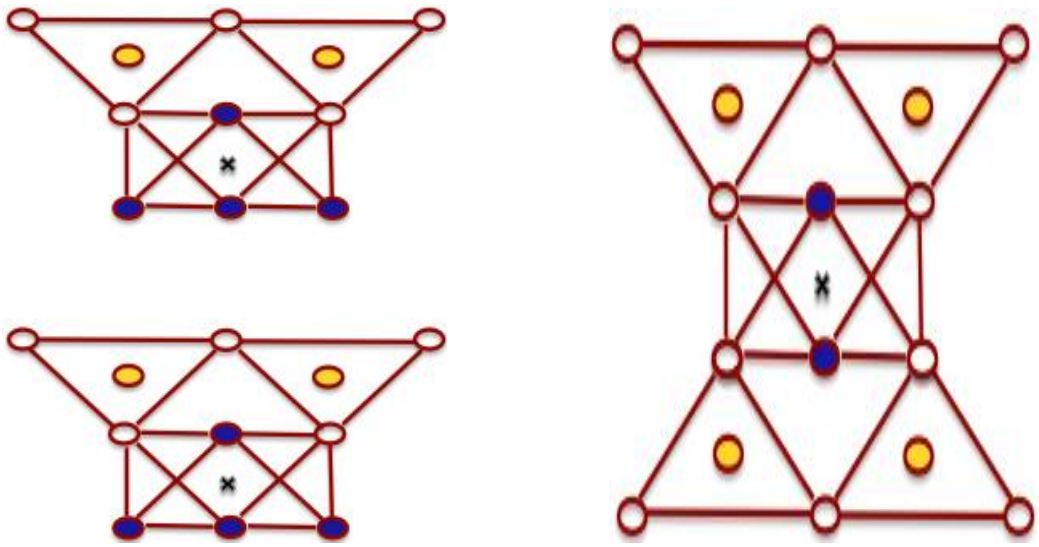

(A) (B)

Figure 1.2: Crystal structures of bilayer phyllosilicate (A), trilayer phyllosilicate (B). The white circles represent oxygen atoms, the blue circles represent hydroxyl groups, the yellow circles represent silicon atoms, and the cross (x) represents aluminum or magnesium atoms.

chlorite. Sometimes, isomorphous substitution of the clay minerals can happen and give rise to layer charge. The layer charge is the charge deficiency on the 2:1 layer due to substitutions in the tetrahedral sheet, octahedral sheet, or in both sheets. The layer charge of illite is ~0.75, and the layer charge of smectite is 0.2–0.6 (Bergaya et al., 2011). The existence of the layer charge for the phyllosilicate layers accounts for the accommodation of interlayer cations to balance the layer charge (K+, Na+, NH4 +, etc.). The lower the layer charge is, the easier for the interlayer cations to exchange with cations in solution (Van Olphen, 1977). The 1:1 bilayer structure gives rise to three distinct surfaces for kaolinite particle: the silica face surface, the alumina face surface, and the edge surface. The three different surfaces of kaolinite are illustrated

in Figure 1.3. Yin et al. reported the wettability of the two basal planes of kaolinite. It was found that the silica face of kaolinite particles is more hydrophobic than the alumina face. This result was confirmed by molecular dynamic simulation as well (Yin, 2012). The AFM charge characterization for all the three surfaces of kaolinite has been done recently at the University of Utah (Gupta and Miller, 2010; Liu, 2015). Gupta and Miller reported the point of zero charge (PZC) of the alumina face surface of kaolinite to be between pH 6 and 8, and the PZC of the silica face surface to be below pH 4 (Gupta and Miller, 2010). In their study, individual kaolinite particles were ordered on substrates, and the prepared surfaces were confirmed by Atomic Force Microscopy (AFM) measurements to be the silica face and alumina face respectively. Until recent years, limited research has been reported on the kaolinite edge surface. The point of zero charge (PZC) of kaolinite edge surface was estimated

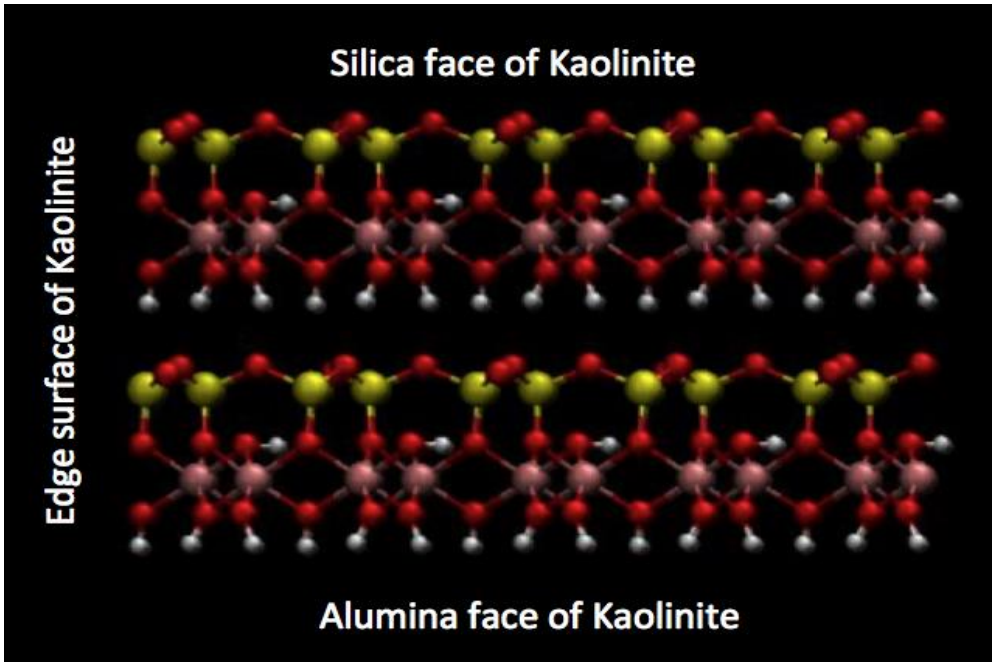

Figure 1.3: Crystal structure of kaolinite illustrating the three different surfaces. Red: Oxygen; Yellow: Silicon; Purple: Aluminum; White: Hydrogen.

to be pH 4.5 by Gupta et al. Recently, Liu et al. prepared well-ordered kaolinite edge surfaces in an epoxy resin sandwich structure that had layered kaolinite particles in the center of the epoxy resin sandwich. The surface charge of the kaolinite edge surfaces was established from AFM surface forces measurement using a super sharp silicon tip. The PZC of the kaolinite edge surface was determined to be below 4, which they believed that lower isomorphous substitution in the silica tetrahedral layer accounted for the lower PZC (Liu et al., 2014). At pH below 6, the alumina face is positively charged whereas the silica face and edge surfaces are negatively charged. (Gupta, 2011). Now we know that the different surfaces of kaolinite exhibit different charges at different pH as shown in Figure 1.4. Electrostatic attractive forces are in play due to the presence of both positively and negatively charged surfaces in the system and this can lead to formation of kaolinite clusters.

1.2 Kaolinite Particle Aggregation

The clay colloidal stability in suspension depends on the mode and extent of particle association in suspension. In the dispersed state, the kaolinite particles can be considered as colloidal particles subjected to Brownian motion. These colloidal particles make collisions at different rates (Yu and Somasundaran, 1997). The modes of particle interaction can be governed by van der Waals force, electrical double layer force, hydrophobic force, hydration force, etc. At higher pH values, these colloids of kaolinite particles form a fairly stable suspension as the electrostatic repulsive force between the negatively charged surfaces prevents aggregation of colliding particles. The effect of other forces on the system is almost negligible. At lower pH, the anisotropic nature of surface charge renders the colloidal system highly unstable. The

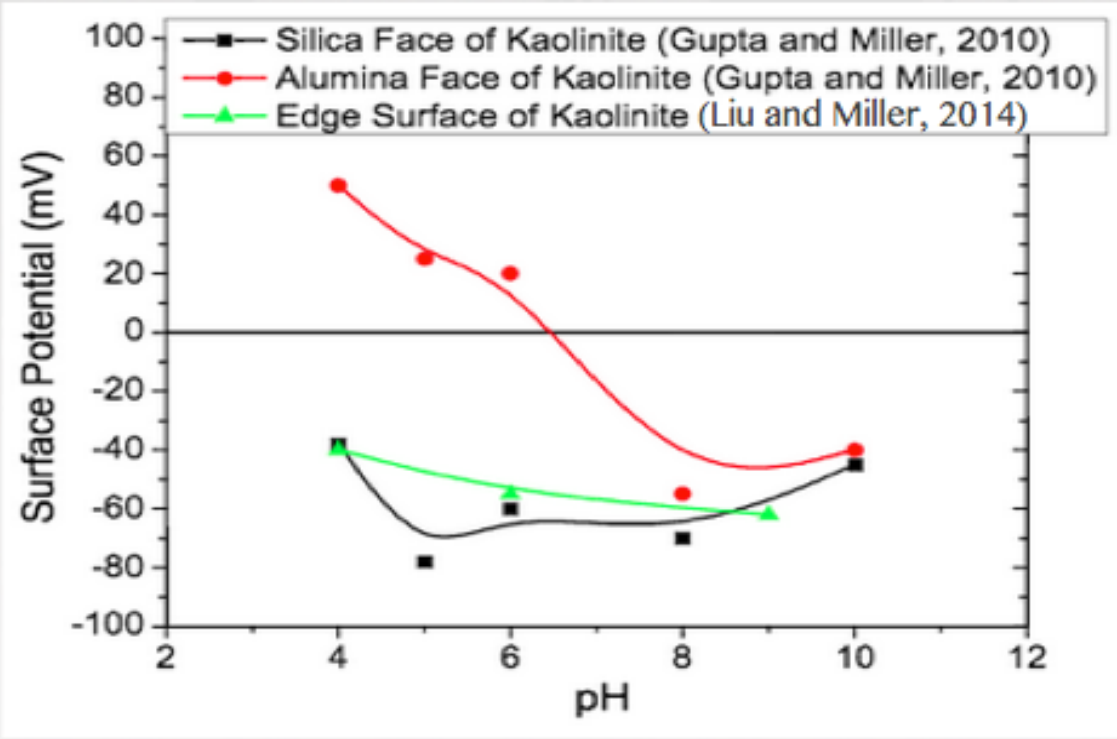

Figure 1.4: Surface potential variation of three different surfaces of kaolinite with pH as determined from AFM surface force measurement (Gupta and Miller, 2010; Liu and Miller, 2014).

presence of oppositely charged surfaces promotes aggregation between the colliding particles leading to the formation of kaolinite clusters. These kaolinite particles become associated with edge-to-edge, edge-to-face, or face-to-face interactions giving rise to a cardhouse type structure as suggested by researchers (Kie, 1954; Van Olphen, 1977). The cardhouse structure of kaolinite clusters has been described using a dynamic coarse grain simulation model as shown in Figure 1.5 (Liu et al., 2015).

The formation of kaolinite clusters in aqueous solution has been studied by many researchers over the past few years. The kaolinite clusters formed in aqueous solution are about 10 μm in size; further increase in the size of aggregates can be obtained by the addition of coagulants or flocculants or both. Addition of polymer-

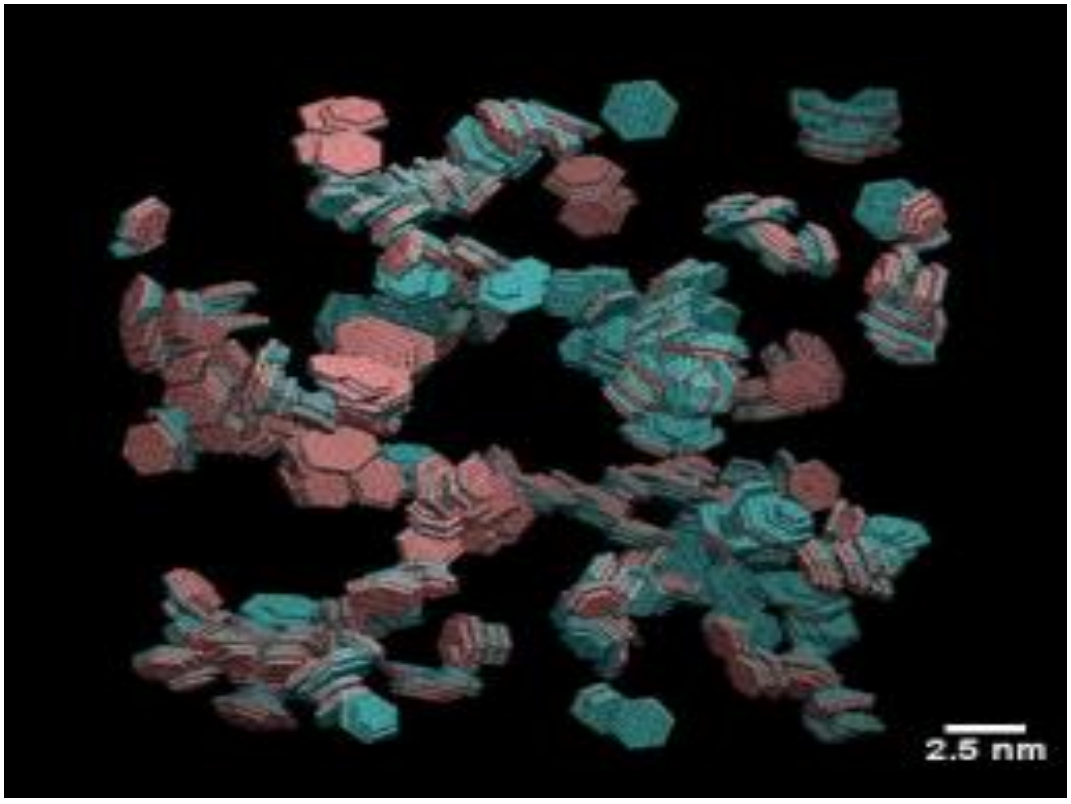

Figure 1.5: Snapshot from the dynamic simulation of kaolinite cluster formation at pH 5 (Jing Liu, 2015). Simulation time was 10 ns.

based flocculants leads to further aggregation and 'flocs' are formed. Polyacrylamide-based polymers (PAMs) are generally used as flocculants for tailings containing kaolinite and other clays. The kaolinite flocs formed on addition of PAM are expected to vary in size, shape, and water content, depending on the conditions of floc formation but their size, shape, and water content has not received much attention due to difficulty in experimental analyses.

1.3 Research Motivation

The oil sands mining and extraction processes in Canada produce large volumes of tailings that are a mixture of mainly water, clay, sand, chemicals, and

bitumen. Kaolinite constitutes about 50-60% of the total clay content. This tailings slurry is approximately 55% solids (82% sand and 18% fines < 44 μm) and is deposited into tailings ponds where sand settles faster to form beaches. Some fines are trapped within the sand matrix of the beaches. However, the remaining thin slurry of fines and water (8% solids) is stored in settling basins where the solids settle gradually to form a densified zone of fine tailings at depth. Released water is recycled back to the processing plant. After a few years, the fines settle to 30 to 35% by weight and are referred to as mature fine tailings (MFT). Further consolidation of the MFT is expected to take centuries (Chalatumyk et al., 2002).

In another example, most of the phosphate deposits in central Florida contain about 10% clay minerals, making the recovery of the phosphate minerals extremely difficult. After phosphate recovery, the tailings, which might contain 30–50% clay, are discarded. It usually takes 3–5 years for sedimentation and consolidation to reach 50–60% solids, requiring a lot of land to be used for tailing disposal (Zhang and Bogan 1995). As of today, 30-40% of the mined lands are being used as clay settling areas.

Therefore, land reclamation and water recirculation are big challenges for operation involving clays such as kaolinite. Dealing with these tailings has significant economic and environmental impacts. The effective flocculation, sedimentation, and consolidation of these fine particles are a major challenge. The tailings settling rate depends on floc size, entrapped water, and surface properties which can be modified by variations in the pH, salinity, and addition of flocculants (Cabrera et al., 2009). There have been discussions about the importance of particle size in gravity separation of clays (Lawler, 1986; O'Melia, 1998). The shape of floc is supposed to

effect the collision efficiency and settling rates (Jiang and Logan, 1991; Johnson et al., 1996; Li et al., 1997; Wiesner, 1992). The settling of flocs is also effected by the water entrapped inside the floc (Hendricks 2016). Therefore, the characterization of floc size, shape, and entrapped water content on addition of suitable polymer will be helpful in understanding and influencing the tailings settling rate, sedimentation, and consolidation.

1.4 Objectives

Although different aspects of kaolinite flocculation have been studied before (Alagha et al., 2013, 2016; Kim and Palamino, 2009; Mpofu et al., 2004; Nasser and James, 2007; Taylor et al., 2002; Yu et al., 2006; Zbik et al., 2008; Zhu et al., 2009), the floc structure for in-situ conditions and the floc structure in sediment have not been compared in previous studies. Not much is known about the 3D characteristics of flocculated kaolinite sediment, such as the water content of individual flocs present in the sediment.

Polymer flocculants have been used in industry for many years to achieve effective flocculation and sedimentation. In this thesis research, the settling characteristics of polymer-induced flocs are compared for different experimental conditions and a few conditions were selected for further more detailed experiments. Further characterization of the flocs formed was done using a pool of analytical techniques. The flocs were analyzed for size, shape, and microstructure.

In summary, the major objective of this research is to study the multiscale features of polyacrylamide induced kaolinite flocs using both 2D and 3D characterization methods. These features include size, shape, and water content.

Analytical tools including Particle Vision Measurement, Dynamic Particle Analyzer, FESEM, WETSEM capsules, and HRXMT are used for characterization of the floc structure. Using the FESEM, the floc fabric was studied and the micro-sized floc nodules were identified in the web created by polymer chains. Using High-Resolution X-ray Microtomography (HRXMT), three-dimensional characterization of the sediment was done and a technique was developed to calculate the water content of each floc present in the sediment.

In most tailings management cases involving clays such as kaolinite, aggregation is necessary prior to its removal by solid-liquid separation processes. Influencing the size, mass, surface area, and number concentration of particles substantially affects their removal by gravity sedimentation and deposition in packed-bed filters (Lawler, 1986; O'Melia, 1998). In addition to size, particle shape affects the behavior of aggregated particles, particularly with regard to collision efficiency (Jiang and Logan, 1991; Wiesner 1992) and settling rates (Johnson et al., 1996; Li et al., 1997). The particle size and solids weight percentage in the slimes determine the settling characteristics and amount of flocculant required to settle the slimes.

The amount of water contained in the flocs is directly influenced by the size of the flocs (Winterwerp and Van Kesteren, 2004) and the rate at which flocculation occurs (Mietta, 2010). The water content of the flocs also influences the settling and self-weight consolidation (Hendricks, 2016). Previously, techniques like the NMR have been used to study the water content in different clays (Fan and Somasundaran, 1999). The analysis of water content for kaolinite flocs is yet to be reported. In this

research, a novel method was developed for determination of water content of sediment flocs using High-Resolution X-ray Microtomography. The X-ray attenuation coefficient for kaolinite was determined and used to analyze the water content in the flocs. Also, size and shape characterization was done for selected flocs. The method developed can be used to determine the relative distribution of water in flocs and channels at different conditions.

1.5 Thesis Organization

The introduction (Chapter 1) includes discussion about kaolinite surface charge and particle aggregation followed by research motivation and objectives.

Chapter 2 considers the mechanism of flocculation mechanism and results from settling experiments. The effect of polymer addition on settling of kaolinite suspension was studied. Parameters including polymer type, polymer dosage, pH, and mixing conditions were varied and their effect on kaolinite settling are reported.

The characterization of kaolinite floc structure was done using in-situ and ex-situ techniques. The results of structure analysis using Particle Vision Microscope (PVM) and Dynamic Laser Diffraction are presented in Chapter 3. The size and shape characterization was done using both techniques and the results are discussed in this chapter.

Chapter 4 deals with 3D characterization of the sediment. Using the High-Resolution X-ray Microtomography and image processing techniques, a method for water content analysis of kaolinite flocs was developed. Individual flocs are identified and analyzed for size and water content. Also, the surface area and volume are calculated for selected flocs.

The floc fabric and structure was further studied using the Scanning Electron Microscope (SEM). The flocs were analyzed using a wet cell as well as using a cryogenic sample preparation method. The results from both methods are discussed in Chapter 5.

CHAPTER 2

SIGNIFICANCE OF OPERATING CONDITIONS ON KAOLINITE SETTLING

2.1 Introduction

Kaolinite primary particles stay dispersed at higher pH due to electrostatic repulsive forces between negatively charged surfaces but show some aggregation and cluster formation at lower pH due to the presence of opposite charges at the particle surfaces. The particle associations can be of edge-face type or face-face type association. The structure of clusters arising from particle interactions is considered to be a manifestation of the interplay of the electrostatic force and the van der Waals force (Mitchell and Soga 1976; Van Olphen 1977; Palomino and Santamarina 2005). These clusters form a card-house type structure and are about 10 μm in size. The presence of polyvalent cations in small amount leads to shrinkage of the electrical double layer. The shrinkage of the electrical double layer brings the particles sufficiently close for interparticle or cationic bridging to occur and in turn leads to an increase in aggregate size (Labille et al., 2005).

In mineral processing operations, particularly tailings disposal, the addition of flocculants is done to obtain larger sized aggregates and hence faster settling rate. Flocculation can be understood as a physical or a mechanical process in which the clusters and/or primary particles are joined together to form bodies of significantly greater size and mass called flocs. This flocculation can be achieved by adding high

molecular weight, water-soluble organic polymers of appropriate charge densities to the suspensions. Interaction of particles, or particle clusters, with the polymers leads to aggregation of clusters, the size of the aggregate increases and, in this way, sedimentation is facilitated. It is very important to gently mix the flocculating agent at a slow speed so that small clusters can easily grow and agglomerate into large flocs, and finally settle at a satisfactory rate. The whole process is extremely sensitive to operating variables. The settling velocity of flocs, and the structure of flocs formed can be easily influenced by change in any of the operating variables. The importance of operating variables will be discussed in subsequent sections of this chapter.

In this work, the effect of polymer flocculants on kaolinite suspensions is studied without the addition of any other coagulants such as polyvalent cations for charge neutralization as the addition of coagulant would influence the surface charge on kaolinite surfaces and hence affect the flocculation characteristics. The scope of this thesis research is limited to the study of polymer-induced flocculation characteristics of kaolinite particles.

In this chapter, results from a series of settling tests for polymer-induced kaolinite flocculation will be considered. The objective of these settling tests is to identify preferred conditions for each operating parameter. These conditions have been used as a basis for further characterization experiments to describe the size, shape, and structure of kaolinite flocs. No claim is made that the conditions used for further experiments are the optimized conditions, as the continuous interactive effect between different operating parameters has not been considered. To establish the interactive effect of different variables, response surface methodology (RSM) should

be used for design of experiments (DOE). RSM is an effective tool for building a multivariable equation and finding their optimal values (Triveni et al., 2001; Yang et al., 2009). In the case of kaolinite flocculation, it can be employed to optimize the conditions of flocculation process and to investigate the interactive effects of experimental factors like dosage, pH, and mixing speed. However, this method can only optimize one output feature of the system. For example, we can optimize the settling rate but not the supernatant clarity at the same time.

2.2 Mechanism of Kaolinite Flocculation

Understanding the mechanism of clay flocculation has been of interest to various researchers for many years (Alagha et al., 2013, 2016; Gregory and Guibai, 1991; Hogg, 1999; Michaels and Bolger, 1962; Nasser and James, 2006, 2009; Ruehrwein and Ward, 1952).

Polymer adsorption on a clay particle surface alters the surface properties of the particle such as surface charge and hence interparticle forces between particles (Theng, 1979). Flocculation of fine particles is a dynamic process and may occur by polymer bridging, charge compensation or neutralization, polymer–particle surface complex formation and depletion flocculation, or by a combination of these mechanisms (Theng, 1979). Of these, bridging and charge neutralization are the commonly encountered mechanisms in the flocculation and dewatering of kaolinite dispersions using high molecular weight ($>10^6$) nonionic polymers or polyelectrolytes (Besra et al., 2002).

Bridging flocculation occurs as a result of adsorption, via hydrogen bonding, of individual polymer chains onto two or more particles simultaneously, forming

molecular bridges between the adjoining particles in the floc. Nonionic polymers and also polyelectrolytes may exhibit this kind of flocculation mechanism (Hogg 1999, 2000). Pefferkorn (1995) discussed interactions between nonionic polyacrylamide and kaolinite in aqueous suspensions in terms of amide-hydroxyl H-bonding. Theng in his book, 'Formation and properties of clay-polymer complexes', discusses in detail the conditions required for interparticle bridging to take place. For an interparticle bridge to take place, it is required that the polymer be adsorbed by two particles at the same time. For charged particles, the polymer chain must be able to span the distance of closest interparticle approach (d_c), which is assumed to be about twice the double layer thickness ($1/\kappa$) (Gregory, 1988). In this regard, the presence of a small amount of electrolyte is helpful in bringing the particles sufficiently close for interparticle bridging to occur in aqueous dispersions (Labille et al., 2005). The presence of electrolytes also enhances bridging by Polymer-Cation-Clay bridging (Laird, 1997). This type of bridging increases with increase in valency of the cation, e.g., Al^{3+} will give more bridging than Na^{+}. Linear chain polymers have better chances for flocculation than branched chain polymers of the same molecular weight as linear chain polymers have better chances of spanning the interparticle distance of closest approach and do not create steric hindrance as expected for branched chain polymers.

The rate of flocculation depends on five rate processes that occur more or less simultaneously (Gregory, 1988). These include mixing of polymer with solid particles, adsorption of polymer at the particle surfaces, rearrangement of adsorbed polymer to an appropriate configuration, collision of particles with adsorbed polymer to form

flocs, and aggregate break-up. After the initial rearrangement is complete, efficiency of flocculation mainly depends on how many of the collisions lead to interparticle bridging. For best results, the polymer should cover sufficient surface of the clay, but interparticle bridging is hindered if most of the clay surface is covered by the polymer. The probability of bridge formation is proportional to the fraction of surface covered by the polymer, θ, and also the fraction of surface uncovered by the polymer, $(1- \theta)$. The collision efficiency, E, can be written as:

$$E = \theta (1 - \theta) \quad \text{(1)}$$

The idea about probability of bridging was introduced and formulated in a series of papers by Mer and Smellie (1962), and Mer and Healy (1963, 1966). Besra et al. (2002) reported that the maximum rate of polyacrylamide induced flocculation for kaolinite suspensions occurs when $\theta = 0.5$.

On the other hand, charge neutralization is a major mechanism for flocculation when significant particle surface sites are of opposite charge. The charge neutralization phenomenon is relatively simple and flocs produced by this method are expected to be smaller in size but stronger.

Sometimes, if the polymer chain is not long enough, the polymer chain can adsorb on the charged surface in "patches" (Theng, 1979). Flocculation then occurs by electrostatic attraction between the positively charged patches on one particle and unpatched negatively charged surface on another particle. A less common mechanism of flocculation is depletion flocculation, which occurs in situations where free non-adsorbing polymer molecules present in the dispersion are excluded from the space

between two approaching particles due to their large size. The resulting osmotic pressure forces the particles to flocculate (Hunter, 1981)

In this study, we have used polyacrylamides of different molecular weights and charge densities. Polyacrylamide is an important water-soluble commercial polymer, it is cost efficient, and can be produced in any ionic form. It has been in wide use by industry since its discovery in the 1970s (Bikales, 1973). Its chemical structure is illustrated in Figure 2.1.

The charge density can be varied by amount of substitutions of the acryl and amide groups. Polyacrylamides interact with clay surfaces via polymer bridging, charge neutralization, complex formation between clay particles and polymer molecules, or a combination of these phenomena (Deng et al., 2006; Laird, 1997; Lee et al., 1991; Mpofu et al., 2003; Ophlen, 1977; Pefferkorn, 1995). The polymer molecule can be adsorbed onto clay particles acting like a bridge between two or

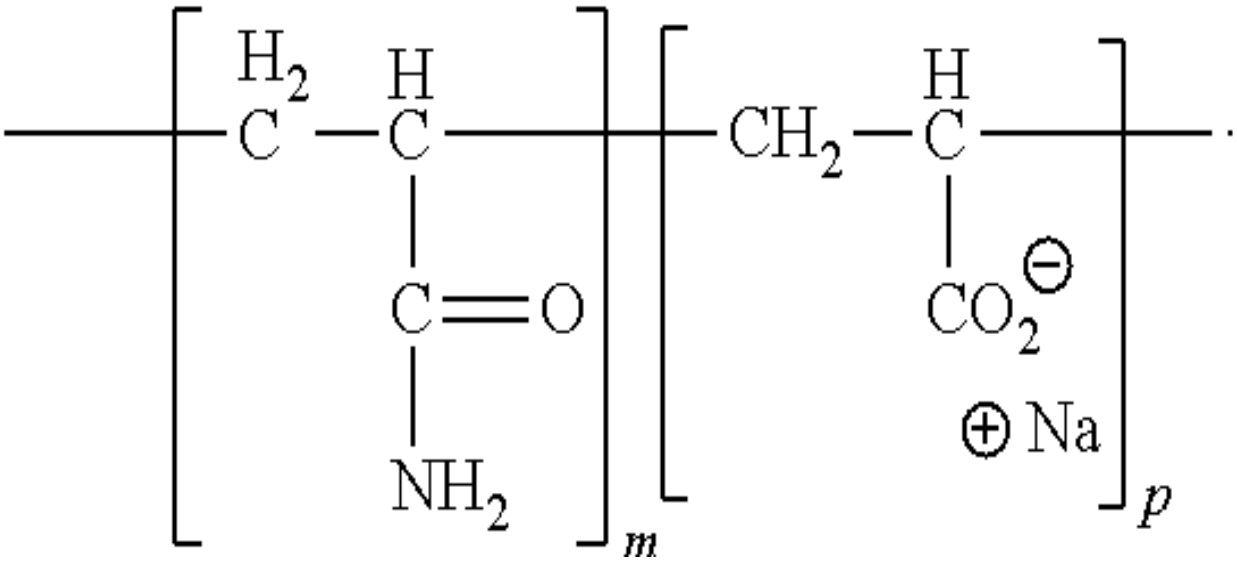

Figure 2.1: Partially hydrolyzed polyacrylamide.

more particles. The aluminol group (Al-OH) on the edge site can bond with the carbonyl oxygen of PAM by hydrogen bonding. The uncharged sites on the siloxane face may have hydrophobic interactions with the hydrophobic backbone (CH_2- CH_2) of the PAM. There is also a possibility of ion-dipole interaction between the exchangeable cations on the clay surface and the carbonyl oxygen of the PAM. Clay-cation-polymer bridging can take place. In the case of cationic polymers, electrostatic attraction is a dominant flocculation mechanism (Kim and Palamino, 2009). Recently, some qualitative analysis of polymer adsorption on different surfaces on kaolinite has been done using the quartz crystal microbalance (Alagha et al., 2013, 2016). It was concluded that the anionic polyacrylamide adsorbs on the alumina basal face by weak electrostatic interaction and hydrogen bonding.

2.3 Materials and Methods

2.3.1 Kaolinite

Acid washed K2 500 kaolinite (U.S.) obtained from Fisher inc. was used in this study. The size analysis of primary particles was done using Dynamic Light Scattering (DLS) manufactured by Wyatt technologies. DLS utilizes the time-dependent fluctuations of scattered intensity, which arise from Brownian motion, in order to determine the diffusion constant. The hydrodynamic radius R_h is then calculated directly as described in DLS theory. Details about DLS theory and other working principles are described in literature (Berne and Pecora, 1976). Kaolinite suspension at pH 8.8 containing 0.1% solids was used. About 1 ml sample was put in a cuvette and the system was sonicated for about 10 seconds. The cuvette was then inserted in

the DLS system and the size analysis was done. Two peaks were observed during the analysis, at about 100 nm and at 600 nm (Figure 2.2).

2.3.2 Polymer Flocculants

Floc screening tests were performed at Pocock industrial, Salt Lake City to examine the differences in flocculation properties for a wide range of polymers and to select a few polymers for further study of kaolinite flocculation. Flocculant screening, selection, and optimization is part of the services offered by Pocock industrial. Floc screening was based on visual observation of the settling and floc properties after adding polymer solution to the kaolinite suspension.

About 50 ml of 4% kaolinite solution was used for each experiment and the different polymers at a concentration of 0.1g/l were added. The testing was done at three different pH: pH 8, pH 5.6, and pH 4.4. The settling characteristics, supernatant

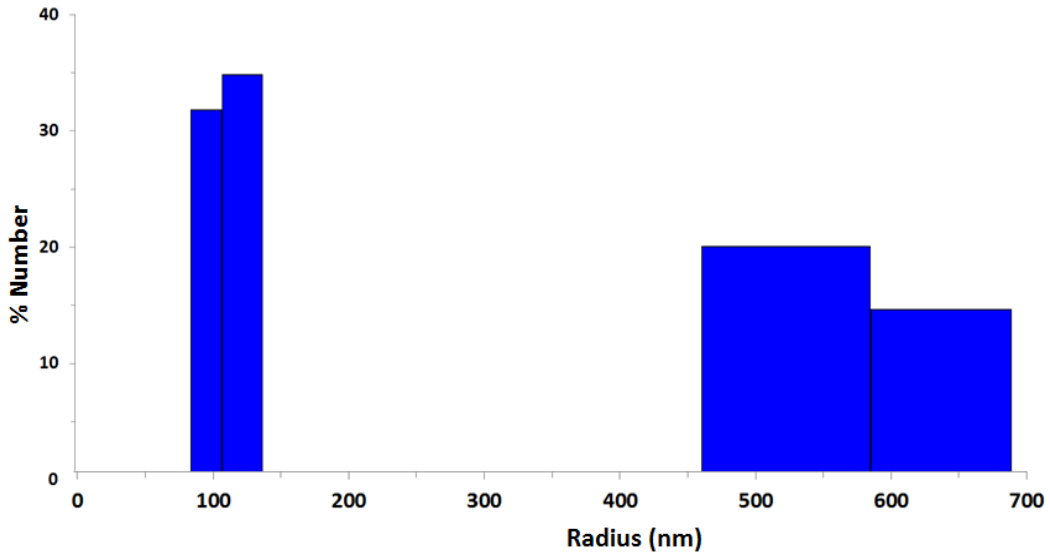

Figure 2.2: Size analysis of kaolinite primary particles using DLS. The kaolinite suspension at pH 8.8 and solid concentration 0.1% was analyzed.

clarity, and structure of floc formed were observed visually and for each condition, polymers were ranked based on their combined performance in these three aspects. The method developed by Pocock industrial does not give quantitative information about settling characteristics and floc properties but it is a time-efficient way to compare the effect of polymers qualitatively. This type of method is very useful for unknown samples and helps in selecting a few polymers from wide range of polymers available. About 12 different polymers were used in the testing; these polymers were polyacrylamide-based and varied in charge density and molecular weight. The cationic polymers were of lower molecular weight than the anionic polymers. The kaolinite suspension at high pH was identified as the most challenging sample; very few polymers gave good settling characteristics. For suspensions at low pH, and natural pH, almost all the polymers worked; a few of them gave better results than the others. It was observed that the supernatant clarity got worse as the charge density on anionic polymers increased, so anionic polymers with low charge density were recommended for further experiments. Cationic polymers with high charge density and lower molecular weight gave contrasting results to the anionic polymers and were included in the study to look at the differences in floc properties. Based on the floc screen test results, the following polymers were selected and used for initial experimentation (Table 2.1).

2.3.3 Sample Preparation

The Fisher K2 500 Kaolinite was added to deionized water to prepare 100 ml of 2% w/v suspension. The suspension was stirred for 60 minutes and sonicated for

Table 2.1: List of polymers selected for further experiments.

Commercial name	Charge density	Molecular weight	Manufacturer
AF 308	40% anionic	12-14 million	Hychem
AF 303	5% anionic	12-14 million	Hychem
NF 301	Nil	12-14 million	Hychem
CP 913	70% cationic	5 million	Hychem

20 minutes. The pH was altered by adding KOH or HCl and the suspension was allowed to equilibrate for 30 minutes while being stirred. The ionic strength was kept less than 2mM for all the samples. The final pH was noted in each case.

Polymer solution used in the settling test was added at 0.1 g/l concentrations. The solid polymer particles in powder form were added to DI water and a stock solution with polymer concentration 1g/l was prepared. The solution was allowed to equilibrate while being stirred for 8 hours at 400 rpm. Right before addition to the kaolinite suspension, some of the polymer was diluted to 0.1g/l and then added to the suspension. Fresh stock solution was prepared every week as the polymer solution showed some aging if stored for longer durations. The aging was evident by change in viscosity and/or a change in color to off-white. The stock solution was always stored at lower temperatures. Polyacrylamide-based polymers take different times to hydrolyze and age depending on their molecular weights. The time-dependent aging of aqueous solutions formed from a number of anionic flocculants was established by

comparing their activities with a standard kaolin slurry (Owen et al., 2002). Keeping these facts and the associated literature in mind, the polymer solutions were not used before 24 hours of aging or after 5 days of aging for all the polymers used.

2.3.4 Procedure for Sedimentation Experiments

During initial experiments, few operating conditions were varied to see the effect of its change on the settling velocity. The procedure is described below using one such set of operating conditions.

100 ml kaolinite suspension at pH 5.5 was transferred to a calibrated measuring cylinder. Polymer solution was added to the kaolinite suspension drop by drop. The polymer solution was added at a concentration of 200-ppm dry weight solids. The suspension was being continuously stirred during polymer addition. The total stirring time was 60 seconds. After 60 seconds, the stirring was switched off and the readings at sediment-suspension interface were taken. The polymer-induced kaolinite flocculation gave quicker settling as compared to kaolinite suspension with no polymer added, as illustrated in Figure 2.3. Adjustments were made for the volume of the magnetic stirrer in final reading. Readings were taken at short intervals for the first few minutes and then at longer intervals until a total time of 60 minutes had elapsed. The readings were also observed after standing overnight. It was observed that three distinct layers developed: the sediment layer, the suspension layer, and the clear supernatant layer. The sediment volume did not show significant change. Using a calibration tape, the volume readings (ml) on the measuring cylinder were converted to height readings (cm) and data were reported as suspension-sediment interface height vs. time for first 60 minutes.

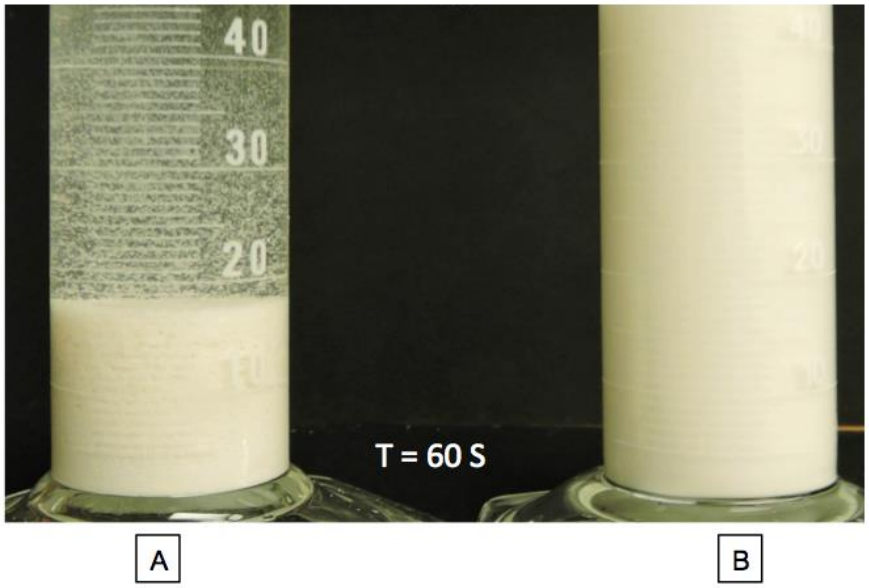

Figure 2.3: Comparison of kaolinite suspension settling after 60 second.
(A) High mol. wt. 5% anionic polymer used as flocculant; (B) no flocculant used.

2.4 Results and Discussion

The effect of polymer type, polymer dosage, pH, and mixing conditions on kaolinite settling characteristics was studied. In effluent treatment, the settling rate or the final sediment volume are the most important properties of the flocculated system. For water recovery and reuse, the supernatant clarity becomes the most important criteria. It is clear from these examples that different properties of the flocculated systems can be the determining criterion in different processes. Different properties of the flocculating system reveal different information about the polymer-kaolinite interaction. The settling rate is a measure of floc size as well as compressibility of the flocs and floc network in later stages. The supernatant clarity is a measure of size distribution of flocs and size-based capture of particles and flocs by the polymer. The sediment volume is an indication of not only floc size and structure but also of adsorbed polymer layers (Somasundaran, 1984).

2.4.1 Effect of Polymer Type

The effect of polymer addition on the settling of kaolinite suspension is shown in Figure 2.4. The length of suspension in column was 18.5 cm initially. The sediment-suspension interface was tracked and their change with time was reported.

It was observed that the anionic polymers provided faster sedimentation and resulted in smaller final sediment volume than the cationic polymers. These results agree with some of the previous work reported. The use of high molecular weight anionic PAM in flocculating negatively charged particles has the advantage of being

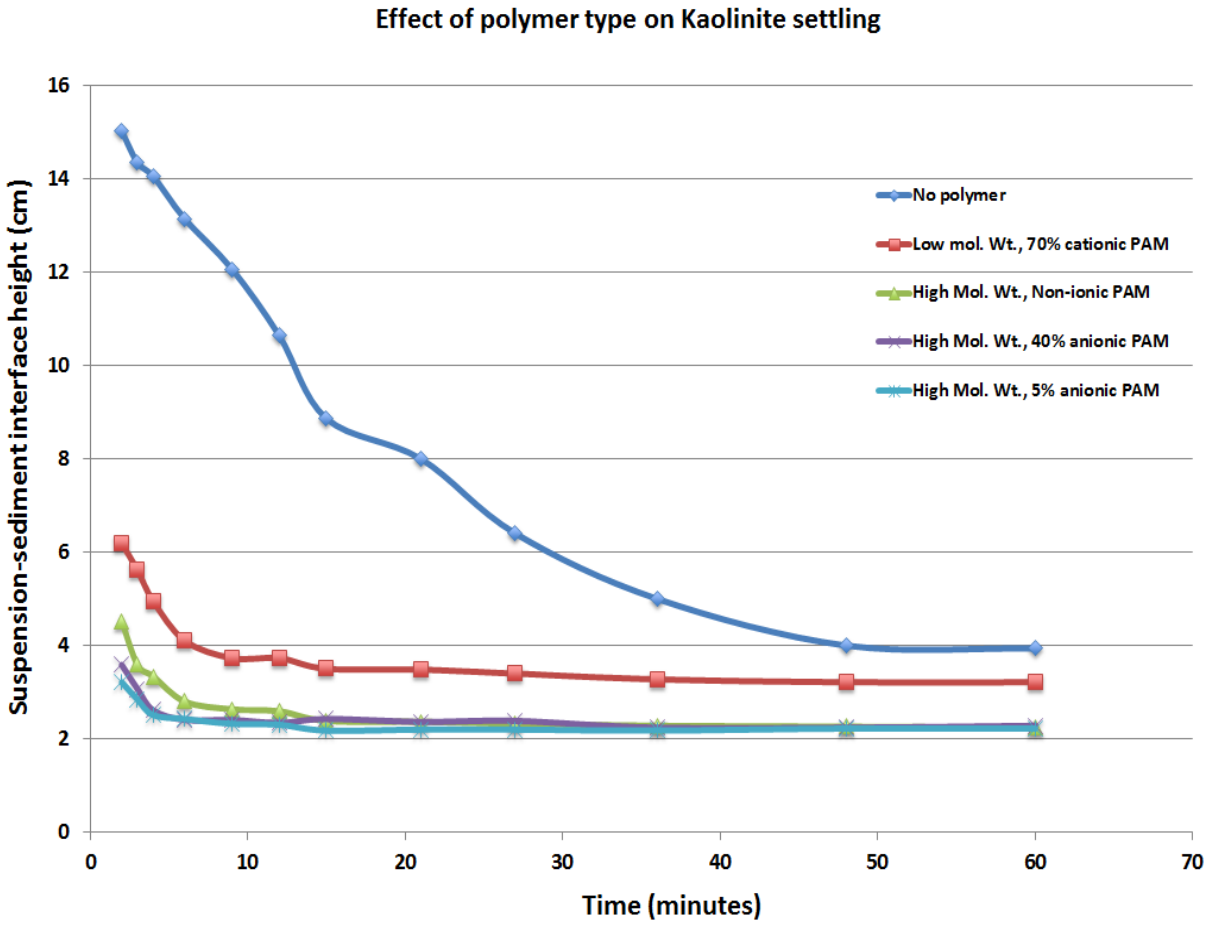

Figure 2.4: Effect of polymer addition of kaolinite settling at 2% solids, 200-ppm polymer dosage, and pH 5.5.

more effective than cationic polymers by increasing settling rate (Somasundaran and Mougdil, 1988). The faster settling rate could be due to the formation of larger sized flocs in case of anionic polymers; this was verified by size analysis of flocs reported in the next chapter.

As we know, interparticle bridging is the dominant mechanism for flocculation in the case of high molecular weight anionic polymer and charge neutralization dominates when a cationic site is present on the polymer chain. Also, polymer molecule expansion arising from charge repulsion in the case of anionic polymers produces loops and tails, which leads to the formation of large open-structure flocs (Nasser and James, 2006).

The charge density of the anionic polymer did not seem to have a huge effect on settling; the 5% anionic polymer and 40% anionic polymer gave almost the same settling characteristics. It was also noticed that the high molecular weight non-ionic polymer gave better settling than the low weight cationic polymer. The results clearly suggests that the effect of molecular weight is more significant than the charge density. It has been established by many researchers that flocculation and settling is dependent on both the polymer charge density and molecular weight. Yoon and Deng (2004) considered that the initial flocculation ability of the polymer is closely related to the molecular weight, but the reflocculation ability is more dominated by the charge density of the polymer.

The supernatant clarity was observed to be better in the case of the cationic polymer as compared to the anionic polymer. As mentioned in the previous section, supernatant clarity is a measure of size distribution of flocs and size-based capture

particles and clusters by the polymer. Poor supernatant clarity in the case of the anionic polymer suggests the incapability of high weight anionic polymers in capturing ultrafine kaolinite particles. At finer particle size, the surface potential effect is expected to dominate the interparticle interactions. It has been shown that finer size clay particles are more responsive to electric field (Shang, 1997). Poor supernatant clarity in case of anionic polymer hints at variation of surface potential with size of kaolinite primary particles. Preliminary experiments at the University of Utah have indicated dependence of surface charge on size of kaolinite particles. It is possible that the finer kaolinite particles carry more negative surface potential and the electrostatic repulsion with the anionic chain dominates other interactions, thus hindering their flocculation. However, in case of cationic polymer, negative surface potential would help in flocculation by charge neutralization, thus giving a clear supernatant.

2.4.2. Effect of Polymer Dosage

It was observed that the dosage has an effect on initial settling rate, final sediment volume, and the total time required to attain that sediment volume; results are shown in Figure 2.5. The settling rate increased and final sediment volume decreased on increasing the polymer dosage up to 100 ppm. Beyond 100 ppm, the increase in polymer dosage led to decrease in the time needed to attain the minimum volume. The optimum dosage of polyacrylamide polymers for kaolinite flocculation has been to be in similar ranges by previous researchers (Kingsley, 2008).

A similar settling test was done using CP 913 and it was found that the sediment volume decreased until 200 ppm polymer dosage. Beyond 200 ppm,

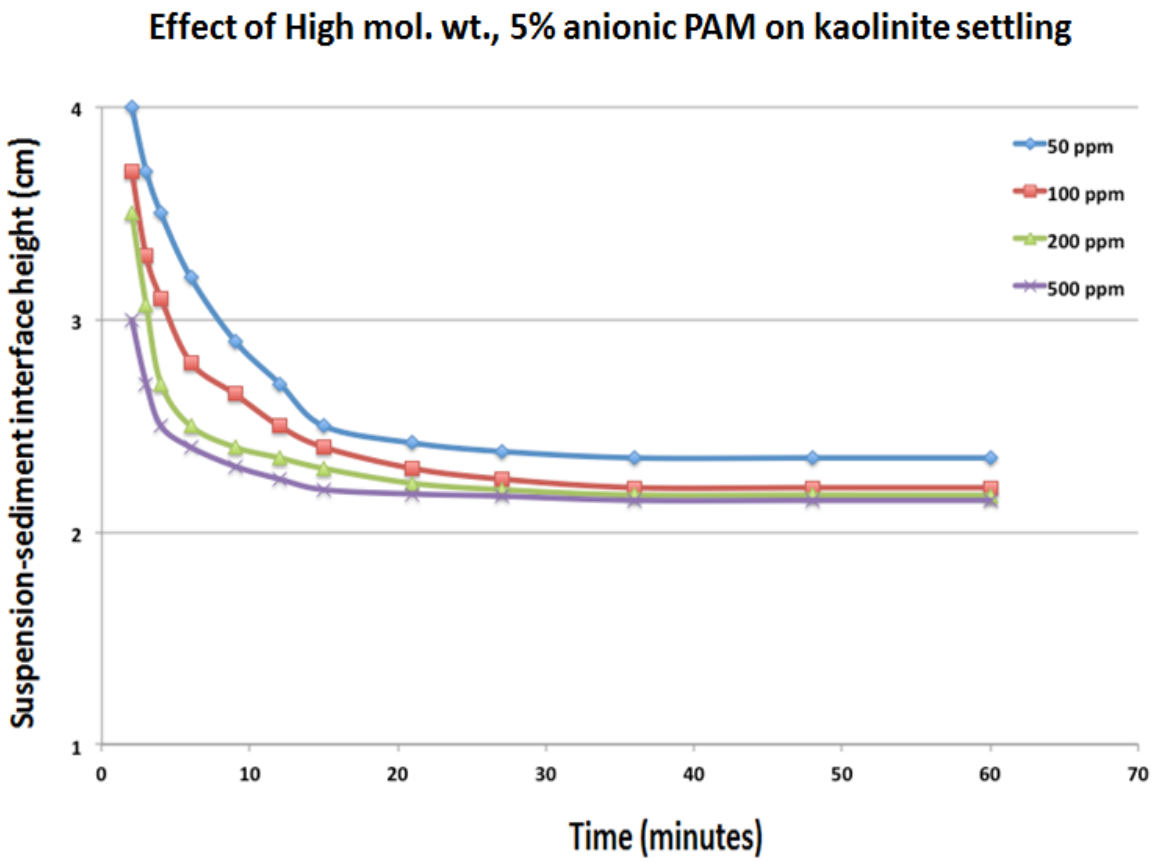

Figure 2.5: Effect of high mol. wt. 5% anionic polymer dosage on kaolinite settling. The solution pH is 5.5, solids content is 2%.

increase in polymer dosage helped the system attain minimum sediment volume quickly.

The difference in optimum dosage for the two polymers is expected due to the difference in their molecular weights and hence chain length. Even though the cationic polymer is able to flocculate kaolinite particles by charge neutralization, bridging is limited due to smaller chain length. Consequently, the optimum dosage required for CP913 is higher than that for AF303. All these experiments were conducted at pH ~ 5.5. The optimum dosage is expected to be different for different pH values.

The floc properties are expected to be different in size, density, and strength based on the dosage of polymer used due to the difference in extent of adsorption. At lower pH, the increase in anionic polyacrylamide dosage increases the strength of flocs formed due to higher adsorption capacity (Taylor et al., 2002). In our experiments, it was observed that at a very low polymer dosage of about 50ppm, the flocs broke under their own weight if left standing for over 24 hours. To get relatively stronger flocs at low pH, a dosage of 200-250 ppm was used for further experiments. For example in the case of HRXMT characterization (Chapter 4), floc dosage was increased further as a stabilized sediment was needed to obtain high fidelity images. Using lower polymer dosage led to some degree of floc breakage and consequent movement which interferes with the HRXMT characterization of the sediment, as will be discussed in subsequent chapters.

Here, it should be noted that in the case of polyacrylamides copolymers, the dosage required is highly dependent on the "age" of the polymer. The optimum dosage at its peak activity time could be significantly lower than at other times (Owen et al., 2002). For these experiments, the effect of aging is considered to be negligible from 24 hours up to 5 days after preparation of the polymer solution.

2.4.3 Effect of pH

The settling characteristics for AF 303-induced flocculation were compared at three different pH values and the results are shown in Figure 2.6. Polymer dosage of 200 ppm was used for all these experiments. It was observed that the lower pH gave better settling characteristics than at the higher pH. It took longer time for the high pH sample to attain a stable volume; the final volume was found to be higher at

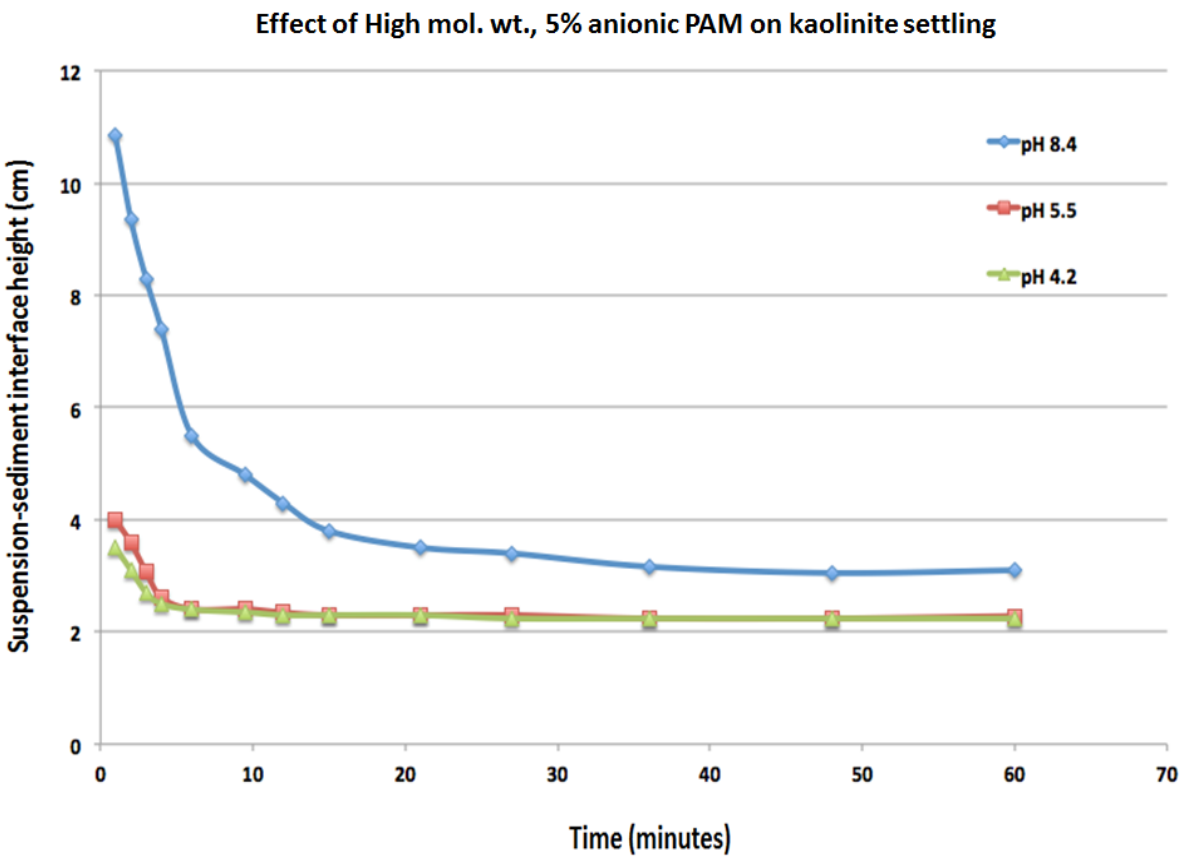

Figure 2.6: Effect of pH on kaolinite settling at 2% solid content, 200-ppm dosage of high mol. wt. 5% anionic polymer.

pH 8.4 as compared to the final volume at pH 5.5 and pH 4.2.

At higher pH since the particles are well dispersed and the whole system is negatively charged, it takes a longer time to form flocs, the flocs formed are smaller in size, and they settle slowly. A similar trend for effect of pH on clay settling in presence of synthetic anionic polymers has been reported in the past (Taylor et al., 2002; Kim et al., 2013).

The overall kinetics at high pH varies from overall kinetics at low pH due to difference in polymer conformation as well as difference in kaolinite surface charges. In case of high pH, all three kaolinite surfaces are negatively charged and therefore

the electrostatic repulsion exists, which indicates low rate of flocculation capacity. It has also been suggested in previous research that the conformation of the polymer chain changes with pH, which influences the interaction of polymer with kaolinite particles. The dissociation of carboxyl group in polyacrylamide is supposed to increase with pH (Graveling et al., 1997). This leads to extended chain at high pH due to an increase in repulsion due to the high number of charged sites (Tjipangandjara and Somasundaran, 1992). Taylor (2002) observed that the extended chain contributes to the final density and strength of the flocs. He suggested that even though the floc size is smaller at high pH, the floc strength and density is higher.

2.4.4 Effect of Mixing Conditions

The mixing speed and time were also varied to see the effect on settling and sediment volume. Insuffiecient agitation does not allow formation of flocs and excessive agitation of a flocculating suspension causes floc breakage. This has an adverse effect on flocculation efficiency as the smaller flocs formed have a lower settling rate. Even though floc breakage leads to exposure of fresh particle surfaces to polymer adsorption, thereby resulting in increased adsorption capacity of the flocculant, the flocs do not reform efficiently as the excess adsorbed polymer causes repulsion. This suggests that optimum dosage for a polymer only holds at a particular degree of agitation. Although the mixing conditions did not effect the settling rate much, the sediment texture showed marked difference. At low mixing speed and time, the sediment was partially present as fine powder due to lack of flocculation (Figure 2.7). At around 400 rpm and 60 seconds mixing time, sediment has a uniform texture

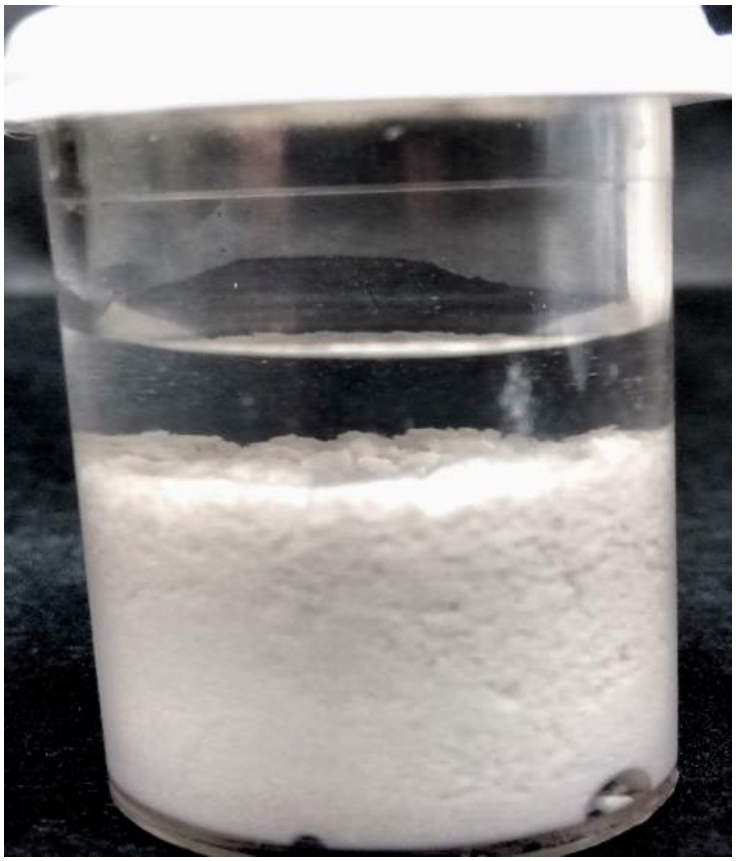

Figure 2.7: Nonuniform texture of sediment formed due to insufficient agitation.

and bigger aggregates were visible. On increasing the mixing speed or time, the delicate flocs got broken and sedimented as finer aggregates. Based on qualitative analysis of sediment texture, 400 rpm and 60 seconds mixing was selected for further experiments.

2.5 Summary

In this chapter, settling tests for polymer-induced kaolinite flocs have been done to identify preferred conditions for few operating parameters. The operating parameters that were varied are polymer type, suspension pH, polymer dosage, and mixing speed.

It was concluded that high molecular weight anionic polymers give faster settling rate and lower sediment volume than low molecular weight cationic polymer. Similar observations have been reported in the past (Somasundaran and Mougdil, 1988). The faster settling rate could be due to the formation of larger flocs in case of anionic polymers; this hypothesis was verified by size analysis of flocs reported in next chapter. Also, the charge density of the anionic polymer did not seem to have a huge effect on settling; the 5% anionic polymer and 40% anionic polymer gave almost the same settling characteristics. It was also noticed that the high molecular weight non-ionic polymer gave better settling than the low weight cationic polymer. The results clearly suggest that the effect of molecular weight is more significant than that of charge density. It has been established by many researchers that flocculation and settling is dependent on both the polymer charge density and molecular weight. Yoon and Deng (2004) considered that the initial flocculation ability of the polymer is closely related to the molecular weight, but the reflocculation ability is more dominated by the charge density of the polymer.

The supernatant clarity was found to be better in case of cationic polymer. Supernatant clarity is a measure of size distribution of flocs and size-based capture of particles and clusters by the the polymer. Poor supernatant clarity in the case of the anionic polymer suggests the incapability of high weight anionic polymers in capturing ultrafine kaolinite particles. Preliminary experiments at the University of Utah have indicated dependence of surface potential on size of kaolinite particles. It is possible that the finer kaolinite particles carry more negative surface potential and the electrostatic repulsion with the anionic chain dominates other interactions, thus

hindering their flocculation. However, in case of cationic polymer, negative surface potential would help in flocculation by charge neutralization, thus giving a clear supernatant.

The optimum dosage for high mol. wt., 5% anionic PAM was found to be around 100 ppm at pH 5.5. Kingsley (2008) has reported similar optimum dosage for anionic PAMs. In case of low mol. wt., cationic PAM, higher polymer dosage of about 200 ppm was required to flocculate the suspension at similar conditions. The difference in optimum dosage for the two polymers is expected due to the difference in their molecular weights and hence chain length. Bridging flocculation is limited in case of cationic polymer due to shorter chain length. The optimum dosage is expected to be different at different pH and "age" of the polymer. The aging time of polymers determines their activity. The optimum dosage at its peak activity time could be significantly lower than at other times (Owen et al., 2002). For experiments conducted in this chapter, the effect of aging is considered negligible from 24 hours up to 5 days after preparation of the polymer solution.

Settling characteristics were compared at different pH using high mol. wt., anionic PAM and it was observed that the lower pH suspension gave better settling all characteristics than higher pH suspension at the same conditions. At higher pH since the surfaces of kaolinite are negatively charged, it takes a longer time to aggregate these particles into flocs. In addition, the flocs formed are smaller and they settle slowly. A similar trend for effect of pH on kaolinite settling in presence of synthetic anionic polymers has been reported in the past (Kim et al., 2013; Taylor et al., 2002). The overall kinetics at high pH varies from overall kinetics at low pH due

to the difference in kaolinite surface charges as well as difference in polymer conformation. It has been suggested in previous research that the conformation of the polymer chain changes with pH; for example, the dissociation of carboxyl group in polyacrylamide is supposed to increase with pH (Graveling et al., 1997). Such factors influence the interaction of polymer with kaolinite particles and hence the settling characteristics are different at different pH.

The mixing speed and time were also varied to see the effect on settling and sediment volume. Insufficient agitation does not allow formation of flocs and excessive agitation of a flocculating suspension causes floc breakage. Although the mixing conditions did not effect the settling a lot, the sediment texture was influenced by change in mixing conditions. At low mixing speed and time, the sediment was partially present as fine powder due to lack of flocculation. At around 400 rpm and 60 seconds mixing time, the sediment has uniform texture and bigger aggregates were visible. On increasing the mixing speed or time, the delicate flocs got broken and sedimented as finer aggregates.

CHAPTER 3

SIZE AND SHAPE OF SUSPENDED FLOCS

3.1 Introduction

Extensive research (Chaiwong and Nuntiya, 2008; McFarlane et al., 2005; Mpofu et al. 2003, 2004; Nasser and James, 2007, 2009; Oliveira and Rubio, 2012; Zbik et al., 2008; Zhou et al., 2004) has been conducted on the relationship between floc properties and slurry settling and sedimentation/dewatering. For sedimentation, larger and compact flocs are required whereas in flotation operations, floc wetting characteristics and strength are important (Liang et al., 2015). It is very important to comprehensively understand the floc properties so as to know whether the flocs are proper for the particular purposes. In addition to other properties, such as strength and compactness, floc size and shape are very important in determining settling and dewatering of suspensions. Floc size and floc shape can influence the slurry rheology (Liu and Peng, 2014) and the interaction between flocs and bubbles (Forbes, 2011). Floc size substantially effects particle removal by sedimentation and filtration. Floc shape affects the behavior of aggregated particles, particularly with regard to collision efficiency and settling rates. Large and compact flocs are wanted both for tailings sedimentation/consolidation and for water recovery (Lemanowicz et al., 2011; Mpofu et al., 2003, 2004; Sabah and Erkan, 2006; Wang et al., 2011).

Kaolinite floc size has received considerable attention from the scientific community in recent years (Chaiwong and Nuntiya, 2008; Li et al., 2006; Nasser and

James, 2006, 2007; Yu et al., 2006; Zhu et al., 2009, and others) but kaolinite floc shape has received less attention. Most of these studies include ex-situ characterization of flocs by various types of particle size analyzers or by empirical methods. Of course, flocs usually form from suspensions and they can be destroyed during handling when they are sampled or poured from one container to another. Imaging is considered to be the most direct and accurate method for studying floc size and shape. For floc analysis, microscope, dynamic image analysis (DIA), and particle vision measurement (PVM) are most frequently used (Liang et al., 2015). In this phase of the research, kaolinite flocs have been studied by using both PVM and DIA.

3.2 Particle Vision & Measurement (PVM)

3.2.1 Equipment Principles

PVM is often used for in-situ determination of particle features in suspension (Greaves et al., 2008; Liang et al., 2015; Liu and Peng, 2014; Nasser and Salhi, 2015; Qi et al., 2015). In this study PVM has been used to observe in-situ flocculation of kaolinite particles. A significant advantage of PVM over DIA is that inconsistency of flow conditions for the primary system in the measurement cell is diminished. Video of around the 1000μ X 1000μ region of the slurry can be captured using a digital camera, so the images recorded at any time can be analyzed. However, this technique suffers from the low resolution for particles/flocs aggregates smaller than 20 μm (Greaves et al., 2008). Using this method, the fully formed flocs could be imaged, but the resolution was not good for observing the primary particles and intermediate states of flocculation. Meanwhile, compared with the in-situ technique Focused Beam Reflectance Measurement *(*FBRM), PVM gives better results in the dilute solutions

having around 0.5% solid concentration (Senaputra et al., 2014).

The PVM probe is shown in Figure 3.1. A sapphire window is present at the probe tip and houses the illumination lenses and imaging lenses. Image acquisition begins at the probe tip with the help of illumination lenses consisting of six pulsed laser diodes and image lens as we can see in Figure 3.2. At any given time, we can use one or more of these lenses to get the best illumination for imaging as required. A camera is present inside the probe which captures images. The focal plane of the imaging lens can be adjusted easily by turning the micrometer knob present at the head. When the focus is on the probe's window surface, it is optimal for viewing the smaller particles. The micrometer is turned clockwise to move the focal point of the probe further into the suspension; this condition is ideal for imaging the larger particles.

3.2.2 Sample Preparation and Procedure

A 1% w/v kaolinite solution was prepared in a 500 ml beaker. The sample was stirred for 2 hours and sonicated for 30 minutes. The pH of the suspension was noted

Figure 3.1: Particle Vision & Measurement probe (source: Mettler Toledo PVM manual).

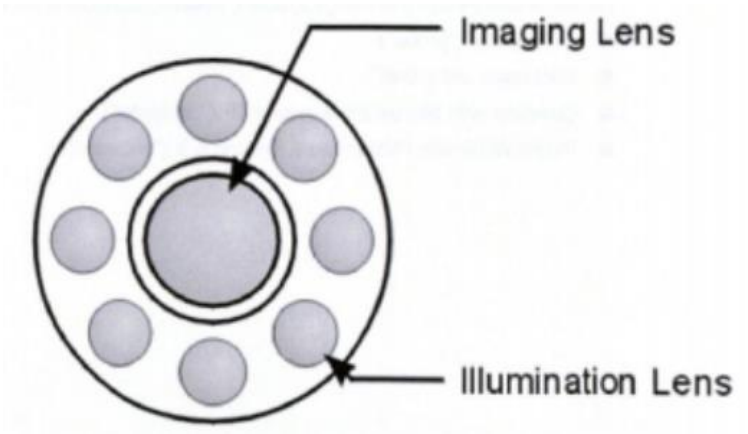

Figure 3.2: Arrangement of illuminating and imaging lens on probe tip (source: Mettler Toledo PVM manual).

to be 5.8. The beaker was kept on a magnetic stirrer. The PVM probe was clamped vertically and the clamp height was adjusted such that the probe tip is around the 250 ml mark in the kaolinite suspension. The magnetic stirrer was turned on at 400 rpm and 0.1 g/l polymer solution was added to the suspension drop by drop until the polymer dosage was 200 ppm. Image acquisition was started while the polymer was being added and was continued till 60 seconds after polymer addition. During this time, a low rpm of 150 was maintained in order to minimize blurriness in images captured. For the initial few seconds of flocculation, cloud-like structures were visible. After a few seconds, some flocs came into focus, but there was a rapid change going on in the floc structure. Towards the end of 30 seconds, the flocs visible were more stable; the images captured after this duration were used for analysis.

3.2.3 Image Processing Tools

Although care was taken to exclude blurriness due to the continuous mixing and dynamic nature of the whole process, many of the images had a certain extent of

blurriness. To remove this blurriness and to carve out the floc boundaries, various image-processing techniques from ImageJ/Fiji were used.

A combination of Gaussian blur, thresholding, level sets segmentation, and erosion function was used to process these images. Blur function replaces each pixel with average intensity of pixel plus neighbor pixels. A matrix of 3X3, 5X5, or 7X7 is generally chosen for calculating the average intensity value. In Gaussian blur function, the weighted average is used instead of average. Smoothing is performed by using the Gaussian function for the entire matrix. The Gaussian function variation is depicted using a 5X5 matrix in Figure 3.3. The intensity values for the blurred image were then subtracted from intensity values for the original image to remove some of the background blurriness.

Using the threshold function, we can interactively set lower and upper threshold values, thus segmenting grayscale images into features of interest and non-interest. This function can be used on 8-bit type image and is a simple and an efficient

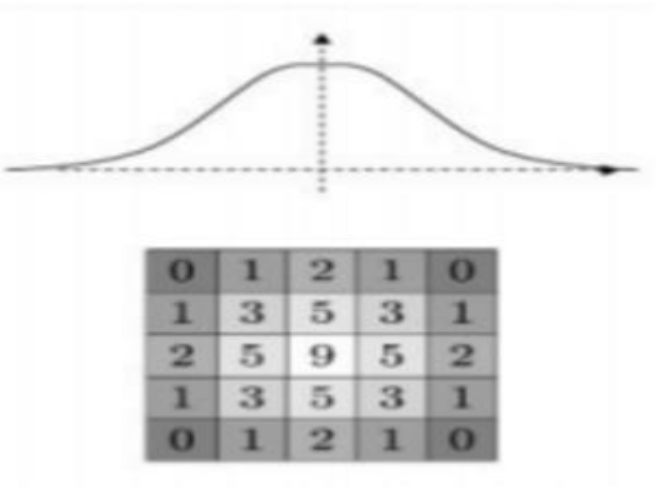

Figure 3.3: Gaussian function variation for a 5X5 matrix.

segmentation tool.

Thresholding worked well to remove some of the unwanted background but was not enough to remove the blurriness at floc boundaries. A few segmentation techniques were tried including the trainable weka segmentation. Finally, level sets segmentation gave good result for removing this blurriness at the floc boundaries. This method is based on partial differential equations and uses them for progressive evaluation of the differences among neighboring pixels to find object boundaries. Fast marching and active contour methods are the two types of algorithms available. A "seed point" is introduced in the image; this point grows in region as the algorithm runs. While growing the region, it constantly calculates the difference of the current selection to the newly added pixels and stops if it exceeds a preselected gray value difference. In order to get satisfactory results from the algorithm, the gray value threshold, distance threshold, level set weight values, and level set convergence criteria should be optimized. The AND function is applied on the original image and level sets output to get the final segmented image, an example of use of level sets has been illustrated in Figure 3.4. This function was used as many times as required on different flocs until the final image was free from blurriness.

The level sets function removes most of the blurriness but a few small protrusions were still left. These were removed by using the erosion function. Erosion function is one of the morphological filters available in Fiji software and is related to Minkowski subtraction. It replaces each pixel with the minimum intensity value in the neighborhood. With binary images, it removes pixels from the edges of black objects. The radius and element type should be chosen carefully, the radius determines the

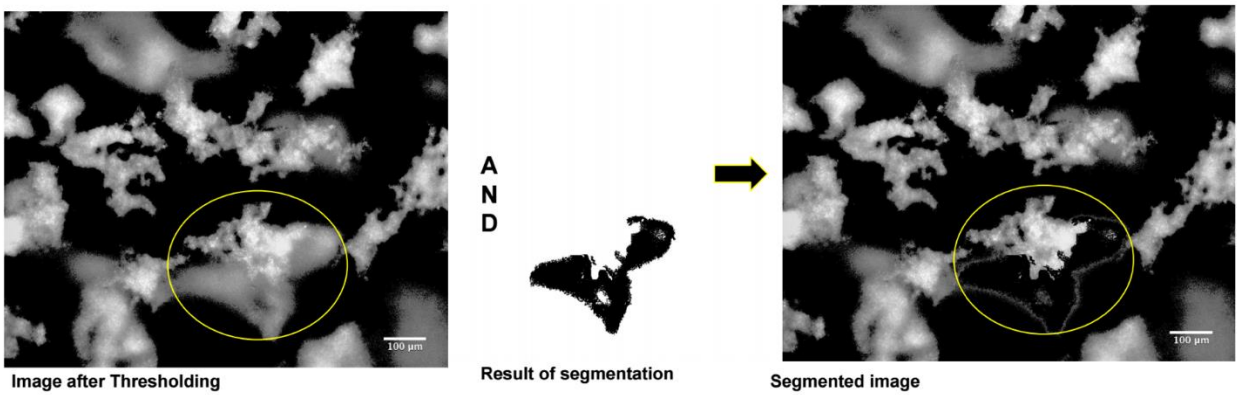

Figure 3.4: Stepwise illustration of how LEVEL SETS segmentation (Fiji plugin) works.

in which it is going to look.

3.3 Dynamic Image Analysis (DIA)

3.3.1 Equipment Principles

Dynamic Image Analysis (DIA) involves imaging a flow of moving particles. It is both similar to, as well as different from, traditional laser diffraction (LD) in detection principle. In both systems, an adaptable beam expansion unit creates a parallel beam of light. This beam of light is directed at the measuring zone of the dispersed system. In the LD system, a Fourier lens transforms the diffracted light to a diffraction pattern, which is recorded by a multi-element photo detector. In a DIA system, imaging lens and imaging sensors are present instead of Fourier lens and multi-element detector, respectively. Using these imaging lenses, the full amplitude and phase distribution of the diffraction pattern is back-transformed to a real image, which is recorded by the image sensor. A comparison of optical set-up for both techniques is shown in Figure 3.5. QICPIC DIA apparatus (Sympatec Inc., Clausthal-Zellerfeld, Germany) was used in the current study. This system combines the basic

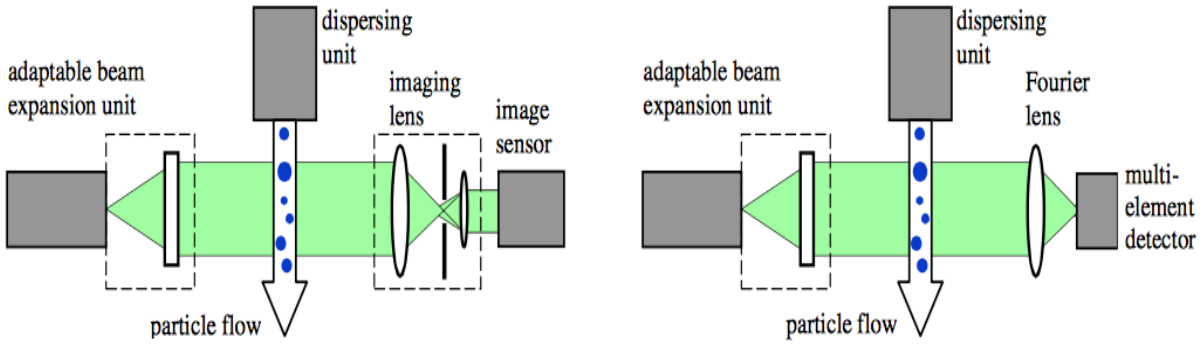

Figure 3.5: Set-up of QICPIC image analysis (left) and HELOS laser diffraction sensor (right). (Source: Sympatec website & user manual).

concepts of a powerful disperser with DIA. The QICPIC uses rear illumination with a visible pulsed light source, the flash rate of the light source is adjustable from 1 to 500 Hz, and is synchronized with the high-speed camera. A well-dispersed particle flow is led through the image plane. Due to the dispersion, the transportation fluid separates the particles from each other and overlapping of particles is avoided. As the particles move across the image plane, attention is paid to a possible motion blur. Special pulsed light source with an exposure time of less than 1 ns is used, this gives a motion blur of less than 100 nm for particles moving with velocity of 100 m/s. 100 nm is less than the smallest pixel size of 1 µm and hence invisible for the camera. So this method gives well-defined particle boundaries.

The camera and the light source are able to operate at any speed from 0 to 450 frames per second (fps); very high particle counts are acquired in a short time. With 100 particles per frame and 450 frames per second, over 1 million particles can be acquired in 25 seconds. In order to detect the edges of the particle precisely, the particle flow is imaged in transmission using a special imaging objective, which only

transmits light rays to the camera, which are nearly parallel to the optical axis. In combination with a parallel illumination, even highly transparent particles are imaged 'black', as long as their diffraction index differs from the surrounding fluid and so their light is deflected. Different objectives mounted on a carrousel allow for the selection a specific measuring range by software.

Finally, a high-speed CMOS camera with 1024x1024, i.e., 1 Mega pixel is used. In combination with a built-in signal processing unit of highest performance and a 1.25 Gigabit-link, all image data can be processed and stored in the database of the PC in real time even at 450 fps.

To measure the particle size in SI length units, the DIA system is calibrated with a certified standard scale. The effective magnification of the imaging lens and the size of the sensor are measured and are thus traceable back to the standard meter. To measure the particle size in SI length units, the wavelength of the light, the scale of the detector, and the exact focal length of the system must be known.

The LIXELL dispersion system was used as the dispersing unit. Its basic construction comprises an open loop flow cell with inlet and outlet connector. Cuvettes with different optical path lengths are available; the location of cuvette position is controlled along the optical axis by the software. This function ensures auto-focus so that we get a very sharp image. It has sample inlets on the front as well as on the top. Either one or both of the inlets can be used.

3.3.2 Sample Preparation

1% kaolinite solution of 50 ml volume was prepared in DI water. Flocs were prepared by adding 0.1 g/l polymer at a dosage of 200 ppm. The flocs formed were

gently transferred to a 500 ml beaker, which was filled with DI water. The objective here was to get a very dilute suspension, so that the particles do not overlap while moving across the image plane. The suspension had to be stirred gently during experimentation to keep the flocs from settling.

Various methods of presampling were tried before it was possible to get reproducible size distribution data. First of all, a couple of 50 ml leur lock syringes were used with the front sample inlets in parallel for sample delivery (the arrangement is shown in Figure 3.6). Sample was filled in one of the syringes and the other syringe was used to suck the sample back and forth. This way it was ensured that the fluid flow is maintained. However, when three consecutive experiments were done, it was noticed that the average floc size decreased continuously, suggesting that the flocs were being sheared. It is possible that the flocs were sheared by being subjected to continuous pressure difference inside and outside the syringe. Since the method is still in the development stage, the difference in results could have been due

Figure 3.6: Sample delivery using two leur lock syringes in parallel.

to problems in sample preparation, incorrect operating conditions, etc. We needed at least two identical runs to be confident about the results.

Next, we tried using one of the inlets on top and one of the inlets in front, creating a perpendicular arrangement (Figure 3.7). The sample was pushed in from the top inlet and back and forth motion of the sample was maintained by using the syringe at the front inlet. In this arrangement, the force applied on syringes was relatively less as the flocs were falling under gravity during a portion of the flow. This method worked better, but the suction force from one syringe was still enough to break the flocs as we could not get reproducible floc size distributions.

It was evident that the flocs are extremely delicate and any kind of external force would break them; the best option was to let them fall freely under gravity. A siphon system was created and joined to one of the inlets on top (Figure 3.8). One of the front holes was used as outlet and the out-coming suspension was collected (not shown in figure).

A large amount of diluted kaolin suspension (around 500 ml) was placed in a beaker siphoned to the LIXELL input. The volume of sample was about ten times larger than in the leur lock syringes and there was no need for recirculation of the sample. The suspension was gently stirred manually while the sample was flowing inside the tubing. The beaker was replenished with water if the solid concentration increased due to continuous settling of flocs. It should be noted here that increasing the stirring speed in order to keep the flocs from settling is not recommended, as it might break the flocs. The sample collected at the front outlet was run a second and third time. The data for first and second runs showed good reproducibility. However,

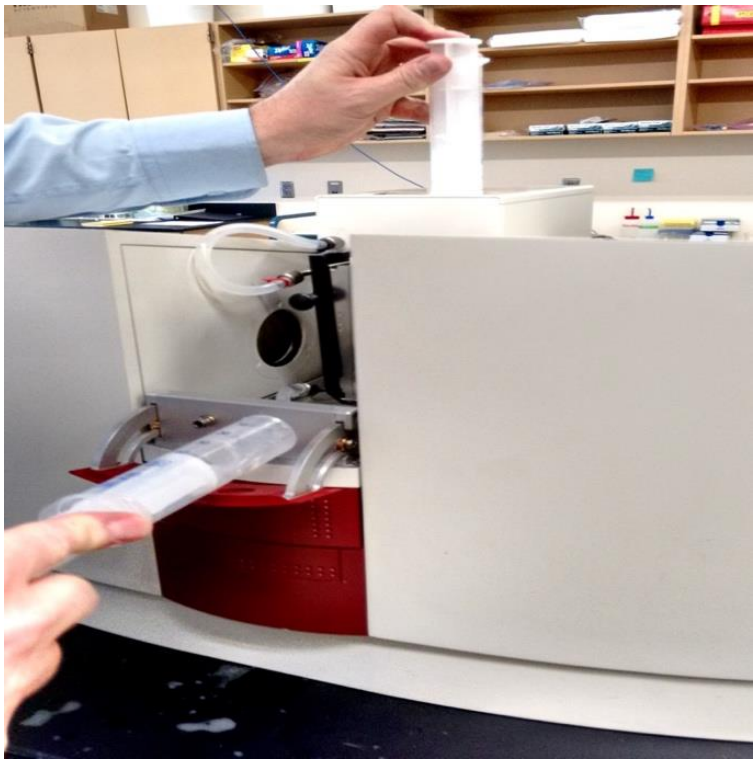

Figure 3.7: Sample delivery using two leur lock syringes in perpendicular arrangement.

Figure 3.8: Sample delivery system using siphon system.

the third time, there was some floc breakage. Even though minimum external force was applied in this arrangement, it is possible that repeated handling and flow led to breakage of some flocs. But it was established that with extreme care, the QICPIC analyzer can be used to get the size distribution of kaolinite flocs. To make the process more consistent, a light magnetic stirrer should be used at low rpm for delivering the suspension into the LIXELL system.

3.4. Results and Discussion

3.4.1. Size and Shape of Flocs Revealed by PVM

Some of the images obtained using the PVM were relatively free of blurriness and did not require a lot of processing, but most of the images had to be processed in order to get useful data out of them. A few examples of before and after image processing are presented in Figure 3.9.

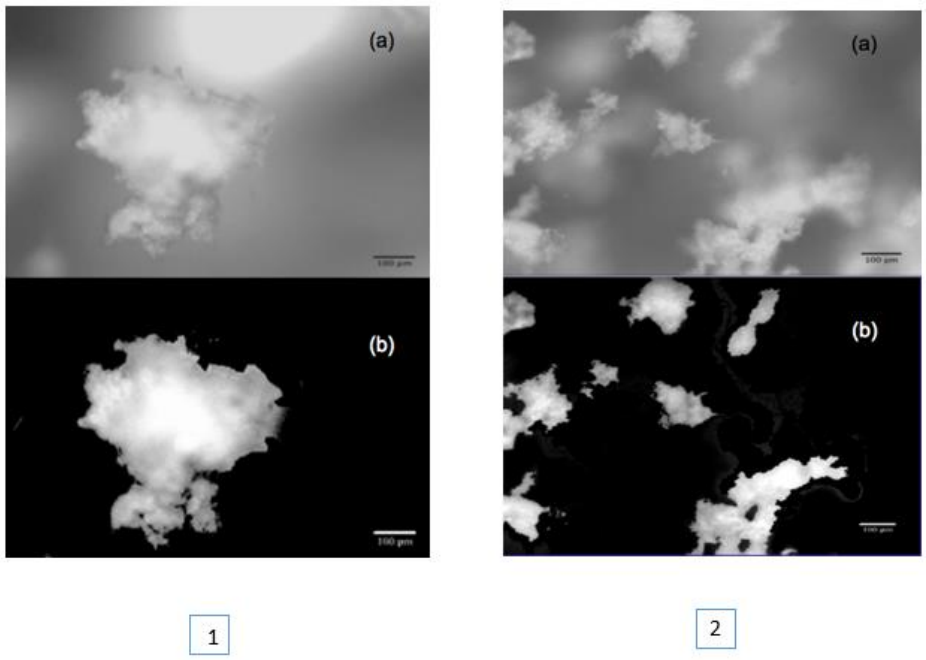

Figure 3.9: Comparison of original image (a) and final image (b) for images 1 and 2.

For better representation and comparison, RGB labeling and numbering of flocs was done (an example is shown in Figure 3.10). Comparison of flocs formed using high mol. wt. anionic PAM and low mol. wt. cationic PAM was done. Five images from both data sets (high mol. wt. anionic PAM and low mol. wt. cationic PAM) were selected for analysis. The images were processed and analyzed for size and shape using the biovoxxel plugin available with Fiji. An example of a processed image is shown in Figure 3.11. Only the flocs, which were completely in the frame, were considered in the analysis. The floc circularity was measured to get information about the shape of the floc. In general, the flocs formed using high mol. wt. anionic PAM were found to be larger and more irregular than the flocs formed using low mol. wt. cationic PAM.

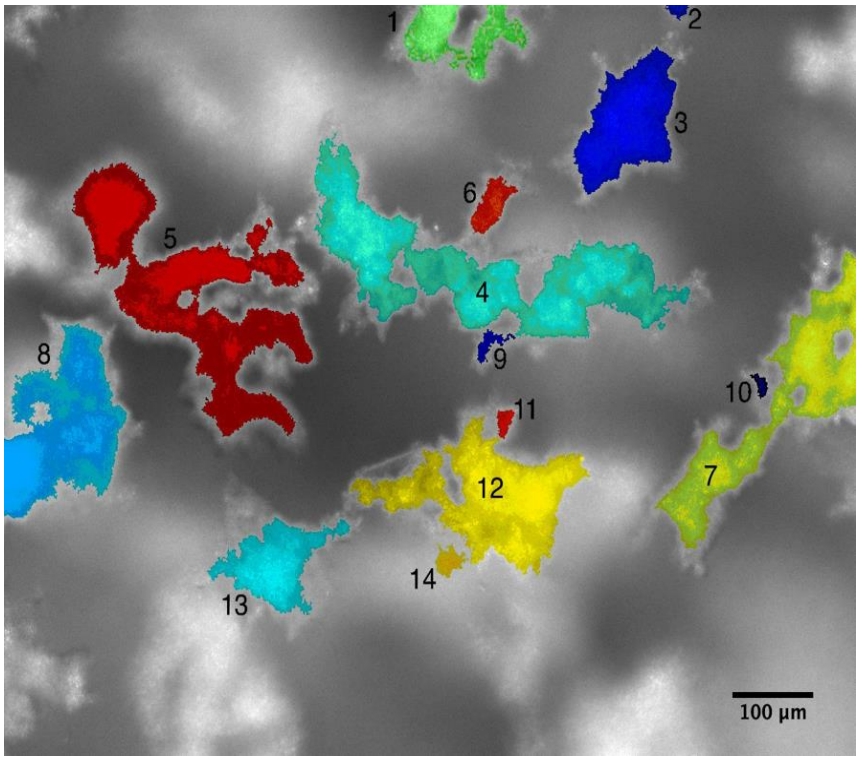

Figure 3.10: Comparison of original and final image using RGB labeling and floc numbering.

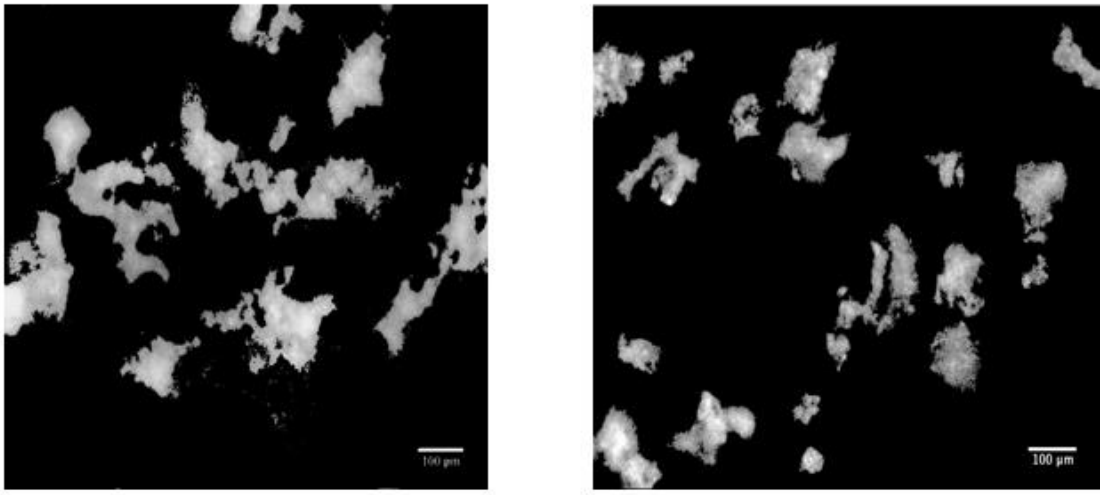

(A) (B)

Figure 3.11: Flocs formed using high mol. wt. anionic PAM (A) as and low mol. wt. cationic PAM (B) as flocculants at pH 5.8 and polymer dosage 200 ppm. The solid concentration was 1%.

Floc size and circularity is compared in Table 3.1. The larger size of high mol. wt. anionic PAM-induced flocs could be attributed to higher bridging capacity of high mol. wt. anionic PAM as compared to low mol. wt. cationic PAM. Also, the difference in floc size explains the difference in settling rate for flocs formed using these two polymers up to some extent.

Various measurements are regarded as the representative characterization of floc size. The equivalent circle diameter is a commonly used method of size representation. It is an accurate measurement of size of spherical particles. However, due to the highly irregular shape of the flocs, equivalent equivalent diameter would not be a true representative of floc size. A simple measure of floc size is the floc longest dimension also known as maximum ferret diameter.

For PVM size analysis data, the maximum ferret diameter has been reported

Table 3.1: Size and shape comparison of flocs formed using AF 303 and CP 913.

Polymer used	Average floc size (µm)	Maximum floc size (µm)	Average floc circularity
AF 303 (High mol. wt. anionic PAM)	223	528	0.26
CP 913 (Low mol. wt. cationic PAM)	145	241	0.34

as the floc size. For biovoxxel plugin, circularity of floc, C, is defined as:

$$C = 4\pi \frac{A}{P^2} \quad \text{……} \quad (3.1)$$

where A and P are the projected area and perimeter of the floc, respectively.

Although the size and shape analysis of polymer-induced kaolinite flocs using PVM has not been reported yet, researchers have found that cationic polymer gives smaller flocs compared to the anionic flocs (Nasser and James, 2006) using an empirical settling equation developed by Michales and Bolgers (1962) for size calculation. In this work, we have been able to validate their conclusions by using experimental methods. The results show some difference in floc circularity and indicate that the anionic polymer flocs are slightly more irregular than the cationic polymer flocs.

3.4.2 Size and shape of Flocs Revealed by DIA

Dynamic Image Analysis is a relatively new technique for size and shape analysis of particles. Since this technique had not been used previously with a delicate sample like kaolinite flocs before, the development of the experimental method was very important. Also, the significance of data collected was our prime concern.

The experiment was repeated a few times for the same sample to be sure of the results obtained. Initially, the data was not reproducible for consecutive runs. This was partly due to breakage of flocs in handling and partly due to high concentration of solid which led to overlap of particles. These factors were adjusted over a few experiments until an arrangement was found that gave reproducible results in two consecutive runs; the size distributions from two runs are compared in Figure 3.12.

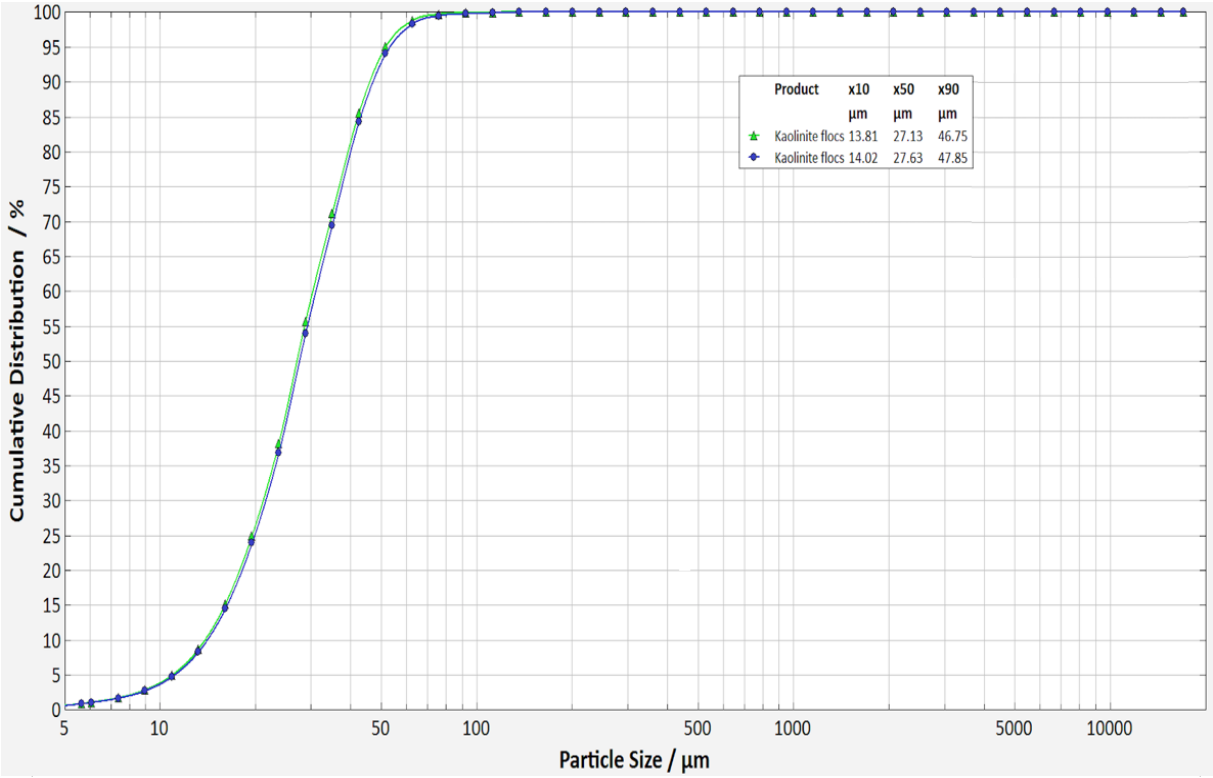

Figure 3.12: Cumulative size distribution comparison for two consecutive runs.

For these runs, same sample, i.e., kaolinite suspension flocculated with high mol. wt. anionic PAM at pH 5.8 was used. The solid content was 0.5% and the particle size reported is the equivalent sphere diameter. Figure 3.12 shows that the consecutive runs give reproducible results. Hence it was established that with extreme care the QICPIC analyzer could be used to get the size distribution of kaolinite flocs. However, extreme care should be taken to avoid floc breakage.

After getting a good signal and satisfactory reproducibility, more tests were conducted by using different solids concentration. The effect of solids concentration on the size distribution was studied using suspensions of three solid contents: 1%, 4%, 8%. A snapshot from an ongoing signal test is shown in Figure 3.13. The particles could be seen moving across the image plane; here we can see how dilute the suspension needs to be in order to get good signal. The size and shape details for the

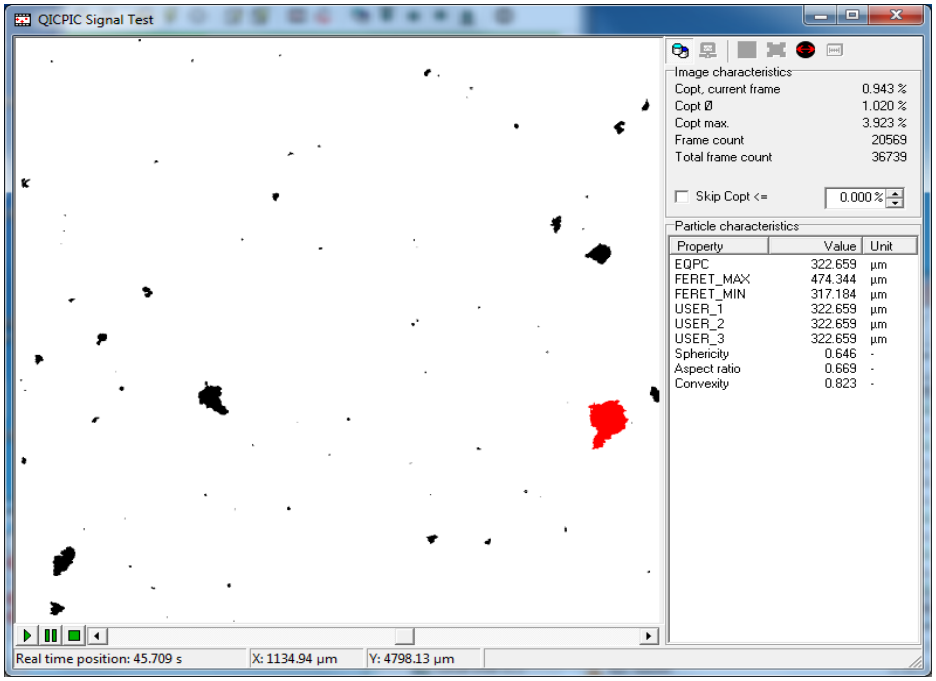

Figure 3.13: Snapshot from QICPIC signal test for 1% solid concentration.

highlighted particles are shown on the left. Using this technique, the size and shape data for each of the flocs can be stored in picture gallery. These data can be retrieved and used for analysis after the run is completed. Over a million flocs were analyzed for each sample. The cumulative size distribution was determined for each solid concentration and the results are compared Figure 3.14. Floc size represented here is the maximum ferret diameter of flocs. The flocs had well-distributed size data as expected. If all the flocs were to have similar size, they would settle at once, giving a clear supernatant and sediment boundary. It was observed that the size of flocs increased with an increase in solid concentration. Similar observations regarding the effect of solid concentration on floc size have been reported in the past (Michaels and

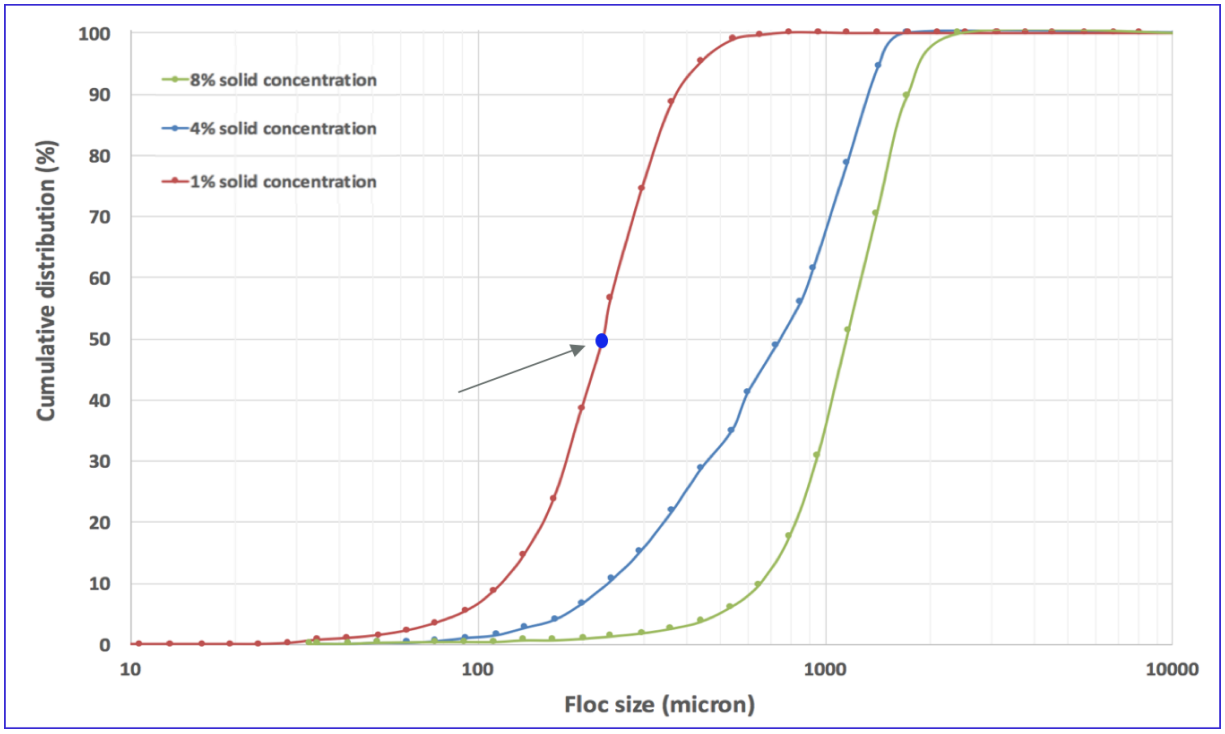

Figure 3.14: Comparison of cumulative size distribution for samples having three different solid content. The samples were prepared by flocculation of 1% solids kaolinite suspension using 200 ppm high mol. wt. anionic PAM at pH 5.8. The floc size reported is ferret maximum diameter.

Bolger, 1962). At higher solid content, the probability of collision of primary particles and clusters increase which has a positive effect on flocculation. It is interesting to note that the increase in floc size decreased with increase in solid concentration. This hints at the existence of a critical solid concentration beyond which the increase in solids concentration would not change the floc size distribution a lot. For QICPIC analysis system, sphericity has been defined as:

$$S = \frac{P_{EQPC}}{P_{real}} \quad \text{...} \quad (3.2)$$

where, P_{EQPC} is the perimeter of equivalent diameter circle, P_{real} is the projected perimeter of the circle. The sphericity of flocs is compared as shown in Figure 3.15. It

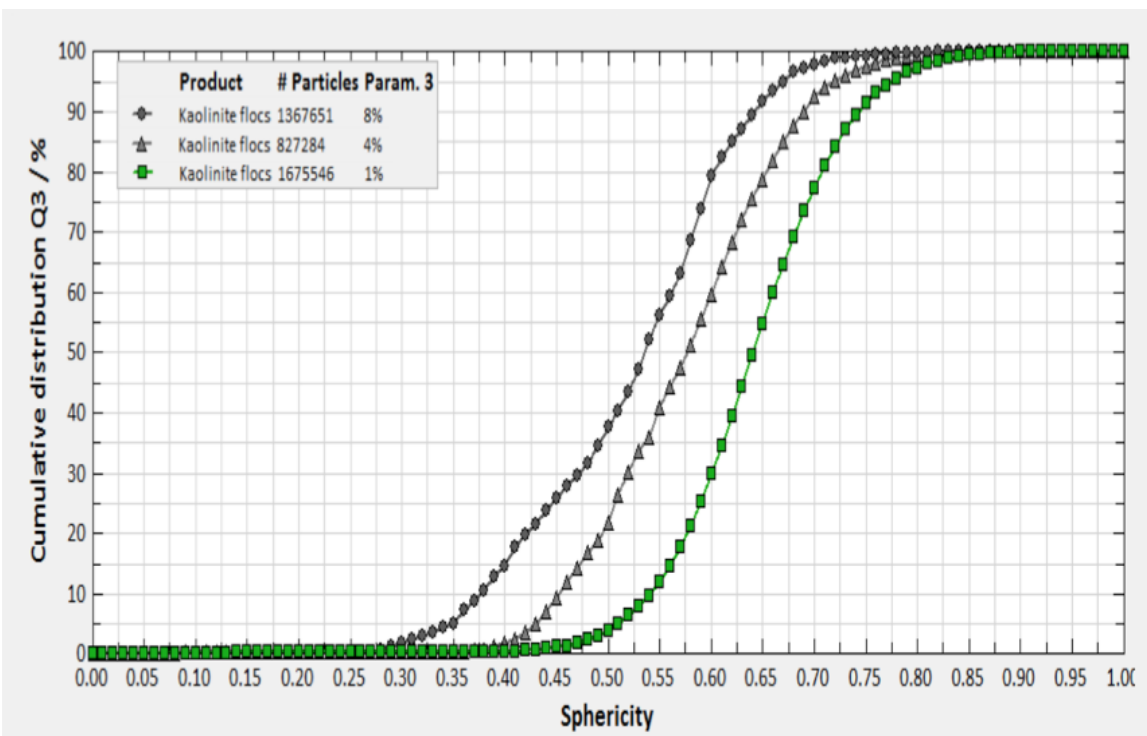

Figure 3.15: Comparison of cumulative distribution of sphericity for samples having three different solid content. The samples were prepared by flocculation of 1% solids kaolinite suspension using high mol. wt. anionic PAM at pH 5.8.

appears that 1% solid concentration flocs, which are smaller in size, are more regular in shape. The sphericity is shown to decrease with increase in solid content. The legend box displays the number of particles analyzed (#Particles) which was the same for both size and sphericity measurement.

3.4.3 Comparison of PVM and DIA Results

PVM is very useful equipment for in-situ image analysis and size characterization. By using PVM the inconsistency of flow conditions for the primary system and measurement cell can be diminished to a large extent. PVM is widely used in industry in conjunction with FBRM for visualization of real-time processes. But the analysis cannot be extended to the entire sample as only a few particles in the field of view are imaged at any given time. The results give a good idea about the general size and shape range for the flocs, but the numbers cannot be reported for the entire sample population. The dynamic image analysis technique can give a lot of information for a larger amount of sample in a short time. About a million particles can be analyzed for size and shape in a few seconds. These two methods complement each other and have their own advantages and disadvantages.

It is interesting to see if the PVM results are in agreement with the DIA results. Since we have represented the floc size by ferret diameter in both cases, comparisons can be drawn. Using PVM, we obtained an average floc size of 223 μ for 1% solids kaolinite suspension. We can estimate the mean floc size given by DIA for a 1% kaolinite suspension by assuming the size data to be normally distributed, as the mean and median are identical for a normal distribution. The median (d_{50}) for the data set is around 230 μm, which is fairly close to the mean floc size given by PVM;

there is a good co-relation between the two methods of size analysis.

The Stokes equation has been described in detail (Stoke, 1851) and is a simple way to determine particle size if terminal velocity and particle density are known. The settling curves (Figure 2.4) were used to get an estimate of terminal velocity of flocs and the floc density was estimated using the water content analysis discussed in Chapter 4. It was assumed that these flocs are rigid and spherical in shape; the solid concentration has no effect on the settling velocity and on the water content of flocs. Laminar flow conditions and no interference between falling floc was assumed. It was also assumed that during sedimentation, these flocs attained terminal velocity in first 120 seconds. The diameter of flocs was found to be 106 micron by this method, it is significantly less than the value obtained by the PVM and DIA analysis. This difference could be attributed to the various assumptions made about the properties of these flocs and their behavior. In the past, attempts have been made to extend Stokes' law to cover nonspherical particles (Andreasen, 1929), to allow for the effect of particle concentration upon settling rate (Hawkesley, 1951; Richardson and Zaki, 1954). Michaels and Bolger (1962) concluded that for a flocculated suspension, the floc rather than the primary particle is the fundamental structural unit in gravity sedimentation. In recent years, some work has been done on characterization of kaolinite floc size (Nasser and James, 2006, 2009) by using the modified Stokes equations developed by Richardson and Zaki, and Michaels and Bolger. However, experimental techniques like the PVM and DIA have been used for size characterization of suspended kaolinite flocs for the first time in this work.

It is not possible to do a quantitative comparison for shape analysis using both

methods because of the different quantities used to represent shape. In the case of PVM, the ratio of projected area and perimeter defines circularity. In the case of DIA, "sphericity" is defined by ratio of perimeter of equivalent circle to the real perimeter. It is an interesting definition of sphericity as generally sphericity implies volume measurement. But the definition used here is based on two-dimensional quantities without any consideration of the third dimension. The PVM involves direct imaging of flocs, whereas in DIA, the amplitude and phase distribution of the diffraction pattern is back-transformed to get a real image. Since the method of detection is different for both the techniques, some difference in values of sphericity/circularity reported by these techniques is expected.

In conclusion, we can say that polymer type and solids concentration have an effect on kaolinite floc size and shape. Anionic high weight polymers give larger and less circular flocs than cationic low weight polymers. The increase in solids content leads to increase in floc size and decrease in floc sphericity. It appears that the flocs grow in such a way that the larger flocs turn out to be more irregular than the smaller flocs, irrespective of the operating variables. This was verified by varying two conditions, the polymer type and the solids content. It would be interesting to investigate which factors dictate floc structure formation during floc growth in a kaolinite suspension.

CHAPTER 4

SIZE AND WATER CONTENT OF SEDIMENTED FLOCS FROM 3D IMAGE ANALYSIS USING HRXMT

4.1 Introduction

The size characterization of kaolinite flocs in the suspended state by using PVM and DIA was reported in Chapter 3. As the flocs settle, they form a sediment bed which contains a network of interconnected flocs and water channels. Size analysis of flocs in a sediment bed is challenging due to the problems in segmentation of the sediment into individual flocs.

The water content of flocs is another important property besides size and shape. The amount of water contained in flocs is directly influenced by the size of the flocs (Winterwerp and Van Kesteren, 2004) and the rate at which flocculation occurs (Mietta, 2010). The water content of the flocs also influences the settling and self-weight consolidation (Hendriks, 2016). Previously, techniques like the NMR have been used to study the water content in different clays (Fan and Somasundaran, 1999). The analysis of water content for individual kaolinite flocs is yet to be reported.

In this part of the thesis research, a novel method was developed for determination of the water content of sedimented flocs using X-ray microtomography and 3D image analysis software. The attenuation coefficients for kaolinite-water mixtures was determined at different water contents and used to prepare a

calibration curve. This curve was then used to find the composition of kaolinite flocs with respect to water content. The size analysis of the flocs was also accomplished and the floc population was divided into four size ranges. The water content variation in each size range was reported.

The use of X-ray microtomography (XMT) in mineral processing applications has increased over the past few years. Its use has been extended to include size, shape, texture, exposure, and liberation of multiphase mineral particle populations (Garcia et al., 2009; Lin and Miller, 2005, 2009). More recently, the High-resolution X-ray microtomography (HRXMT) has been used for 3D particle characterization and multiphase particle segmentation and analysis at the University of Utah (Alvaro and Lin, 2010; Yan and Lin, 2015). The HRXMT along with image processing and visualization tools like imagej, medical image processing, analysis & visualization (MIPAV), and drishti which are powerful tools for particle segmentation and structure analysis.

Although HRXMT has been used for studying multiphase solid particles before, it has never been used for studying water content of aggregates in a sediment bed. In this part of the thesis research, water content and size analysis of kaolinite flocs has been done by using the HRXMT and various image processing techniques. The kaolinite floc sediment bed was treated as a two-phase system containing water and kaolinite and the principles of multiphase particle segmentation were applied to the sediment bed to isolate and identify individual flocs. The polymer flocculant is present at a very small dosage, hence the system can still be considered to be a two-phase system.

4.2 Materials and methods

4.2.1 Materials and Sample Preparation

Fisher 500 kaolinite obtained from Fisher Scientific was used in this study. The polymer flocculant used was high weight anionic polyacrylamide with a charge density of 5%. The polymer was obtained from Hychem. More details about the materials can be found in Chapter 2.

Pure water and kaolinite suspensions at different solid content were prepared and scanned for calibration. About 50 ml kaolinite suspension with 80% solid content was prepared. The suspension was transferred to a 20ml test tube and was allowed to settle for about 6 hours. It was scanned using the HRXMT and the scaled CT number was found. The process was repeated for four different solid concentrations. Using the scaled CT numbers, a calibration curve was plotted for scaled CT number variation with water content.

The sedimented kaolinite floc was prepared from a 5% w/v kaolinite suspension of 80 ml volume. The sample was allowed to stir for 1 hour at 400 rpm and sonicate for 20 minutes. The pH of suspension was noted to be 5.8. High mol. wt. 5% anionic polymer was added to the suspension drop by drop until the polymer concentration was 1000 ppm. The mixing was carried out at 500 rpm for 90 seconds and the sample was carefully transferred to a 13 ml container (inside diameter ~ 3.5 cm). The sample was allowed to settle for 24 hours and then scanned using the HRXMT machine. The sample Figure 4.1 was scanned in the middle portion. This was done to avoid the sheared flocs that might be present in the top and the bottom portion.

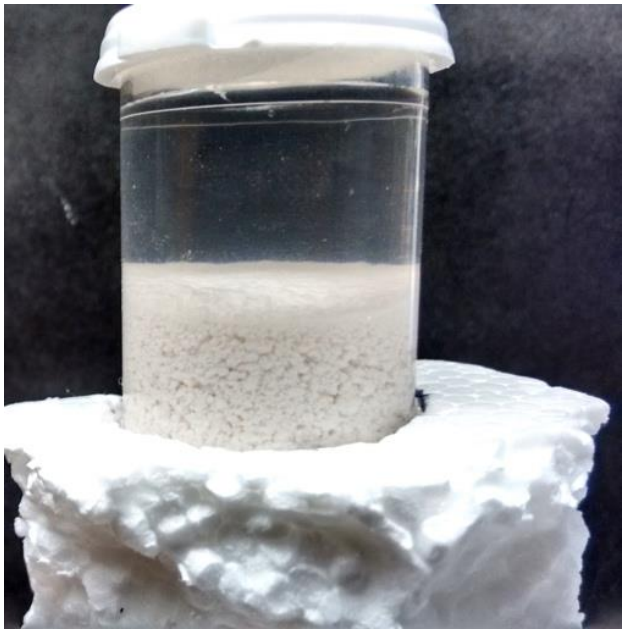

Figure 4.1: Kaolinite floc sediment before HRXMT scan.

During the HRXMT scan, the sample is well-confined and held by frictional forces in a cylindrical container. The sample container as well as the sample inside the container should be completely stable in order to get useful data. Any small movement will cause reconstruction failure and errors. During the initial scans of sedimented kaolinite flocs at low polymer dosage and less mixing, the coalescence between kaolinite flocs was affecting the stability of the sediment. The polymer dosage, mixing time, and settling time were optimized to get a stable sample. After a few attempts, it was possible to get a sample that was stable during the 2 hour scan.

4.2.2 Data Acquisition

4.2.2.1 X-ray Microtomography

The high-resolution XMT (MicroXCT- 400, Xradia) at the University of Utah was used for this study. The basic layout is shown in Figure 4.2. More details about

its principles and operation are available in the literature (Hsieh, 2012). The basic principle of X-ray microtomography is discussed here.

The X-ray beam can be considered as a beam of photons. In vacuum, all X-ray photons leaving the source reach the detector. However, when a medium is present between the source and the detector, some of the photons interact with the medium and not all photons leaving the source reach the detector. As these X-ray photons pass through the medium, they are attenuated, or weakened, following the Lambert-Beer's law. According to this law, when a monochromatic beam with energy, E_o , and incident photon flux density or intensity, I_o , passes through a medium of thickness x, the intensity, I , of the emerging beam is given by equation 4.1.

$$I = I_0 \exp\left[-\mu(\rho, Z, E_0)x\right] \quad \text{.....} \quad (4.1)$$

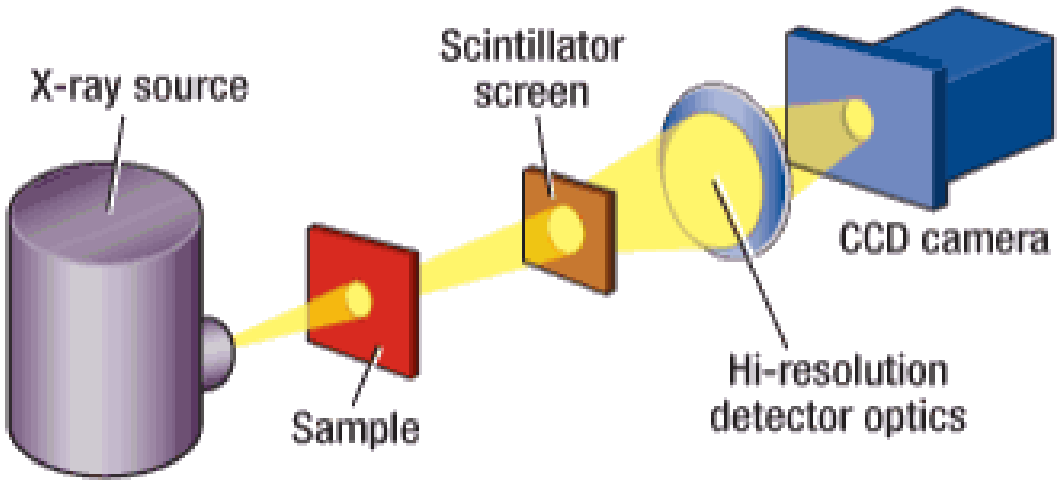

Figure 4.2: Layout of the HRXMT instrument, the Zeiss Micro XCT 400.

where,

μ : Linear attenuation coefficient.

ρ : Density of the absorber.

Z : Atomic Number.

The linear attenuation coefficient, μ , depends on the energy of the photon, and the density and atomic number of the material (medium) placed between the source and the detector. As μ is dependent on material characteristics, it can be used to describe the internal structure of any material kept in between the source and detector.

When the X-ray photons travel across a heterogeneous object, which contains materials of different attenuation coefficients, the linear attenuation coefficient is a space variant function dependent on the distribution of material in the sample being interrogated (Videla, 2006). This difference in attenuation coefficient is exploited for 3D segmentation of multiphase particles. The scaled CT number is a representative of the attenuation coefficient, μ, of material and has been used for this work. Typical CT number used in the medical field is given by equation 4.2.

$$\text{CT number} = \frac{\mu\,(material) - \mu\,(water)}{\mu\,(water)} \times 1000 \qquad \ldots\ldots\ldots\ldots\ldots\ldots\ldots\ldots \qquad (4.2)$$

CT number for air and water is -1000 and 0, respectively. The detection of the photon beam is by a 2D detector that acquires a projection, formed by a set of line-integrals of the attenuation coefficients of the material. The sample is rotated to get the projection at various angles. The output from HRXMT is the back-projected image of

the sample which is a 3D spatial reconstruction of the attenuation coefficients based on integral linear projections and Fourier transform filtering.

The volume elements of this image are the voxels which represent cubes of the material in the field of view. The size of these voxels depend on the magnification used. The value of the attenuation coefficient assigned to each voxel is a material property and represents the average value of the material occupying the cubic space. A set of transform functions and algorithms are applied to reconstruct the three-dimensional images of the sample from the projection data, which have been described in the literature (Lin and Miller, 2002; Videla, 2006). Figure 4.3 represents a schematic of data acquisition and reconstruction process using the HRXMT.

4.2.2.2 Experimental Considerations

Experimental considerations are very important to achieve the desired results. In this work, the same experimental conditions were used for all the samples scanned. It is very crucial to scan the kaolinite floc sediment at the same conditions as the samples used for calibration. Change in conditions would make the whole analysis pointless as the relationship established between scaled CT number and water content during calibration would no longer be valid.

The difference in attenuation coefficients between various phases of sample determines the image quality of the HRXMT scan. The scan conditions for HRXMT analysis are determined by the difference in attenuation coefficient of the phases we are trying to scan. After the scan, reconstruction of data is also a very important step in HRXMT analysis. A detailed discussion on HRXMT scan conditions and reconstruction considerations is available elsewhere (Hsieh, 2012). Here, a brief

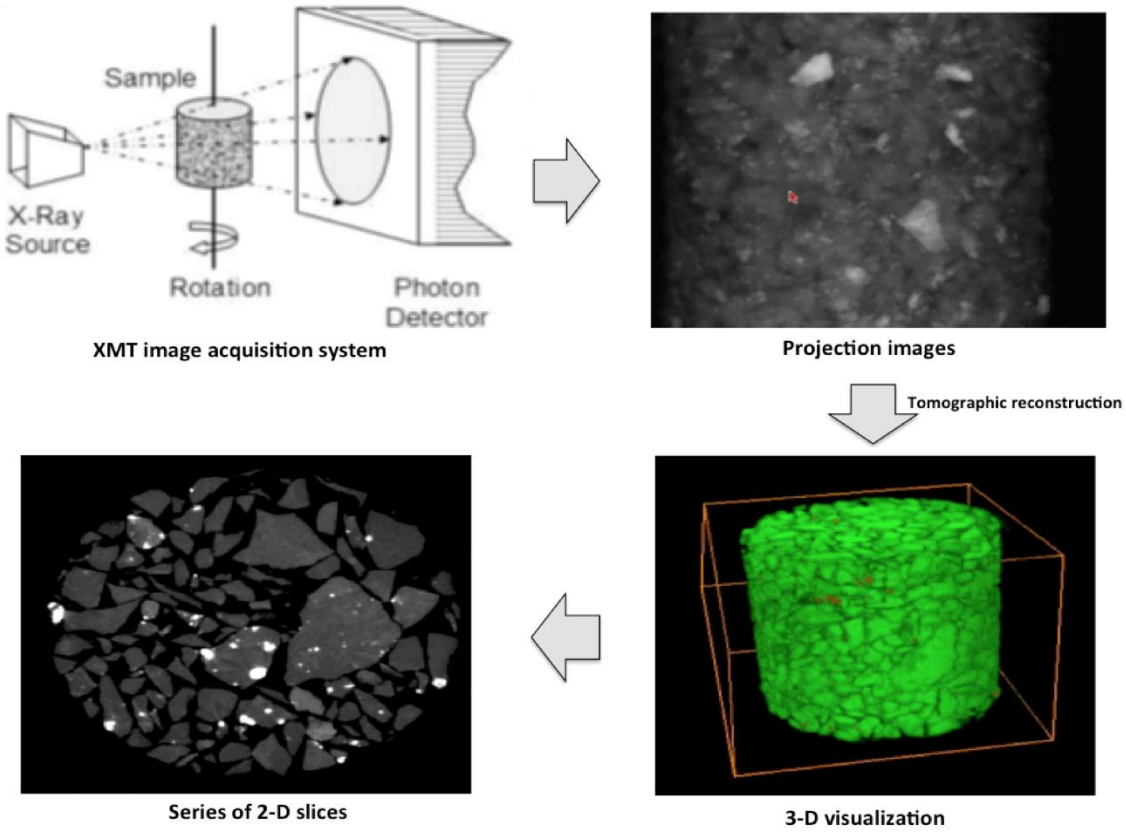

Figure 4.3: Schematic illustration of HRXMT data acquisition and reconstruction processes. The data are constructed in 3D as is typically presented as a series of 2D slice which is used for further processing.

discussion on the experimental conditions used for the analysis of sedimented kaolinite flocs will be done.

According to Beer's law (discussed in previous section), the linear attenuation coefficient is mainly determined by beam energy, density, and atomic number of material. Hence, the X-ray source voltage plays a key role in determination of the attenuation coefficient. The Micro XCT 400 system has a polychromatic source, having an energy level from 40KV to 150KV. Silica and low-density materials can be

scanned at 40KV, while copper minerals and molybdenite require a higher energy level around 80KV (Hsieh, 2012). For extremely high-density samples, 150 kV is used along with long exposure time and a suitable filter, although care is taken to avoid overexposure. For our analysis, 60 kV X-ray voltage was used.

Exposure time is another decisive factor for the CT scan. Material density and elemental composition decides the energy level (voltage), but exposure time determines the attenuation coefficient reading for the sample. Exposure time should be such that there is enough transmission of the X-ray photons to achieve more than 3000 counts on the detector, but care should be taken to avoid over-exposure. For these experiments, exposure time of 1.5 seconds was used.

The five X-ray lenses on the turret are 0.5X, 4X, 10X, 20X, and 40X. Each lens has its own magnification scale and resolution. For our analysis, the 0.5X lens was used. The reconstructed resolution was about 18.5 μm. Magnification is decided by a consideration of mostly resolution, field of view, sample composition, and exposure time. The lower magnification means more X-ray photons will be measured on the detector, with lower resolution and larger field of view. Higher magnification means fewer X-ray photons captured by detector, higher resolution, and a smaller field of view.

Since the X-ray source generates a polychromatic beam, a filter should be used to remove the low and high energy X-rays. Use of a filter decreases the contrast of different minerals, but ensures no overexposure error. The cut-off energy is the linear attenuation coefficient of the filter material. X-ray photons below the energy level will be absorbed, in other words, “filtered” by the material. Here we have used 150 μm

glass filter.

Image resolution is also an important issue of the HRXMT scan. The maximum image resolution does not only rely on the magnification, but also depends on the quality and the setting of the detector. The maximum image size that the detectors can acquire is 2048x2048 pixels according to the XRadia MicroXCT 400 manual specification. For our analysis, we used an image resolution of 1024x1024.

Mass attenuation coefficient increases with an increase in X-ray photon travel distance. A larger ratio of source-sample distance to sample-detector distance gives better image contrast at a high energy level and long exposure times. However, the X-ray intensity counts are also reduced in this regard. To obtain an image with good quality contrast and enough counts of X-ray intensity, a combination of distances and exposure time is necessary. For our analysis, source-sample distance and source detector distances of 60 mm and 120 mm were used. The Field Of View (FOV) is determined by designed magnification and distance for source and detector. The FOV should be chosen such that, the whole sample area is covered in the scan. For our analysis, FOV of 19 mm was used.

Moving the source and detector forward or backward in a certain range can control resolution and field of view. The voxel resolution is a function of the X-ray source size, the distance between source and sample, and the detector resolution. In our case, the reconstructed voxel resolution was 18.52 μm.

The projection counts greatly affect the quality of the reconstructed image. In general, the radiograph set (projection) is collected and transformed using the Fourier Slice Theorem. By using the back projection method, the reconstructed image

can be visualized as a 3D view with linear attenuation coefficients attached as CT numbers. The image is displayed by phase contrast based on the grey scale established for different materials. For our analysis, a projection count of 1000 was used.

Using these scan conditions, data were collected in unsigned short (u16) form. It basically means that the 16-bit detector was used. The 16-bit detector can identify the color depth levels from 0 to 65535 in an unsigned short format. Thus, the maximum reading of X-ray intensity can never be over 65535. A CT number can be assigned in this range according to the light intensity measured by the detector.

After the projections have been acquired from every angle, an application called "XMReconstructor" was used for reconstruction purposes. It helps users evaluate and determine which variables to vary in order to obtain the best image quality, and reduce the artifacts. Center shift and beam hardening are the prime concerns during reconstruction. Center shift happens when the field of view is not centered on the object and deviates from the center line. To correct this artifact, we can adjust the offset distance and acquire a higher quality image. Although filters can remove low energy X-ray beams, the dispersed energy levels of X-ray beams cause various attenuation coefficients of one specific mineral phase due to the distance through which the photon passes. The measured linear attenuation coefficient is lower in the center, where the X-ray passing distance is longer, and higher at the edge, where the X-ray passing distance is shorter. In other words, the X-ray beam looks "Hardened" at a higher energy level in the boundary area. Calibrating the CT number profile, or using a software algorithm to remove the artifact, can correct the beam-

hardening condition.

The tomography file is based on voxel geometry and is saved in XRM format. The XRM file contains information of coordinates, angles, exposure time, source voltages, distances, etc. A collection of XRM files is processed with the help of tools like XMReconstructor, XMController, and XM3DViewer. Finally, a raw format file containing a 3D dataset is obtained which is then used with various image processing software for data analysis. Typical scan and reconstruction time for each sample at the specified conditions is 2 hours.

4.2.3 Image Processing Tools

4.2.3.1 Feature-based Classification

Segmentation is known as the process of separation of an image into objects of interest and noninterest. The segmentation process involves two major steps: first, the separation of the image in the foreground and background such as thresholding; and second, the separation of the foreground as individual particles. In a segmented 3D image, the elementary elements are no longer voxels but connected sets of voxels or regions, which allow analysis of individual particles.

Due to the complexity of the floc structure, thresholding is not sufficient to obtain the desired result. In this case, feature-based classification was selected for separation of background and foreground. Feature-based classification is a machine learning method to extract useful features for a specific image processing procedure. Feature-based classification is used for selection of important features and image segmentation. Trainable weka segmentation (TWS), an ImageJ/Fiji plugin, was used as the feature-based classification method for this study. TWS is a versatile tool for

image segmentation based on voxel classification. The software has a library of methods and a user friendly interface. It combines the image processing toolkit Fiji with state-of-the-art machine learning algorithms provided in the latest version of data mining and machine learning toolkit Waikato Environment for Knowledge Analysis (WEKA). The graphical user interface enables the user to load an image or stacks of images and perform automatic segmentation by interactive learning.

Trainable weka segmentation considers not only the voxel intensities but also a wide range of image features to determine particle boundaries. There are 20 features used in TWS. A list of features for the "Trainable weka segmentation" (Fiji, 2015) is shown in Table 4.1.

The user selects image features and adds them to different classes. The TWS then trains the whole image according to the selection initially provided. Based on the segmentation results, more annotation can be added for misrepresented regions and retraining of the classifier can be done until satisfactory segmentation results are obtained. While training, the algorithm basically extracts image features from different aspects of image content, such as voxel statistics, filtering, texture etc. for each voxel is calculated. The calculation time for each feature might vary; for example, utilization of anisotropic diffusion is time consuming. Also some features are not efficient for accurate analysis.

Based on the image segmentation quality and computation time, Gaussian blur, Sobel filter, Hessian, Membrane projections, and Difference of Gaussians were selected for training to improve segmentation of the floc particles form the background.

Table 4.1 List of features of “Trainable weka segmentation” (Fiji 2015)

Gaussian blur	Hessian	Membrane projections	Anisotropic diffusion	Mean
Maximum	Lipschitz	Gabor	Laplacian	Entropy
Sobel filter	Difference of Gaussians	Variance	Minimum	Median
Bilateral	Neighbors	Structure	Kuwahara	Derivatives

An example of use of TWS for feature-based segmentation is shown in Figure 4.4.

A stack of 370 images from the middle portion of the scan was used for analysis. The output image after TWS was used as a model to train the stack of the remaining 369 images used for analysis.

4.2.3.2 Watershed Segmentation Process for 3D Images

In addition to the segmentation of solid phase from background, different particles in the solid phase need to be separated from one another. 3D watershed segmentation has been developed at the University of Utah for segmentation of packed particle beds. The sedimented kaolinite flocs can be treated as a particle bed with two different phases. The 3D watershed segmentation method was used with binary images for separation of touching flocs. The process involves marker-controlled watershed segmentation and has been described in detail elsewhere (Videla, 2007; Wang, 2016). A simple algorithm of the process developed by these researchers is shown in Figure 4.5.

The key concept behind watershed segmentation is the interpretation of an image as a topographic surface with mountains and valleys. If a drop of water falls on

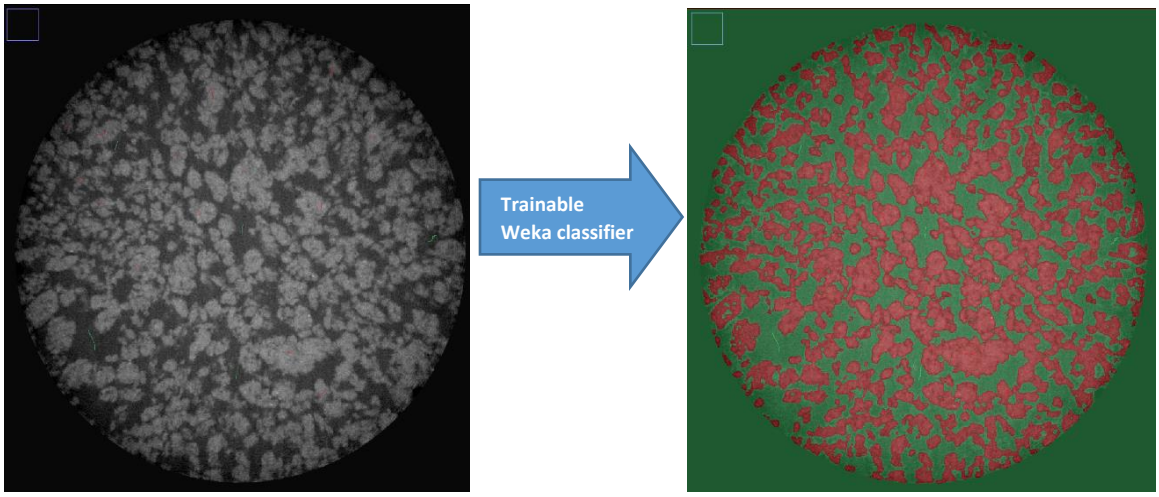

Figure 4.4: Illustration of use of trainable weka segmentation on a 2D slice of sedimented kaolinite flocs (image on left). As evident from the images, the separation of foreground from background was done (image on right).

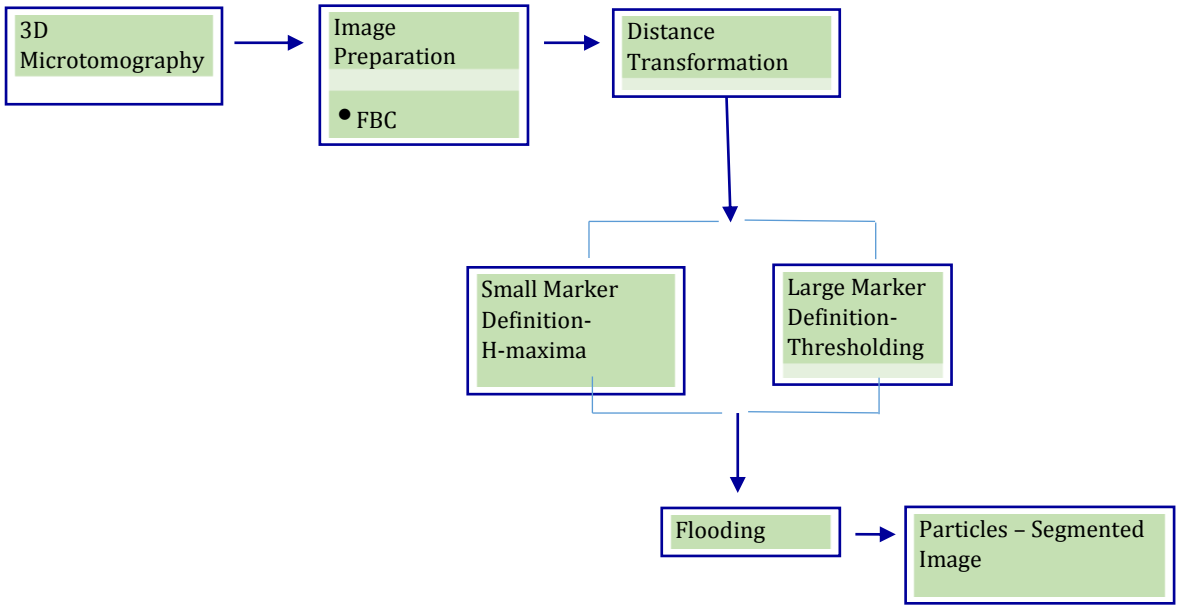

Figure 4.5: Algorithm for marker-controlled watershed segmentation

such a topographic surface, it follows the steepest path until it reaches a minimum point. All sets of points on the surface whose steepest path belongs to the same minimum constitutes the catchment basin associated with this minimum. The watersheds are known as the zones dividing adjacent catchments basins. This is the underlying concept of watershed segmentation. Various processes are done on the raw image in order to get a good segmentation. The feature-based classification method was used for image preparation. The trainable weka segmentation plugin available with Fiji was used for separation of background and foreground. The distance transform is an image operation process that converts a binary image with feature (white) and no feature (black) elements to a picture where each voxel has an intensity value that approximates the Euclidean distance of the voxel itself to the nearest nonfeature element. In other words, in a binary image, the distance transform operation calculates the distance from each white voxel to the nearest black voxel. Figure 4.6 illustrates the use of this function on original image. The most important step in complex segmentation applications is marker extraction. Markers represent unique regions of space, which distinguish unique particles. This is very important to avoid over segmentation. Image distance transform presents the local maxima values somewhere inside the boundaries of the particles. These maxima values can then be used as a marker for the position of a particle in the image. Larger markers are directly obtained by thresholding the distance-transformed image. For smaller markers, H-maxima is defined. Before proceeding with the flooding process, it is necessary to label each marker (regional maxima) with a unique number using connect component labelling.

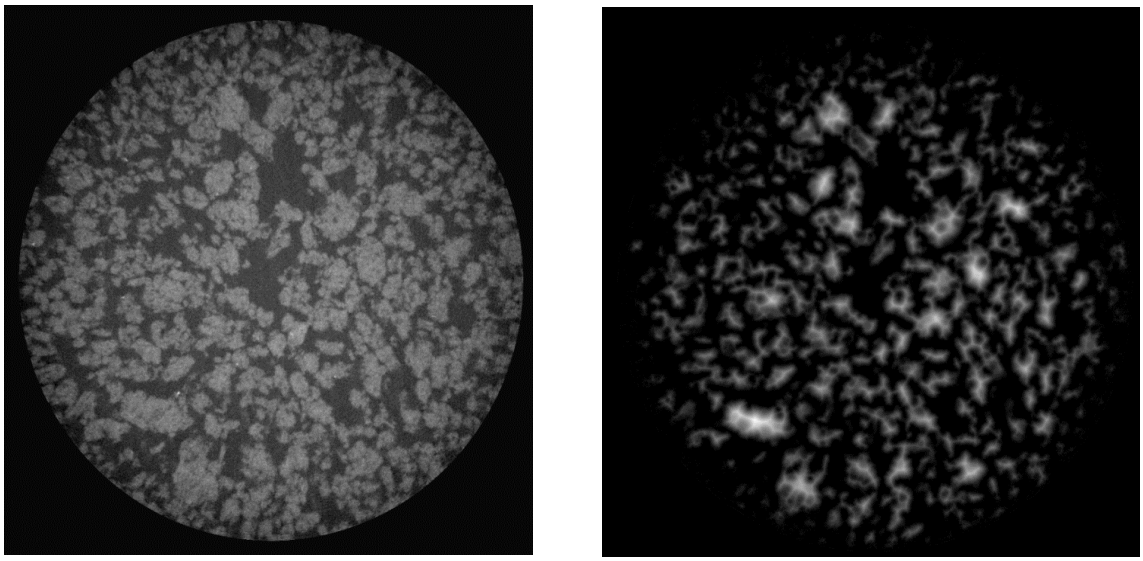

Figure 4.6: Illustration of distance transform function. Original image (left); image after distance tranform (right)

In this way, its identification number will differentiate each particle that will emerge from those markers from the rest of the particles.

Next, the process to segment the particle image is carried out using the watershed transform or flooding process. In the topographic interpretation stated earlier, the complement of the distance transform image is analogous to the elevations in topography of a surface with valleys and peaks where the maxima distance is the bottom point of the valley. In this growing method, the valleys are flooded with water at a constant rate and during the process, dams are erected when two different valleys merge together. The line formed between these two minimum or valleys will be the boundary between the two different particles. Figure 4.7 compares the original image with the segmented image after these steps have been followed. Flocs are labelled by using different colors for better visualization. The label on each marker was used to separate individual flocs.

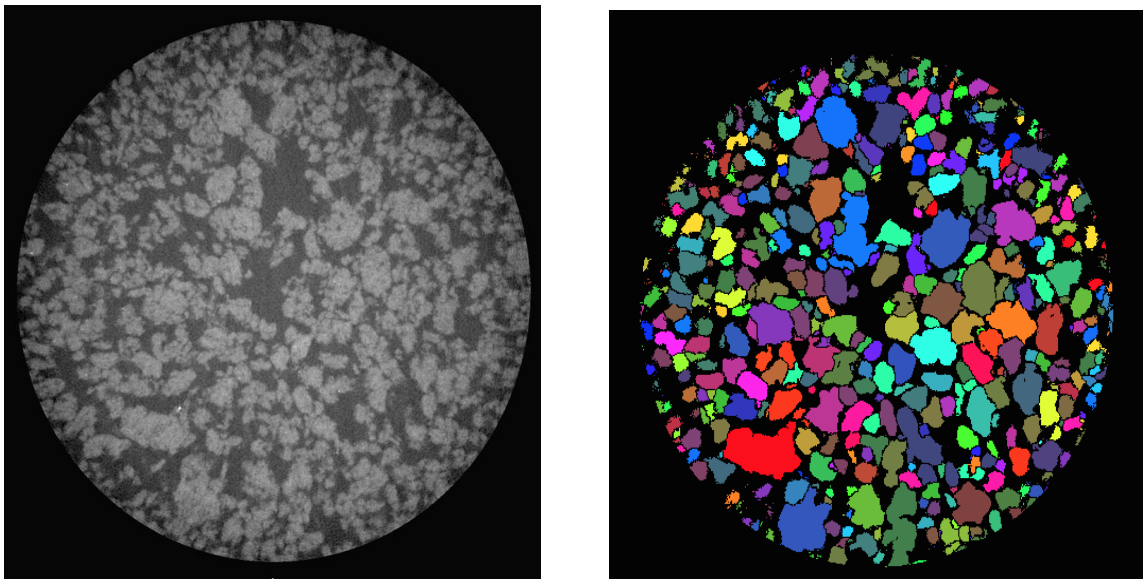

Figure 4.7: Original image (left); segmented image (right). Segmented flocs are represented by different colors.

4.2.4 Floc Size and Water Content Analysis

The kaolinite floc sediment was isolated into individual flocs. Before the flooding process, each marker (regional maxima) in the segmented image is labelled with a unique number. This serves as an identification number to differentiate each floc from rest of the flocs.

Using the MIPAV software, thresholding can be done to include only a single floc in the image. Each floc can be visualized by doing AND operation on original image and the isolated floc from watershed segmented image. In the results section, images of a few isolated flocs are presented.

For size and water content analysis, all individual flocs with total volume greater than 11 voxels were considered. The equivalent sphere diameter for each floc was calculated using the total voxel volume as shown below:

Total voxel in a floc * Volume of single voxel = Volume of a floc

Volume of a floc = $\frac{\pi d^3}{6}$ …… (4.3)

where, *d* is the equivalent spherical diameter of the floc.

The calibration curve for water-kaolinite system was plotted using scaled CT numbers for kaolinite suspensions with different water content. The calibration curve is shown in Figure 4.8. Using the fitted function, water content of unknown samples can be found if we know the scaled CT number for them.

The calibration curve establishes a relationship between the rescaled CT number and the water content. This equation can be used to find the water content of individual flocs by using the average CT number for each floc.

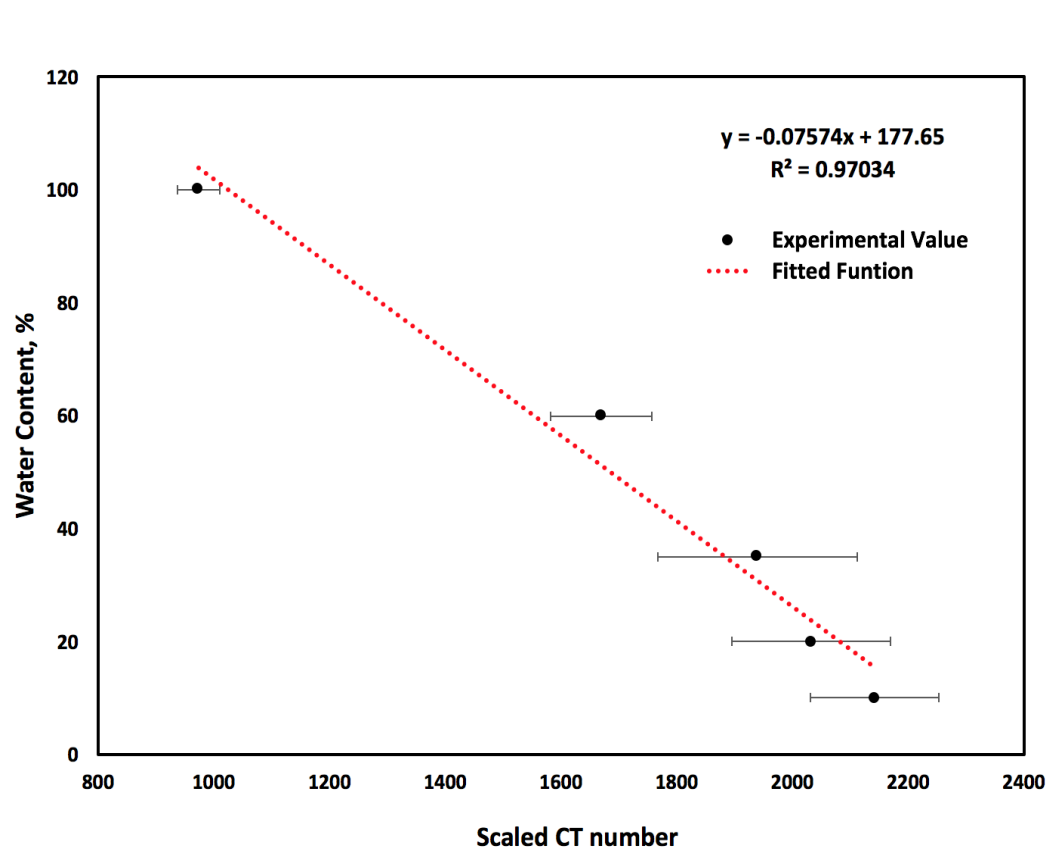

Figure 4.8: Calibration curve used for water content analysis of flocs. The standard deviation for each data point and the line of best fit are displayed.

Water content % (Y) = Intercept + Slope * (scaled CT number, X)

$$Y = 177.65 - 0.07574 * X \quad \text{..... (4.4)}$$

Using this relation, the intensity value (scaled CT number) was converted to water content for each voxel. Such a conversion makes the direct visualization of water content distribution possible. A 2D slice from the water content raw file is shown in Figure 4.9. The intensity value at each voxel in this image gives the water content at that voxel. A stack of such images was used to get the water content for each voxel. Once the flocs have been isolated, surface area, volume, aspect ratio, and sphericity can be calculated for individual flocs by using methods of shape analysis

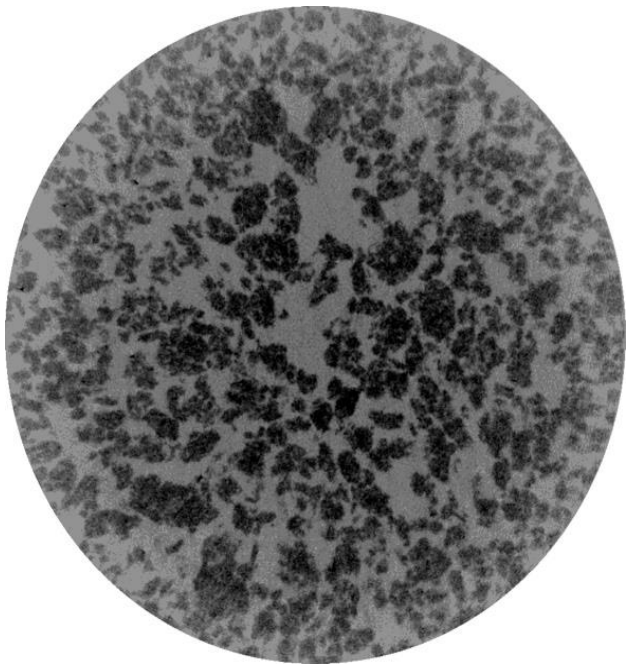

Figure 4.9: Image representing water content value at each voxel. Dark grey represents lower water content than light grey.

for 3D particles. The shape analysis including these features has been done for 10 flocs. The details about shape analysis for 3D particles by using XMT can be found in literature (Lin and Miller, 2005).

4.3 Results and Discussion

4.3.1 Water Content and Size Distribution of Flocs

The kaolinite floc sediment was scanned using the same conditions as were used for calibration. The floc network was carefully segmented by using the method for segmentation of multiphase particles developed previously at the University of Utah. A 3-dimensional view of the sediment with isolated flocs before and after segmentation is shown in Figure 4.10. By comparison of floc voxel volume with total voxel volume, the composition of sediment bed with respect to water was calculated. The sediment bed was found to contain 63% inter-aggregate water by volume. For this calculation, it was assumed that water channels contain 100% water with no solid particles. The total water content was found to be around 80% by volume (including both inter-aggregate and intra-aggregate water).

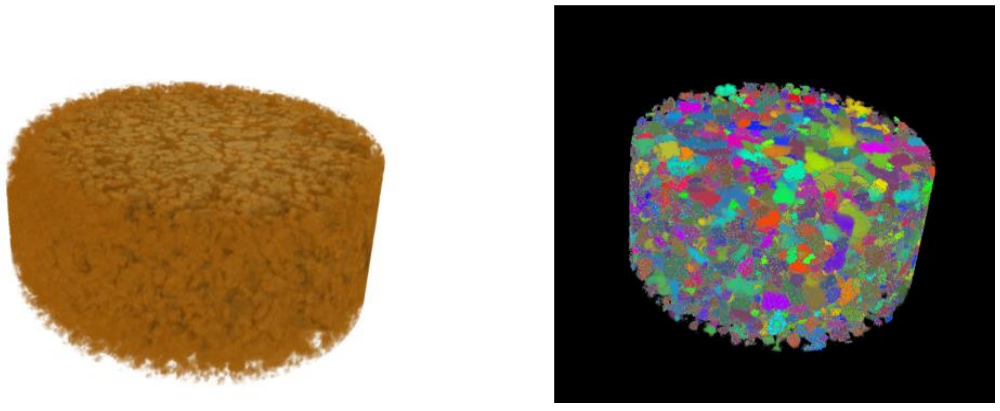

Figure 4.10: Unsegmented sediment bed (left); Sediment bed after segmentation (right). Different color represents different flocs in the segmented image.

For further analysis, individual flocs were isolated and analyzed for size and water content. Figure 4.11 summarizes the steps followed. Figure 4.12 shows few isolated flocs along with their size and water content. The method for calculating the size distribution and water content distribution of flocs has been described in previous section.

The segmented bed contains about 13 thousand flocs. Some of the very fine flocs were not considered for analysis. A threshold of 11 voxels was applied and flocs with volume more than 11 voxels were considered for further analysis.

Each of the flocs were analyzed for water content using a script based on equation 4.4. The results suggest a normal distribution of water content for these flocs, with mean water content of 53.9% and standard deviation of 11.8%. The water content distribution of flocs is shown in Figure 4.13.

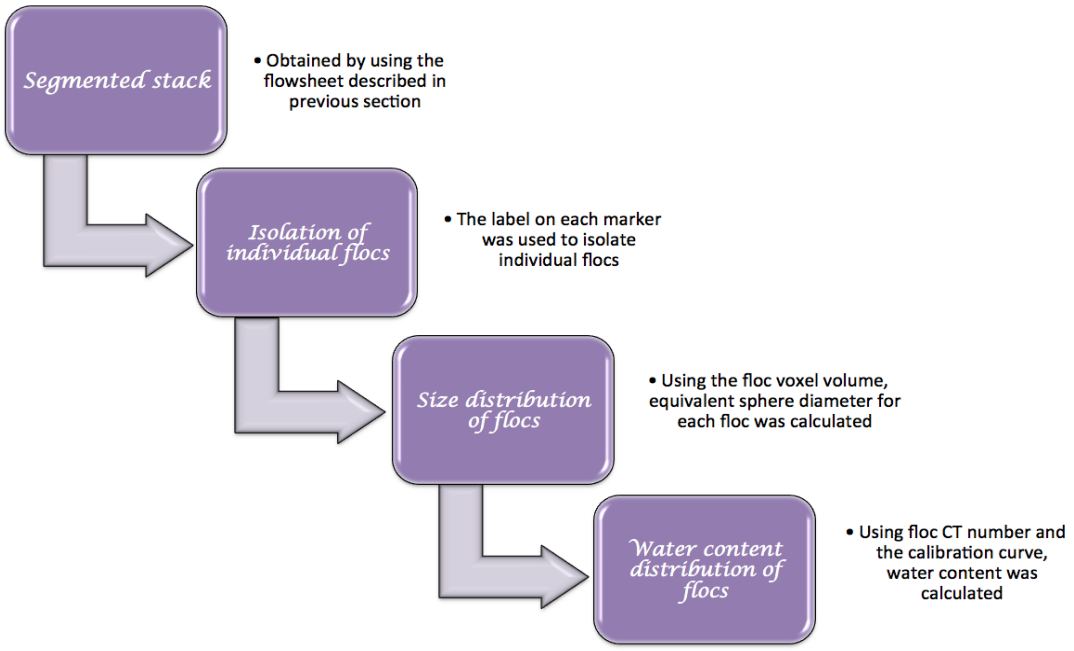

Figure 4.11: Flowchart of steps followed in the analysis.

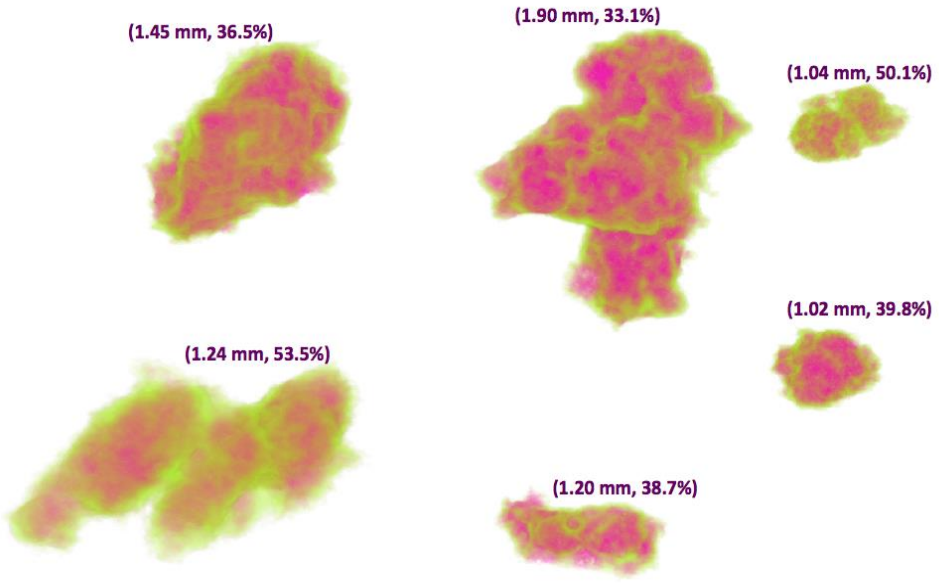

Fig 4.12: Selected individual flocs with floc size and water content respectively in parentheses. The water content increases from pink to green.

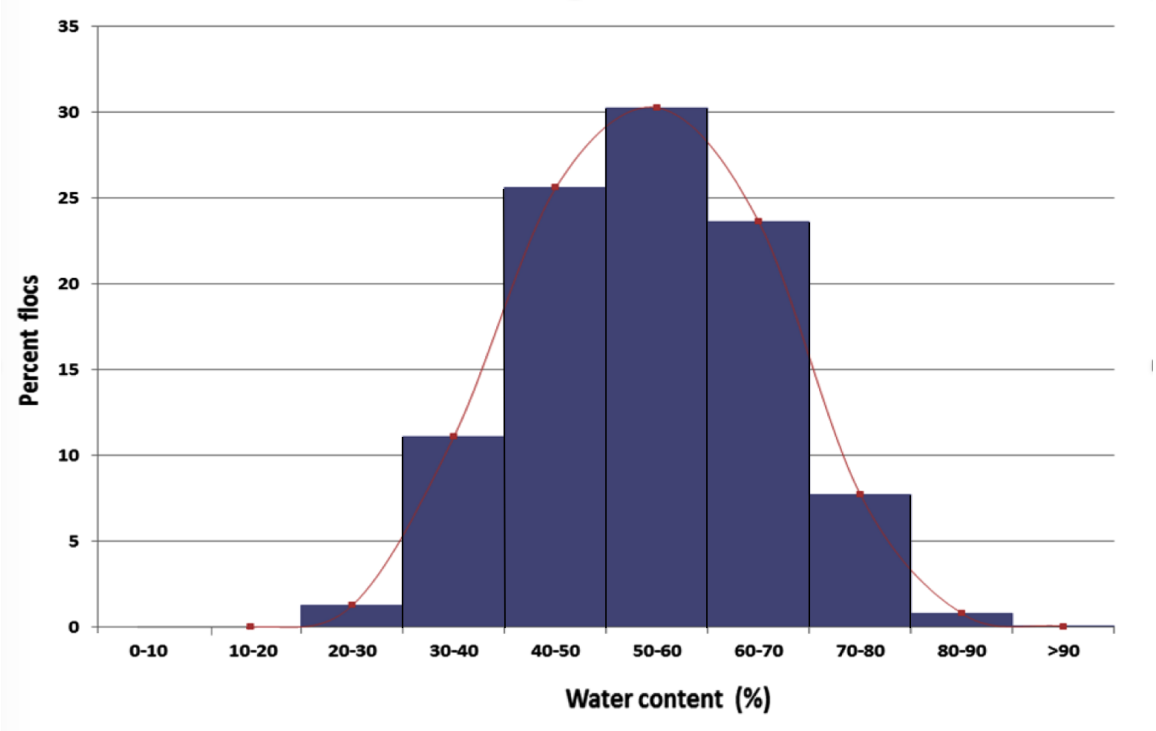

Figure 4.13: Water content distribution for kaolinite flocs. The sample was prepared at pH 5.8, 5% solids, 1000 ppm of high mol. wt. 5% anionic polymer and allowed to settle for 24 hours.

Water content class of 50-59% has the maximum number of flocs, 30.3%, and about 98% of the flocs have water content in the range 30-80%.

Size analysis of flocs was done using a script based on equation 4.3. The equivalent sphere diameter was calculated and reported as the floc size. It should be noted that this distribution is based on voxel volume and not voxel number. The cumulative floc size distribution is shown in Figure 4.14. About 90% of the flocs were found to be less than 1.5 mm in size. Around 40% of the flocs had a size range of 0.5-0.85 mm. The flocs were divided into four size ranges and water content analysis for each size range was done. It was observed that the average water content of flocs increases with a decrease in floc size. Smaller flocs have more entrapped water than the larger flocs. Also, most of the flocs were found to be in the size ranges 0.12-0.85

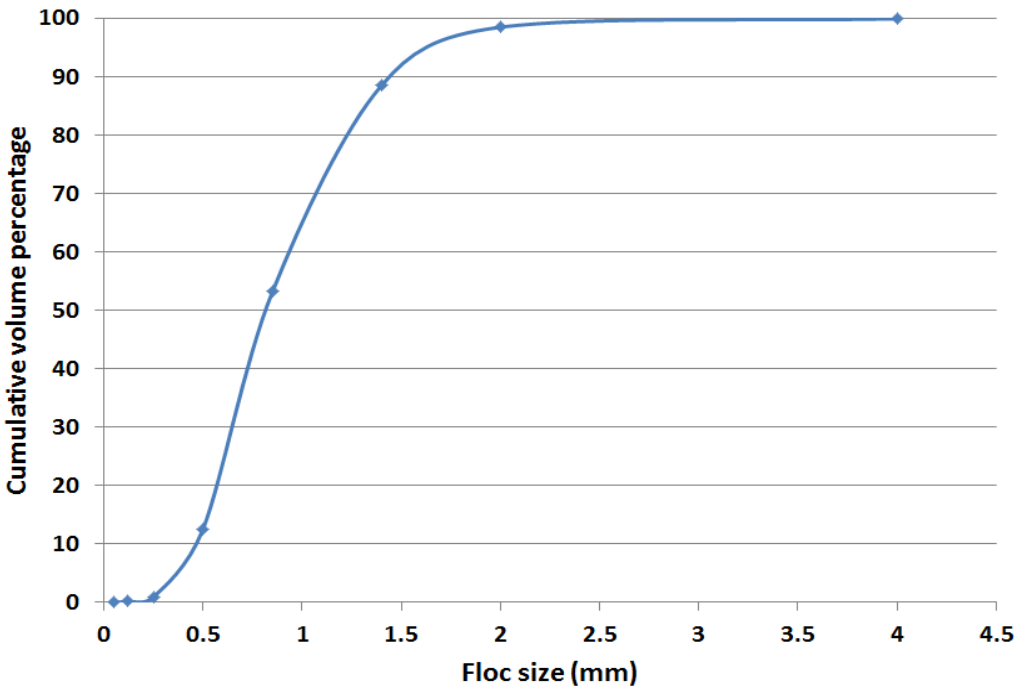

Figure 4.14: Floc size distribution of kaolinite flocs. Equivalent sphere diameter is reported as floc size. The sample was prepared at pH 5.8, 5% solids, 1000 ppm of high mol. wt. 5% anionic polymer and allowed to settle for 24 hours.

mm and 0.85-2 mm. The results are provided as continuous scatter plots in Figure 4.15.

In conclusion, the water content distribution and size analysis was done successfully for these flocs. For further investigation of floc structure, the shape analysis was done for select flocs.

4.3.2 Shape Analysis of Selected Flocs

The isolation of individual flocs makes it possible to analyze various features of these flocs. The floc shape can be characterized by calculating the floc surface area, volume, aspect ratio, and sphericity. These features of 3D particles can be calculated

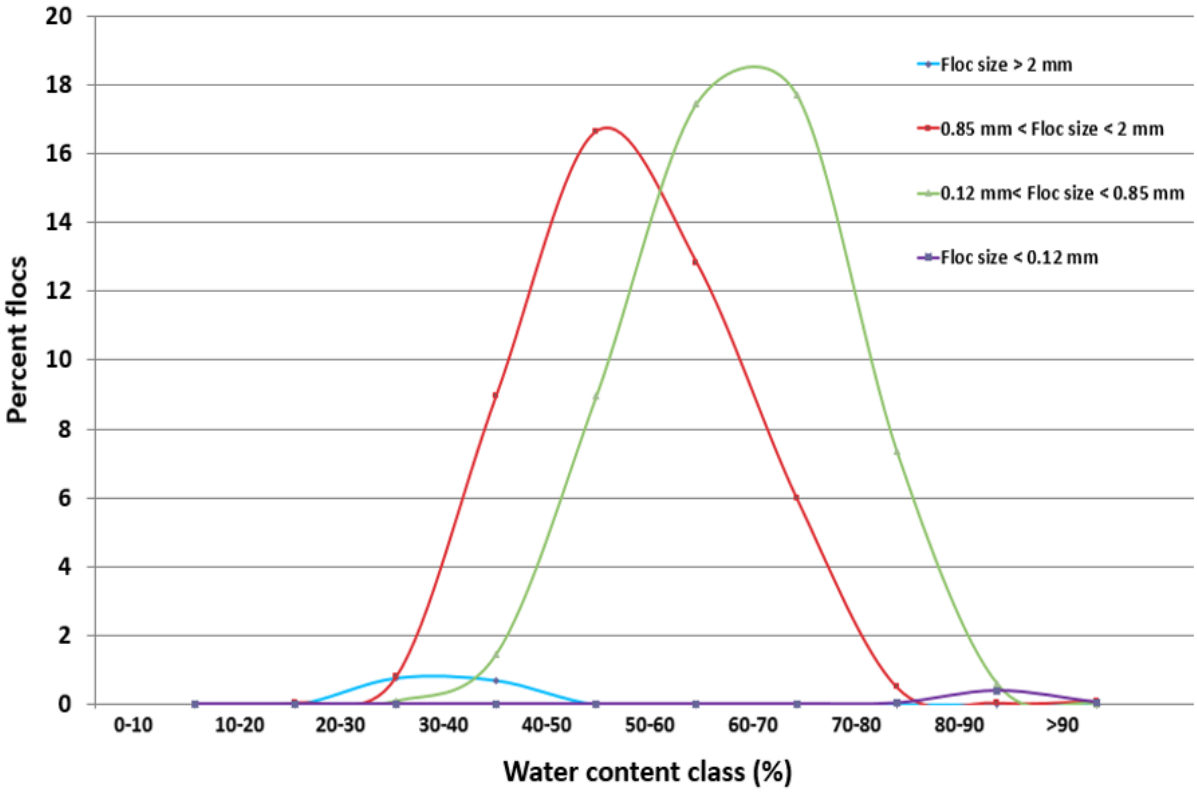

Figure 4.15: Water content distribution of flocs in various floc size ranges. The sample was prepared at pH 5.8, 5% solids, 1000 ppm of high mol. wt. 5% anionic polymer and allowed to settle for 24 hours.

by using the method of shape analysis for 3D particles developed by Lin and Miller (2005). Shape analysis was done for 10 flocs and is reported along with water content and size in Table 4.2. The floc number given in table is based on the labelling done during sediment segmentation and serves as an identifier for individual flocs.

The shape analysis was not done for the entire population of 13 thousand flocs and the results for 10 individual flocs cannot be extrapolated to include the entire floc population. Due to highly irregular shape of these flocs, there were complications in finding the surface area of some flocs, especially for the ones with high water content. A single floc was sometimes identified as a combination of flocs by the program. Manual analysis of each individual floc should be done in case of such irregular and porous particles to avoid errors.

Table 4.2: Shape analysis of selected flocs in the sediment bed

Floc no.	Size (mm)	Water Content (%)	Volume $(mm)^3$	Surface Area $(mm)^2$	Aspect Ratio			Sphericity
					Length	Width	Height	
1	1.5	62.4	4.13	25.57	1.38	1.21	1	0.061
2	1.9	33	3.39	24.07	1.79	1.19	1	0.101
3	2.3	28.2	2.41	31.90	1.64	1.1	1	0.108
4	0.54	60	1.67	13.71	3.18	2.08	1	0.109
5	1.43	43	1.17	10.08	2.13	1.95	1	0.11
6	1	54.7	0.85	7.46	2.29	1.67	1	0.113
7	0.81	56	0.25	3.79	1.95	1.65	1	0.113
8	1.26	31	0.09	1.97	1.95	1.55	1	0.118
9	1.2	38.7	0.31	3.89	1.53	1.1	1	0.128
10	0.79	43.4	0.01	0.08	1.73	1.37	1	0.139

4.4 Summary

Kaolinite-water mixtures at different water content were scanned using HRXMT to establish the scaled CT number for each sample. The scaled CT number and water content for each sample was plotted to obtain a calibration curve. The scaled CT number for a sample of unknown water content can be used to get the water content for that sample by using this calibration curve.

The kaolinite floc sediment bed was scanned using HRXMT and the rescaled CT number for each voxel was obtained. The floc network was carefully segmented by using the method for segmentation of multiphase particles. Individual kaolinite flocs were isolated within the sediment bed. About 13 thousand flocs were identified by using this method. Size and water content analysis for each floc was done. The results suggest a normal distribution of water content for these flocs, with mean water content of 53.9% and standard deviation of 11.8%. Water content class of 50-59% has the maximum number of flocs, 30.3%, and about 98% of the flocs have water content in the range 30-80%.

About 90% of the flocs were found to be less than 1.5 mm in size. Around 40% of the flocs had a size range of 0.5-0.85 mm. The flocs were further divided into four size ranges and water content analysis for each size range was done. The results are provided as continuous scatter plots in Figure 4.15. It was observed that the average water content of flocs increases with a decrease in floc size. Smaller flocs have more entrapped water than the larger flocs. The size range of sedimented and suspended flocs were found to be comparable, but due to difference in sample preparation conditions, exact comparisons could not be made. DIA analysis of suspended flocs

indicated a mean ferret maximum diameter of 0.74 mm at 4% solids and 1.02 mm at 8% solids; polymer dosage was 200 ppm. The analysis of sedimented flocs using HRXMT indicated a mean equivalent sphere diameter of about 1 mm at 5% solids and 1000 ppm polymer dosage. Although the flocs have similar size ranges in suspended and sedimented state, it is difficult to compare the sizes due to difference in sample preparation conditions.

Since flocs have been successfully isolated from the sediment bed, it is possible to analyze various features of the floc shape including but not limited to surface area, volume, aspect ratio, and sphericity. This has been demonstrated by analyzing these features for 10 flocs. It should be noted that shape characterization for the entire floc population has not been reported and results for 10 flocs should not be generalized to represent the entire floc population.

The HRXMT procedure developed in this work has allowed not only the determination of floc structure but also the water content of individual flocs. The procedure developed can be extended for water content and size distribution analysis of flocs formed from industrial tailings at different conditions. This would enable us to study the effect of different parameters on the water entrapped in individual flocs as well as on the size distribution of the floc population. Both size and water content of flocs are crucial in determining the settling and self-weight consolidation of flocs.

CHAPTER 5

SCANNING ELECTRON MICROSCOPY ANALYSIS OF FLOC MICROSTRUCTURE

5.1 Introduction

Various aspects of kaolinite floc structure and rheological properties have been studied in detail. Many researchers have tried to verify their results by scanning electron microscopy characterization (Kim and Palamino, 2009; Mpofu et al., 2003; Zbik et al., 2008). The results from all these studies are interesting and give information about floc structure during different stages of sedimentation (Zbik et al., 2008), the effect of polymer concentration (Kim and Palamino, 2009), and the effect of polymer type (Kim and Palamino, 2009; Mpofu et al., 2003). Most of these studies focus on the type of primary particle interaction, i.e., edge-edge, egde-face, face-face at different conditions. Kim et al. concluded that with an increase in polymer concentration, face-face interaction increases giving rise to higher density of flocs. They also investigated the effect of polymer type and concluded that cationic polymers give more porous flocs than the anionic polymer induced flocs. Mpofu's research suggests that free settling flocs show predominant E-E interaction whereas settled flocs show more F-F interaction. Although we have some idea about the structure of kaolinite aggregates, we have limited information on the structure of polymer chains and how these chains bridge the smaller aggregates and create flocs of millimeter size. In this thesis research, an attempt has been made using cryogenic SEM to visualize the kaolinite floc microstructure as well as polymer bridges

connecting these microstructures. Such visualization will enhance our understanding of kaolinite floc formation in presence of polyacrylamide flocculant. This information can in turn help in selection of appropriate polymers and operating conditions for flocculation.

The flocs were visualized in hydrated state by using wet SEM capsules. A wetsem capsule (QX-102, QuantomiX Ltd., Israel) allows the SEM imaging of fully hydrated kaolinite suspension at high vacuum (Barshack, 2004). Liu et al. (2015) have reported the structure of kaolinite clusters in absence of polymer at different pH conditions using wet SEM capsules. In this thesis research, polymer-induced kaolinite floc structures were visualized in the hydrated state using the wet SEM capsules.

5.2 Materials and Methods

5.2.1 Equipment Principles

The scanning electron microscopy (SEM) has been widely used for studying microstructure of kaolinite aggregates as mentioned in introduction. The SEM has a large magnification range, allowing examination of samples at magnifications well over 100,000 times. Besides magnification capabilities, SEM is capable of giving large depth of field for images, which provides a three-dimensional perspective. Thus, an SEM image provides much more information about a specimen's topography and surface structures than light microscopy at the same magnification. The first prototype SEM was constructed by Knoll and von Ardenne in Germany, after a series of refinements the first commercial SEM became available in 1963. The SEM can be subdivided into a number of components such as the electron optical system, specimen stage, electron detector, and vacuum system. An electron optical system is

involved in the focusing and control of the electron beam. A specimen stage is needed so that the specimen may be inserted and situated relative to the beam. When the beam of electron interacts with the sample, more than one type of electrons are emitted. The main types are secondary electrons and backscattered electrons. The capabilities of the electron detector can vary depending on which emitted beam we are interested in detecting. The emitted beam is collected using a suitable detector and processed to generate a signal that is amplified and ultimately displayed on viewing and recording monitors. A vacuum system is necessary to remove air molecules that might impede the passage of the high energy electrons down the column as well as to permit the low energy secondary electrons to travel to the detector. Greater details about SEM principles and operation are available in the literature (Goldstein and others, 1990).

For this work, we have used Sigma 500 FESEM from Ziess and Novanao SEM from FEI. The Sigma 500 SEM has a powerful lens system and more efficient detectors and vacuum system. More details about both these equipment is available on the respective websites of Zeiss and FEI (links provided in reference section).

5.2.2 Materials and Sample Preparation

The kaolinite used in this study is acid washed K2 500, obtained from Fisher scientific. The polymer used is high molecular wt., 5% anionic PAM, obtained from Hychem. More details about the materials used are given in section 2.3, Chapter 2. A kaolinite suspension (1% w/v) was prepared using DI water. The suspension was allowed to stir for 1 hour followed by 20 minutes sonication. The solution pH was 5.7. High mol. wt. anionic polymer was added to the suspension at a dosage of 400 ppm

and stirring was continued for 60 seconds at 400 rpm. The flocculated suspension was then allowed to settle for 1 hour and the top layer of the sediment bed was carefully transferred to another container.

For wet SEM analysis, about 15 µl of the floc volume was injected into a well-sealed WETSEM capsule. The sample was separated from the interior of the electron microscope by a thin, electron-transparent partition membrane. This membrane is strong enough to sustain a 1 atm pressure difference and, in this way, the sample inside the capsule can be maintained at atmospheric pressure while the SEM chamber reached high vacuum. The electrons coming from the electron gun penetrate a few micron into the wet cluster and an SEM image of the cluster structure is obtained. Figure 5.1 shows schematic working of the wet SEM capsule. The wet SEM analysis was done using the Sigma 500 FESEM: Figure 5.2 shows a snapshot of the wet SEM capsule in the specimen chamber of the Sigma 500.

Wet SEM analysis of kaolinite clusters formed without addition of polymers has been reported previously by Liu et al. (2015). At pH 4.3, the cluster size varied from1.5 µ to 0 µ whereas at pH 8, the kaolinite was found to be in a dispersed state. The wet SEM analysis of kaolinite flocs formed after addition of polymer has not been reported in literature.

For cryogenic sample preparation, a few flocs (about 2-3) were carefully placed on the conductive carbon tape glued to the metal stub used for SEM imaging. The stub was immersed horizontally in a container full of liquid nitrogen with help of tweezers. The stub was taken out immediately and imaged at once before the devitrification could take place. By using this method, the microfloc structure could

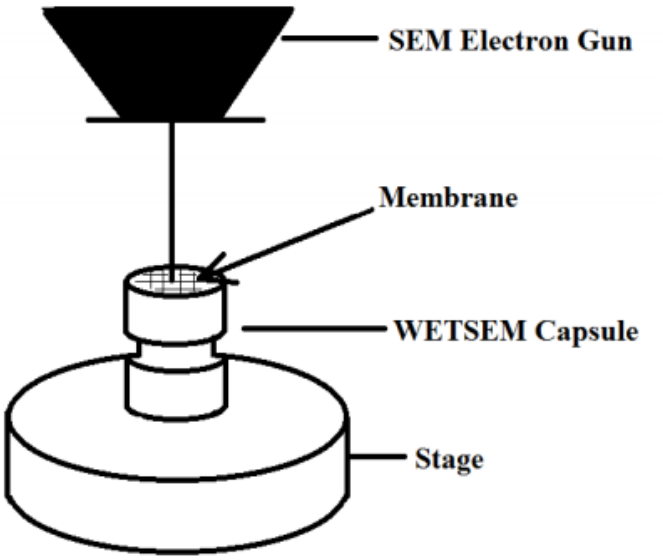

Figure 5.1: Schematic drawing of wet SEM capsule on the stage.

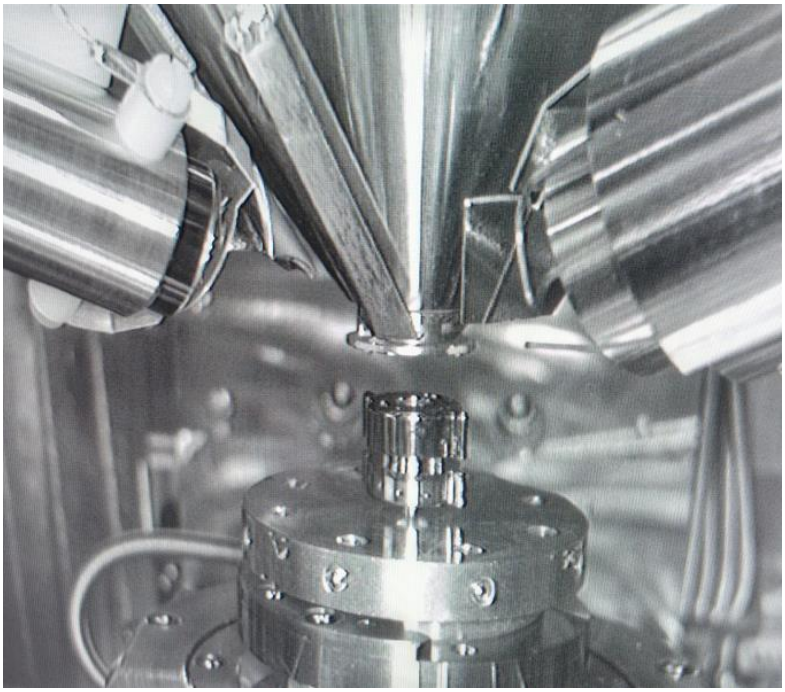

Figure 5.2: Wet SEM capsule in the specimen chamber of Sigma 500 FESEM.

be visualized; however, visualization of the polymer chain needed optimization with respect to a few conditions. After various attempts, it was found that adjustment of the sample quantity on the stub, time for which the sample is dipped in liquid nitrogen and imaging time were very crucial and determine the image quality for visualization of the polymer chain.

For visualization of the polymer chain, the sample should be dipped in sample for long enough to immobilize the water molecules but not so long that the whole sample is frozen and a thick frost layer is formed. Since a cold stage was not used for imaging, the frosted sample started melting after a few seconds inside the sample chamber. This is not desired as the melted water led to movement within the sample and sample features were not clear. However, if the sample is super cooled to immobilize the water and polymer chains, the polymer chains could be seen. It is doubtful, even with use of a cold stage, that visualization of polymer chains at such low polymer dosage would be possible as frosting could break the delicate polymer chains present in the sample. However, visualization of polyacrylamide chain in DI water at higher polymer concentration by using the cryogenic method has been reported before (Sui et al., 2015).

The sample was dipped in liquid nitrogen for about 5-10 seconds and imaged immediately. If imaging is delayed by more than 2-3 minutes, the water molecules are mobilized again and the sample is similar to a wet sample. For visualization of polyacrylamide polymer chain in water, a thin sample layer is recommended (Sui et al., 2015). Since the amount of polymer in our sample was less and concentration of kaolinite was much higher, we could not see the polymer chains by using a very small

amount of sample. Larger amounts of sample lead to contamination of the lens. A balance is needed to get the desired results. For all cryogenic samples, a very low voltage was used (less than 2kV); higher voltage led to charging of the sample.

5.3 Results and Discussion

5.3.1 Floc Structures in Hydrated State Using Wet-SEM capsules

The wet SEM analysis reveals the presence of aggregates of varying size; these aggregates range in size from few µm to about 50 µm. Some of these aggregates are interconnected to form larger aggregates. Figure 5.3 shows one larger aggregate of about 77 µm in size made up of smaller aggregates. The aggregate could be considered

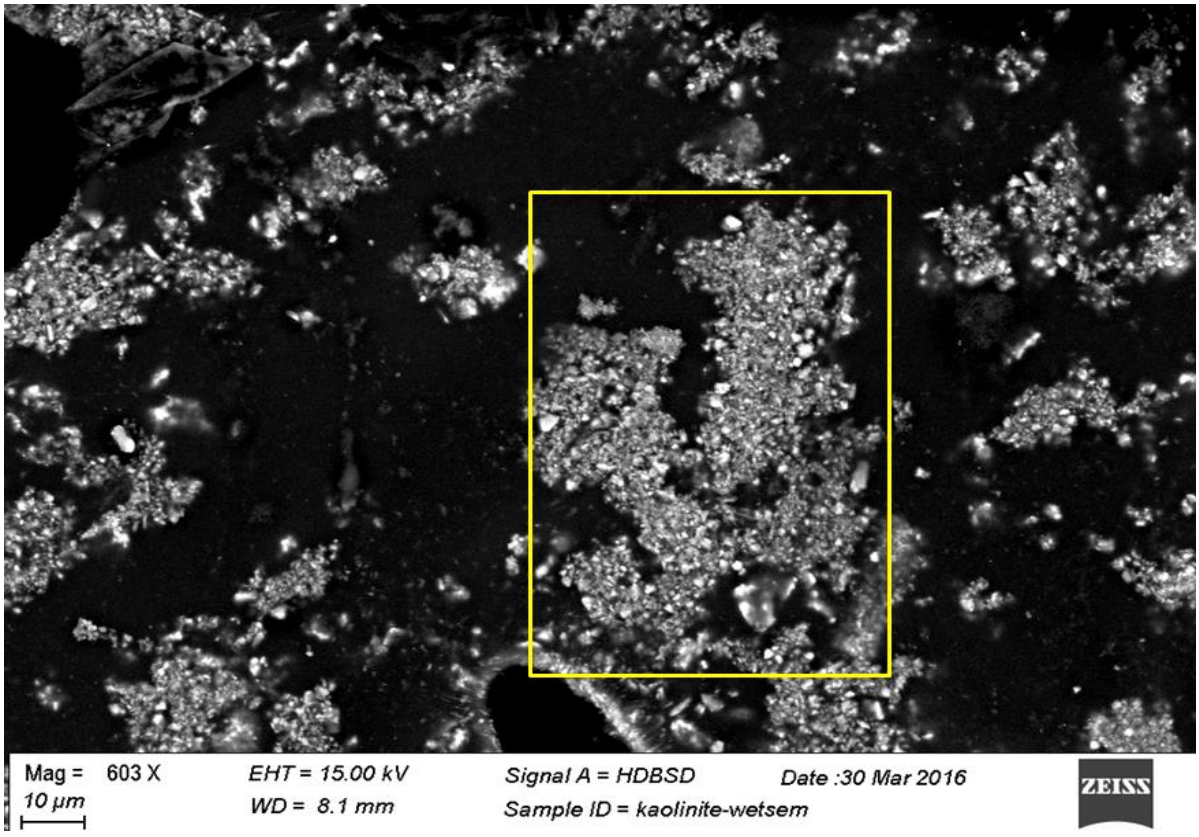

Figure 5.3: Wet SEM analysis of kaolinite floc at pH 5.7. The highlighted microfloc is about 77 µm in size.

to be an individual floc (microfloc) within a larger floc (millifloc).

In Figure 5.4, a few primary kaolinite particles can be seen in different orintations. Due to the low resolution of the image, not much information about the orientation of primary particles could be obtained. For further investigation of the microstructure, the cryogenic method was used.

5.3.2 Cryogenic Visualization of Microflocs Including Images of the Polymer Chain

By use of cryogenic method, better resolution was obtained and the orientation of primaty particles could be seen (Figures 5.5 and 5.6).

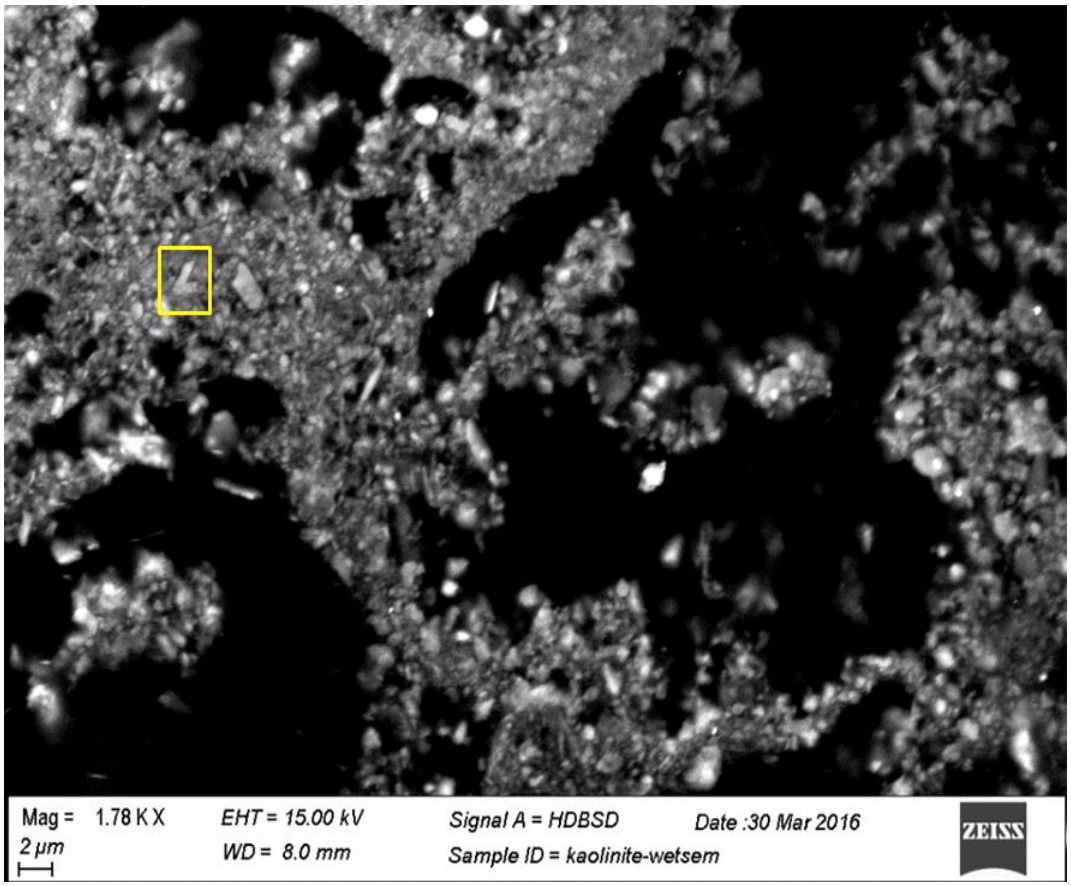

Figure 5.4: Wet SEM analysis of kaolinite floc at pH 5.7. The primary particle interactions (as shown in highlighted box) are not clear due to low resolution.

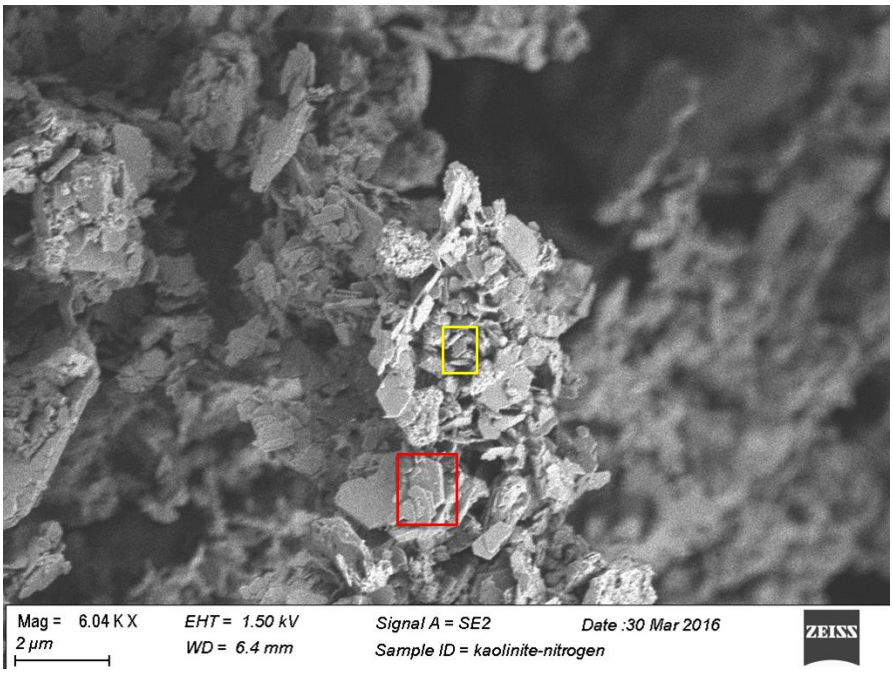

Figure 5.5: SEM image of kaolinite microfloc at pH 5.7. The primary particles show edge-face interaction (highlighted in yellow) and face-face interaction (highlighted in red).

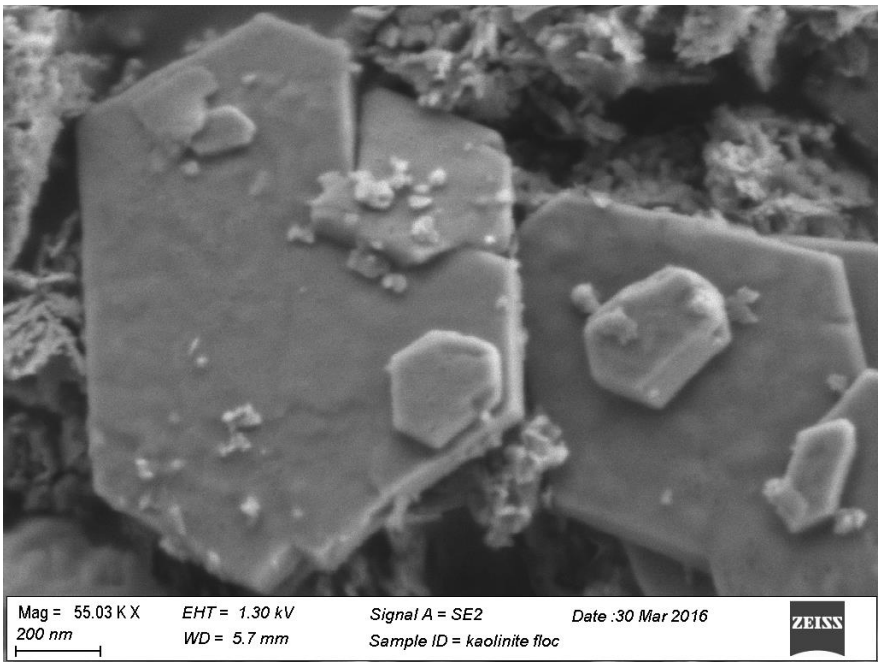

Figure 5.6: High magnification SEM image of kaolinite primary particles within the microfloc. Face-face interaction between primary particles is revealed.

The microscale investigation of floc by using the cryogenic method reveals that microflocs from 0.5 μm to about 10 μm in size are interconnected by polymer chains (Figure 5.7). These polymer chains can vary in dimensions as can been seen in these images; the thicknees could vary from a few nm to about 80 nm. These polymer chains seem to be elastic in nature, capable of changing dimensions based on the force exterted from different ends. The smaller microflocs could be attached to the ends of a single polymer chain but the larger microflocs were found to be intertwined between many chains. It appears that more than one attachment point between the larger flocs and the polymer chain is necessary for structural stability. It was also noticed that the chain length between two consecutive microflocs varies a lot, from almost continuous microflocs to about 5 μm polymer chain in between flocs. It appears that breakage of these delicate chain structures occurs under shear and hence the well known sensitivity of floc stability to turbulence level. For different polymers, there would be a critical chain length beyond which breakage occurs thus restricting the size to which floc grows.

Here, it should be noted that the varation in polymer chain dimension could be due to stacking of fine polymer chains giving rise to thicker chains or due to the presence of undissolved polymer chains. The polyacrylamide chain contains both positive and negative sites in hydrated state. Depending on the relative orientaion of these groups in the polymer chain, there is a chance of aggregation due to electrostatic forces. It is also possible that the loss in water due to cryo freezing and sublimation leads to collapse of fine poymer network giving rise to thicker polymer chains. The polymer chains form close ended web like stuctures, bridging various

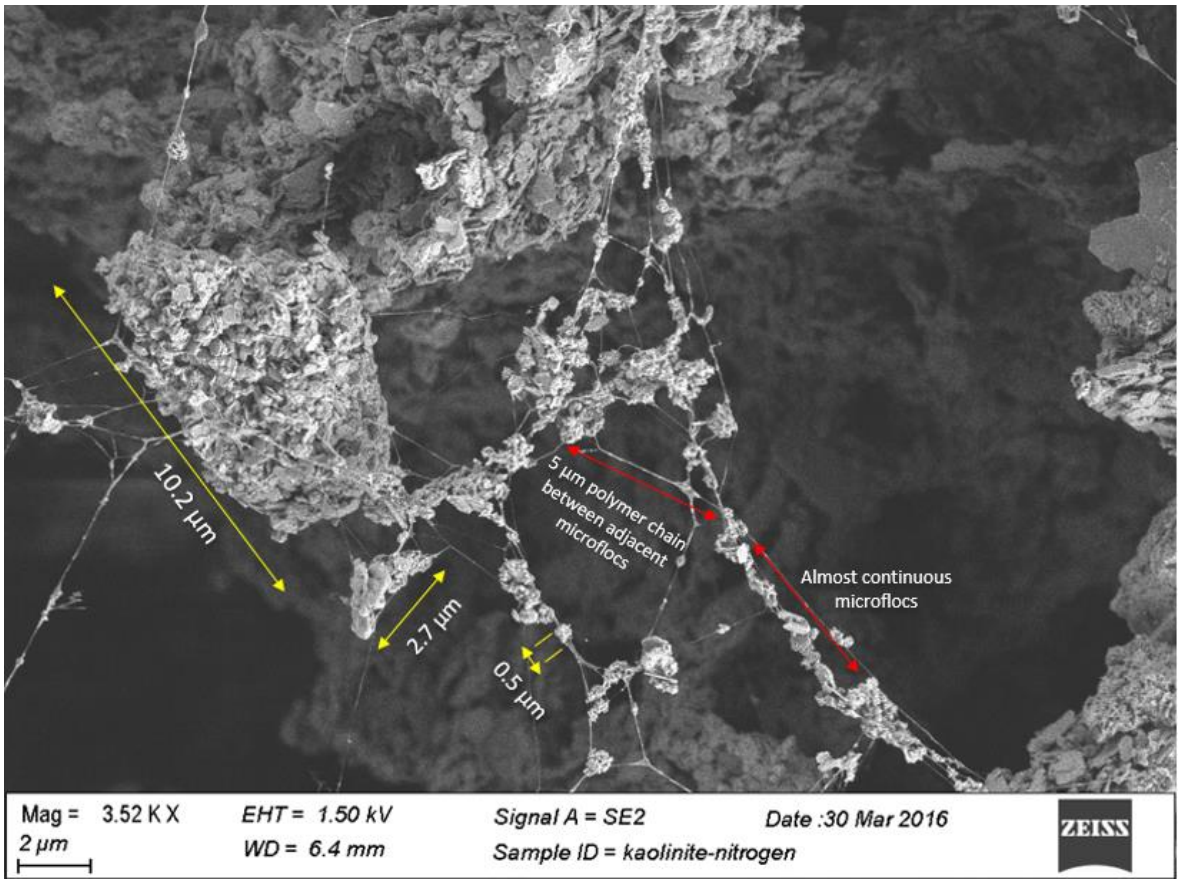

Figure 5.7: Microstructure of kaolinite floc as revealed by FESEM. The microflocs vary in size from 0.5 µm to 10 µm (highlighted in yellow). The microflocs could be almost continuous or have a significant length of polymer chain in between adjacent microflocs (highlighted in red).

microflocs to one another (see Figure 5.8). Due to the limitations of 2-dimensional visualization, it is difficult to say to which surface of the kaolinite particle these polymer chains attach. It appears that the polymer bridges are formed by attachment to both surfaces: the base surface and the edge surface. It is possible that the anionic polymer chain attaches to the alumina face which is positively charged at pH 5.8 while the interaction of edge surface with the anionic polymer chain is via hydrogen bonding. High magnification reveals polymer chain-edge surface attachements with some clarity (Figure 5.9).

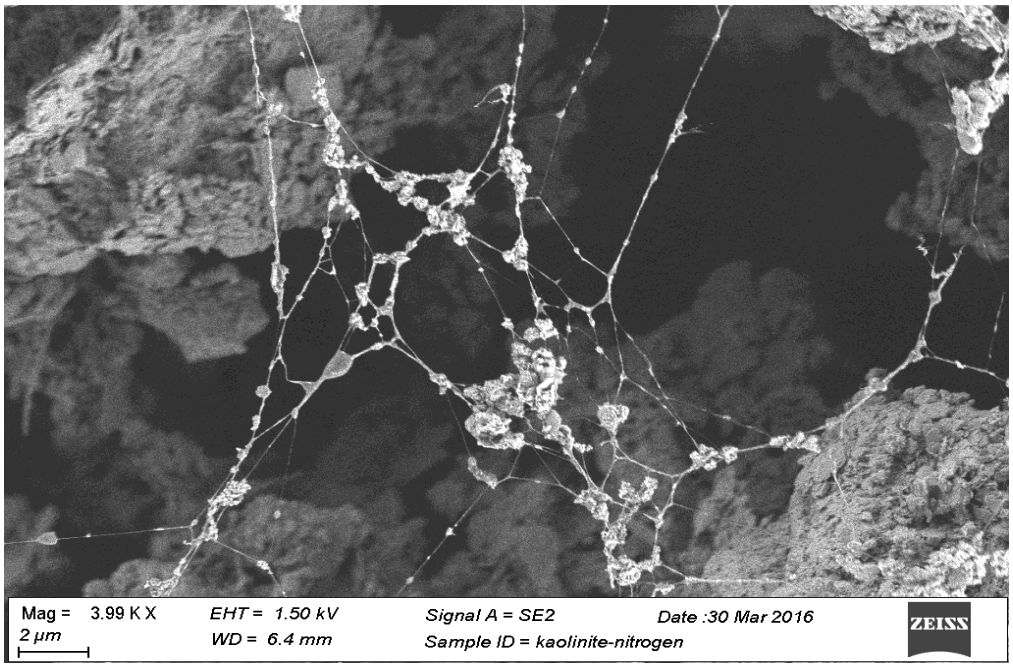

Figure 5.8: Web-like structures formed by polymer chains. These polymer chain show a lot of variation in thickness and length.

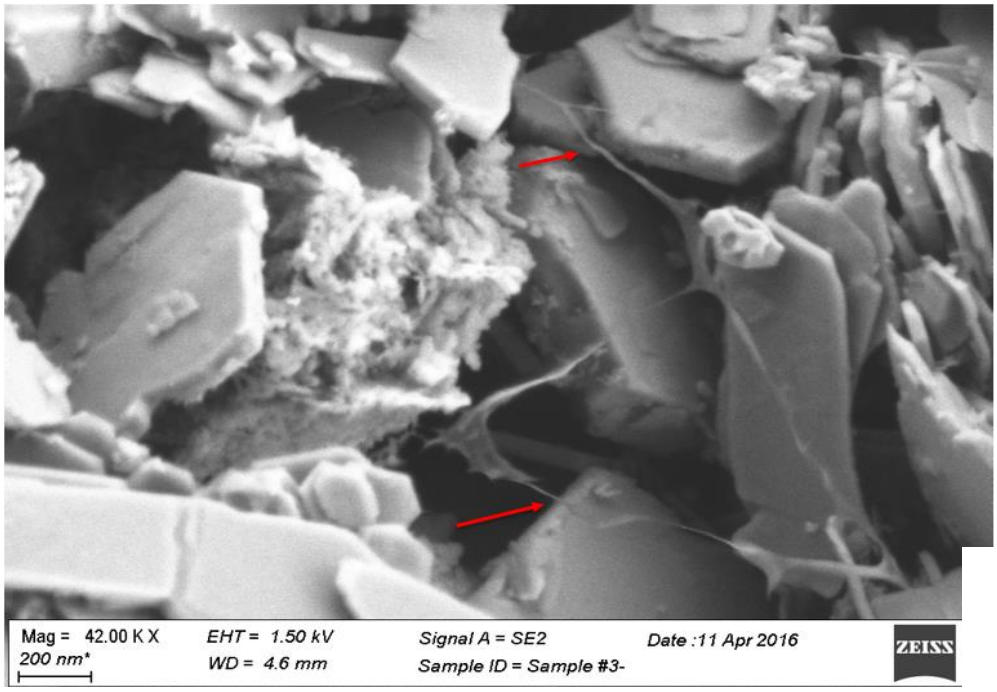

Figure 5.9: Microstcucture of kaolinite floc at higher magnification. Interaction between kaolinite edge surface – polymer chain is evident (marked using red arrows).

CHAPTER 6

THESIS SUMMARY AND CONCLUSIONS

In this thesis research, the flocculation of primary kaolinite particles was achieved using a suitable polymer and operating conditions. The primary particles had a bimodal size distribution with peaks at about 100 nm and 500 nm. These submicron kaolinite particles could be aggreated into flocs of about 1 mm in size under appropriate conditions of polymer concentration and pH. The structure of suspended kaolinite flocs was analyzed in 2D using the Particle Vision & Measurement (PVM) and Dynamic Image Analysis (DIA). The structure of sedimented kaolinite flocs was also analyzed in 3D using High Resolution X-ray Microtomography (HRXMT) and Scanning Electron Microscopy (SEM) as well as image processing softwares including fiji, MIPAV, and drishti.

The analysis of the suspended flocs by PVM and DIA revealed a mean floc size of about 230 μm for the high molecular weight, 5% anionic polyacrylamide-induced flocs. The lower molecular weight, 70% cationic polymer-induced flocs were found to be smaller in size (mean size 145 μm). DIA was used to analyze the flocs at different solids concentration. It was found that an increase in solids concentration leads to an increase in floc size from mean size of 230 μm at 1% solids concentration to 740 μm at 4% solid concentration and to 1020 μm at 8% solids concentration. Floc circularity was also analyzed using both of these methods. The major objective of this research was to do the multiscale analysis of the sedimented kaolinite flocs, a pictorial

summary of research is provided (Figure 6.1). A calibration curve was prepared from kaolinite-water suspension at different solids concentration. Using HRXMT, a 3D image of sedimented kaolinite flocs was constructed. The sediment bed of 3.5 cm diameter was segmented by using image processing techniques and about 13 thousand individual flocs were isolated. These individual flocs were then analyzed for size and water content. The results suggest a normal distribution of water content for these flocs, with mean water content of 53.9% and standard deviation of 11.8%. About 98% of the flocs had a water content in the range of 30-80% by volume (Figure 4.13, Chapter 4). About 90% of the flocs were found to be in the size range 0.5-2 mm (Figure 4.14, Chapter 4). From this 3D analysis, the water compositions of the individual flocs were established for the first time and the floc size distribution was reported. The mean size of these

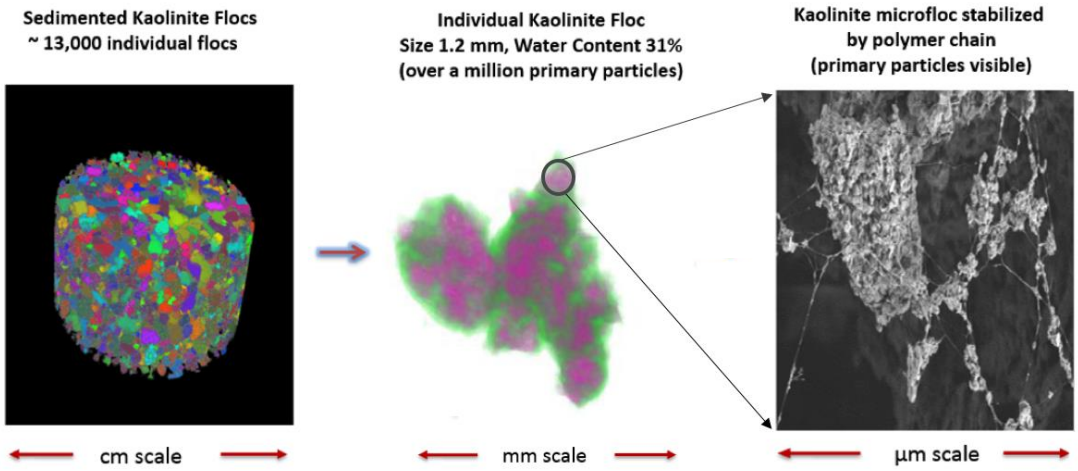

Figure 6.1: Multiscale analysis of kaolinite flocs. The sediment bed (on left) was segmented and individual flocs were isolated. One individual floc of about one mm size is shown in middle. The water content analysis of individual flocs was done. The water content increases from pink to green. The individual floc was further investigated for its microsctructure by using SEM and cryo sample preparation to indentify kaolinite primary particles and polymer (on right).

flocs in sedimented state is comparable to the mean size of flocs in suspended state. However, exact comparisons cannot be drawn due to different conditions used for sample preparation in both cases.

Further investigation of individual flocs was done using FESEM in order to understand the floc microstructure. In the SEM analysis, microflocs of varied size were revealed. These microflocs appear to be composed of kaolinite clusters and were interconnected by polymer bridges which formed a web like structure which accounts for floc size and staility. Thus multiscale analysis of flocculated kaolinite is reported for the first time (see Figure 6.1).

The HRXMT procedure developed in this work has allowed not only the determination of floc structure but also the water content of individual kaolinite flocs for the first time. The procedure developed can be extended for water content and size distribution analysis of flocs formed from industrial tailings at different conditions. This would enable us to study the effect of different parameters on the water entrapped in individual flocs as well as on the size distribution of the floc population. Both size and water content of flocs are crucial in determining the settling and self-weight consolidation of flocs.

Finally, the use of SEM for visualization of floc microst ructure and polymer chain reveals the stabilization of kaolinite microflocs in the web formed by polymer chains. The morphology of the polymer chain as well as the interaction between microflocs and polymer chain is a key to understanding floc growth and stability.

REFERENCES

Alagha, L.; Guo, L.; Ghuzi, M.; Molatlhegi. O.; Xu, Z. Adsorption of hybrid polyacrylamides on anisotropic kaolinite surfaces: Effect of polymer characteristics and solution properties. Colloids and Surfaces A: Physicochemical and Engineering Aspects. 2016, 498, 285-296.

Alagha, L.; Wang, S.; Yan, L.; Xu, Z.; Maslivah,J. Probing Adsorption of Polyacrylamide-Based Polymers on Anisotropic Basal Planes of Kaolinite Using Quartz Crystal Microbalanc. Langmuir. 2013, 29, 3989–3998.

Andreasen, A.; Jensen, W; Lundberg, J. Ein Apparat fur die dispersoidanalyse und einige Untersuchungen damit, Kolloid-Zeitschrift. 1929, 49, 253-265.

Barshack, I.; Kopolovic, J.; Chowers, Y.; Gileadi, O.; Vainshtein, A.; Zik, O.; and Behar, V. A novel method for "wet" SEM. Ultrastructural pathology. 2004, 281, 29-31.

Bergaya, F.; Theng, B.K.; and Lagaly, G. Handbook of clay science. Vol. 1: Elsevier Science, New York, 2011.

Berne, B.J.; Pecora, R. Dynamic Light Scattering: With Applications to Chemistry, Biology, and Physics. John Wiley & Sons, Inc., New York, 1976.

Besra, L.; Sengupta, D.K.; Roy S.K.; Particle characteristics and their influence on dewatering of kaolin, calcite and quartz suspensions, Int. J. Miner. Process. 2000, 59, 89–112.

Besra, L.; Sengupta, D.K.; Roy, S.K.; Ay, P. Polymer adsorption: its correlation with flocculation and dewatering of kaolin suspension in the presence and absence of surfactants. International Journal of Mineral Processing. 2002, 66, 183-202

Bikales, N.M. Preparation of acrylamide polymers. Water soluble polymers: Polymer Science and Technology. 1973, 2, 213-225.

Cabrera, S.C.M.; Bryan, J.; Komishke, B.; and Kantzas, A. Study of the settling characteristics of tailings using nuclear magnetic resonance technique. International Journal of Mining, Reclamation and Environment. 2009, 23, 33–50.

Chaiwong, N., Nuntiya, A. Influence of pH, electrolytes and polymers on flocculation of kaolin particle. Journal of Science. 2008, 35, 11-16.

Chalaturnyk, R.J.; Scott, J.D.; Ozum, B. Management of oil sands tailings. Pet. Sci. Technol. 2002, 20, 1025-1046

Deng, Y.; Dixon, J.B.; White, G.N.; Adsorption of polyacrylamide on smectite, illite, and kaolinite. Soil Science. 2006, 70, 297-304

Fan, A.; Somasundaran, P.; Turro, N.J. Proton Nuclear Magnetic Resonance Study of Water in Flocs. Langmuir. 1999, 15, 4922-4926,

FEI website, 2015 <http://www.fei.com/products/sem/nova-nanosem/

Forbes, E. Shear, selective and temperature responsive flocculation: a comparison of fine particle flotation techniques. Int. J. Miner. Process. 2011, 99, 1–10.

Garcia D.; Lin C.L.; Miller J.D. Quantitative Analysis of Grain Boundary Fracture in the Breakage of Single Multiphase Particles Using X-Ray Microtomography Procedures. Minerals Engg. 2009, 22, 236-243.

Goldstein J.; Newbury D.E.; Echlin P.; Joy, Romig A.D.; Lyman, Charles C.E.; Fiori, Lifshin, E. Scanning Electron Microscopy and X-Ray Microanalysis. Plenum, New York 1990.

Govoreanu, R.; Saveyn, H.; Van der Meeren, P.; Nopens, I.; Vanrolleghem, P.A. A methodological approach for direct quantificationof the activated sludge floc size distribution by using different techniques. Water Sci. Technol. 2009, 60, 1857–1867.

Graveling, G.J.; Ragnarsdottir, V.K.; Allen, G.C.,Eastman, J.; Brady, P.V.; Balsley, S.D.; Controls on polyacrylamide adsorption to quartz, kaolinite, and feldspar. Geochemistry et. Cosmochimica. Acta. 1997, 61, 3515-3523

Greaves, D.; Boxall, J.; Mulligan, J.; Montesi, A.; Creek, J. Sloan, E.D.; Koh, C.A. Measuring the particle size of a known distribution using the focused beam reflectance measurement technique. Chem. Eng. Sci. 2008, 63, 5410–5419.

Gregory, J.; Guibai, L. Effects of dosing and mixing conditions on polymer flocculation of concentrated suspensions, Chemical Engineering Communications. 1991, 108, 3–21.

Gregory, J.; Polymer adsorption and flocculation in sheared suspensions. Colloids Surf. 1988, 31, 231-253.

Grim, R.E. Clay mineralogy. Mc-Graw Hill, New York, 1953.

Gupta, V. Surface charge features of kaolinite particles and their interactions. PhD Dissertation, University of Utah, Salt Lake City, 2011.

Gupta, V.; Hampton, M.A;, Stokes, J.R.; Nguyen, A.V.; and Miller, J.D. Particle interactions in kaolinite suspensions and corresponding aggregate structures. J. Colloid Interface Sci. 2011, 359, 95-103.

Gupta, V.; Miller, J.D., Surface force measurements at the basal planes of ordered kaolinite particles. J. Colloid Interface Sci. 2010, 344, 362-71.

Hawkesley, P. G. W. Some Aspects of Fluid Flow. Arnold & .Co., London, 1951.

Hendricks, H.C.M. The effect of pH and the solids composition on the settling and self-weight consolidation of mud. Master of Science Thesis, Tu Delft, Netherlands, 2016.

Hogg, R. Flocculation and dewatering. Int. J. of Mineral Proces. 2000, 58, 223- 236.

Hogg, R. The role of polymer adsorption kinetics in flocculation. Colloids and Surfaces A: Physicochemical and Engineering Aspects. 1999, 146, 253–263.

Hsieh, C.H. Procedure and analysis of mineral samples using high resolution x-ray microtomography. Master of Science Thesis, University of Utah, Salt Lake City, 2012.

Hunter, R.J. Zeta Potential in Colloid Science. Academic press, London, 1981.

Jiang, Q.; Logan, B. E. Fractal dimensions of aggregates determined from steady state size distributions, Environ. Sci. Technol. 1991, 25, 2031- 2038.

Johnson, C. P.; Li, X.; Logan B. E. Settling velocities of fractal aggregates. Environ. Sci. Technol. 1996, 30, 1911-1918.

Kaya, A.; Oren, A.H.; Yukselen, Y. Settling of kaolinite in different aqueous environment. Mar. Georesour. Geotechnol. 2006, 24, 203–218.

Kie, T.T. Investigations of the rheological properties of clays. PhD thesis, Technical University of Delft, Netehrlands, 1984.

Kim, M.; Kim, S.; Kim, J.; Kang, S.; Lee, S. Factors affecting flocculation performance of synthetic polymer for turbidity control. J. of Agricultural Chem. and Environ. 2013, 2, 16-21

Kim, S.; Palomino, A.M. Polyacrylamide-treated kaolin: A fabric study. Applied Clay Sc. 2009, 45, 270-279.

Kingsley E.K. Studies on flocculation of kaolin suspensions and mature fine tailings. Master of Science Thesis, University of Alberta, Canada, 2008.

Kuroda, Y.; Nakaishi, K.; Adachi, Y. Settling velocity and structure of kaolinite floc in sodium chloride solution. Clay Sc. 2003, 12, 103-107.

Labille, J.; Thomas, F.; Milas, M.; Vanhaverbeke, C. Flocculation of colloidal clay by bacterial polysaccharides: effect of macromolecule charge and structure. J. Colloid Interface Sc. 2005, 284, 149-56.

Lagaly, G.; Bergaya, F. Handbook of clay science: Elsevier., Boston, 2013.

Laird, D.A.D. Bonding between polyacrylamide and clay mineral surfaces. Soil Sc. 1997, 162, 826–832

Lawler, D. F. Removing particles in water and wastewater. Environ. Sci. Technol. 1986, 20, 856-861.

Lee, T.; Rahbari, R.; Lecourtier, J.; Chauveteau, G. Adsorption of polyacrylamides on different faces of kaolinites. J. Colloid Interface Sci. 1991, 147, 351-357.

Lemanowicz, M.; Jach, Z.; Kilian, E.; Gierczycki, A. Ultra-fine coal flocculation using dual-polymer systems of ultrasonically conditioned and unmodified flocculant. Chem. Eng. J. 2011, 168, 159–169.

Lemieux, P.R.; Rumpf, D.S. Lightweight oil and gas well proppants. US5030603, July 9, 1991.

Li, T.; Zhu, Z.; Wang, D.; Yao, T. Characterization of floc size, strength and structure under various coagulation mechanisms. Powder Technology. 2006, 168, 104-110.

Li, X.; Logan, B. E. Collision frequencies between fractal aggregates and small particles in a turbulently sheared fluid. Environ Sci. Technol. 1997, 31, 1237-1242.

Liang, L.; Peng Y.; Tan J.; Xie G. A review of the modern characterization techniques for flocs in mineral processing. Minerals Engg. 2015, 84, 130–144.

Limaye, A. Drishti: a volume exploration and presentation tool. Proc. SPIE – The International Society for Optical Engineering. Baltimore, USA. October, 2012.

Lin, C.L.; Miller, J.D. 3D characterization and analysis of particle shape using X-ray microtomography (XMT). Powder Techn. 2005, 154, 61-69

Lin, C.L.; Videla, A.R.; Yu, Q.; Miller, J.D. Characterization and analysis of porous, brittle solid structures by X-ray micro computed tomography. J. of Metal. 2010, 62, 86– 89.

Liu, D.; Peng, Y. Reducing the entrainment of clay minerals in flotation using tap and saline water. Powder Technol. 2014, 253, 216–222.

Liu, J.; Lin, C.L.; Miller, J.D. Simulation of cluster formation from kaolinite suspensions. International J. of Mineral Proc. 2015, 145, 38-47.

Liu, J.; Sandaklie-Nikolova, L.; Wang, X.; and Miller, J.D. Surface force measurements at kaolinite edge surfaces using atomic force microscopy. J. Colloid Interface Sci. 2014, 420, 35-40.

Lyklema, J. Fundamentals of Interface and Colloid Science, Volume II: Solid Liquid Interfaces. Academic Press, London, 1995.

McAuliffe, M; Lalonde, F; McGarry, D; Gandler, W; Csaky, K; Trus, B. Medical image processing, analysis and visualization in clinical research. Proceedings of the 14th IEEE Symposium on Computer-Based Medical Systems. Maryland, July, 2001.

McFarlane A.J.; Addai-Mensah J.; Bremmell K. Rheology of flocculated kaolinite dispersions. Korea-Australia Rheology Journal. 2005, 17, 181-190.

Mer, L.; Healy, V.K. Adsorption flocculation reactions of macromolecules at the solid-liquid interface. Rev. Pre Applied Chemistry. 1963, 13, 112-133

Mer, L.; Healy, V.K. Filtration of colloidal dispersions flocculated by anionic and cationic polyelectrolytes. Discuss. Faraday Society. 1966, 42, 248-254

Mer, L.; Smellie, R.H. Theory of flocculation, subsidence and refiltration rates of colloidal dispersions flocculated by polyelectrolytes. Clay and Clay Minerals. 1962, 9, 295-314.

Michaels, A.S.; Bolger, J.C. Settling rate and sedimentation volumes of flocculated kaolin dispersions. I & EC Fundamentals. 1962, 1, 24-33.

Mietta, F. Evolution of the floc size distribution of cohesive sediments. PhD Thesis, TU Delft, Netherlands, 2010.

Miller, J.D., and Lin, C.L. “Three-dimensional analysis of particulates in mineral processing systems by cone beam X-ray microtomography”, Minerals and Metallurgical Processing. 2003, 21, 113-124.

Mitchell, J.K.; Soga, K. Fundamentals of soil behavior. Wiley, New York, 1976.

Mpofu, P.; Addai, M.J.; Ralston J. Influence of hydrolyzable metal ions on the interfacial chemistry, particle interactions, and dewatering behavior of kaolinite dispersions. J. Colloid Interface Science. 2003, 261, 349-59.

Mpofu, P.; Addai, M.J.; Ralston J. Temperature influence of nonionic polyethylene oxide and anionic polyacrylamide on flocculation and dewatering behavior of kaolinite dispersions. J. Colloid Interface Science. 2004, 271, 145-56.

Murray, H.H. Overview—clay mineral applications. Appl. Clay Sci. 1991, 5, 379-395.

Murray, H.H. Traditional and new applications for kaolin, smectite, and palygorskite: a general overview. Appl. Clay Sci. 2000, 17, 207-221.

Nasser, M. S.; James, A. E. Settling and sediment bed behaviour of kaolinite in aqueous media. Separation and Purification Technology. 2006, 51, 10-17.

Nasser, M. S.; James, A. E. The effect of electrolyte concentration and pH on the flocculation and rheological behavior of kaolinite suspensions. Journal of Engineering Science and Technology. 2009, 4, 430 – 446.

Nasser, M.S.; James, A.E. The effect of polyacrylamide charge density and molecular weight on the flocculation and sedimentation behaviour of kaolinite dispersions. Separation and Purification Technology. 2006, 52, 241-252

Nasser, M.S; and James, A.E. Effect of polyacrylamide polymers on floc size and rheological behavior of kaolinite dispersions. Colloids and Surfaces A: Physicochemical and Engineering Aspects. 2007, 301, 311-322.

Nasser, W.; Salhi, F. Kinetics determination of calcium carbonate precipitation behavior by inline techniques. Powder Technol. 2015, 270, 548–560.

O’Melia, C.R. Coagulation and sedimentation in lakes, reservoirs and water treatment plants. Water Sci. Technol, 1998, 37, 129–135.

Oliveira, C.; Rubio, J. Kaolin aerated flocs formation assisted by polymer coated microbubbles. International Journal of Mineral Processing. 2012, 106, 31–36.

Olphen, H.V. An Introduction to Clay Colloid Chemistry: For Clay Technologists, Geologists and Soil Scientists. Interscience, New York, 1963.

Ovenden, C;, Xiao, H. Flocculation behavior and mechanisms of cationic inorganic microparticle/polymer systems. Colloids & Surfaces A: Physicochemical and Engineering Aspects. 2002, 197, 225-234.

Owen, A.T.; Fawell, P.D.; Swift, J.D. The preparation and ageing of acrylamide/acrylate copolymer flocculant solutions. Inter. J. Min. proc. 2007, 84, 3-14.

Owen, A.T.; Fawell, P.D.; Swift, J.D.; Farrow, J.B. The impact of polyacrylamide flocculant solution age on flocculation performance. Inter. J. Min. proc. 2002, 67, 123-414.

Palomino, A.M.; Santamarina, J.C. Fabric map for kaolinite effects of pH and ionic concentration on behavior. Clays Clay Miner. 2005, 53, 211-223.

Pefferkorn, E. The role of polyelectrolytes in the stabilization and destabilization of colloids. Adv. Colloid Interface Science. 1995, 56, 33-104

Qi, L.; Meng, X.; Zhang, R.; Liu, H.; Xu, C.; Liu, Z.; Klusener, P. Droplet size distribution and droplet size correlation of chloroaluminate ionic liquid–heptane dispersion in a stirred vessel. Chem. Eng. J. 2015, 268, 116–124.

Richardson, J. F.; Zaki, W. N. Sedimentation and fluidization. Part 1. Trans. Inst. Chem. Eng. 1954, 32, 35-53.

Ruehrwein, R.A.; Ward, D.W. Mechanism of clay aggregation by polyelectrolytes. Soil Sci. 1952, 73, 485-492.

Sabah, E.; Erkan, Z.E. Interaction mechanism of flocculants with coal waste slurry. Fuel. 2006, 85, 350–359.

Schindelin, J.; Arganda-Carreras, I; Frise, E. et al. Fiji: an open-source platform for biological-image analysis. Nature methods 2012, 9, 676-682

Senaputra, A.; Jones, F.; Fawell, P.D.; Smith, P.G. Focused Beam Reflectance Measurement for monitoring the extent and efficiency of flocculation in mineral systems. AIChE J. 2014, 60, 251–265.

Shang J. Q. Electrokinetic dewatering of clay slurries as engineered soil covers, Can. Geotech. J. 1997, 34, 78–86.

Somasundaran, P.; Chia, Y.H.; Gorelik, R. Adsorption of Polyacrylamides on Kaolinite and its Flocculation and Stabilization. Amercian Chemical Society symposium series. 1984, 240, 393-410.

Somasundaran, P.; Moudgil, B.M. Reagents in Mineral technology. Marcel–Dekker, New York, 1988.

Stokes, G.G. On the effect of the internal friction of fluids on the motion of pendulums: Cambridge Philosophical Society, Transactions. 1851, 9, 287.

Sui, X.; Wang B.; Wu H.; Dong J.; Feng S. Morphology of polyacrylamide in solution: effect of water quality on viscosity. Polymers for advanced technologies. 2015, 26, 1326-1330

Taylor, M.L.; Morris, G.E.; Self, P.; Smart, R. Kinetics of adsorption of high molecular weight anionic Polyacrylamide onto kaolinite: the flocculation process. Journal of Colloid and Interface Sc. 2002, 250, 28–36

Theng, B.K. Formation and properties of clay-polymer complexes. Developments in Clay Science, Elsevier, Amsterdam, 1979.

Tjipangandjara, K.F.; Somasundaran, P. Effects of the conformation of poly acrylic acid on the dispersion-flocculation of alumina and kaolinite fines. Advanced Powd. Tech. 1992, 3, 119-12.

Triveni, R.; Shamala, T.R.; Rastogi, N.K. Optimised production and utilization of exopolysaccharide from Agobacterium radiobacter. Process. Biochem. 2001, 36, 787– 795

Van Olphen, H. An Introduction to Clay Colloid Chemistry: for Clay Technologists, Geologists, and Soil Scientists. Wiley, New York, USA, 1977.

Videla, A.; Lin, C.L.; Miller, J.D. Watershed functions applied to a 3D image segmentation problem for the analysis of packed particle beds. Part. Part. Syst. Char. 2006, 23, 237-245.

Videla, A.R. Development of Three-dimensional Image Computer Tools for X-ray Computed Tomography Analysis of Multiphase Particulate Systems. Master's Thesis, University of Utah, 2006.

Wang Y.; Lin C.L.; Miller, J.D. Improved 3D Image Segmentation for X-ray Tomographic Analysis of Packed Particle Beds. Minerals Engineering. 2015, 83, 185-191.

Wang, J.; Chen, Y.; Wang, Y.; Yuan, S.; Yu, H. Optimization of the coagulation-flocculation process for pulp mill wastewater treatment using a

combination of uniform design and response surface methodology. Water Resources. 2011, 45, 5633– 5640.

Wang, S.; Alagha, L.; Xu, Z.; Adsorption of organic-inorganic hybrid polymers on kaolin from aqueous solutions. Colloids and Surfaces A: Physicochemical and Engineering Aspects. 2014, 453, 13-20

Wellington S.L.; Vinegar H.J. X-Ray Computerized Tomography. Journal of Petroleum Techn. 1987, 885-886.

Wiesner M. R. Kinetics of aggregate formation in rapid mix. Water Res. 1992, 26, 379-387.

Winterwerp, J. C.; Kesteren, V. Introduction to the physics of cohesive sediment in the marine environment. Developments in Sedimentology, Elsevier, 2004.

XRadia, MicroXCT-200 and MicroXCT-400 User's Guide, XRadia, 2010, pp.87, 155, 175, and 283-284.

Yang, Z.H.; Huang, J.; Zeng; Ruan; Zhou; Li. Optimization of flocculation conditions for kaolin suspension using the composite flocculant of MBFGA1 and PAC by response surface methodology. Bioresource Technology. 2009, 100, 4233–4239.

Yin, X. Anisotropic surface features of selected phyllosilicates. PhD Dissertation, University of Utah, 2012.

Yoon, S.Y.; Deng, Y.L. Flocculation and reflocculation of clay suspension by different polymer systems under turbulent conditions. J. Colloid Interface Sci. 2004, 278, 139–145.

Yu, J.; Wang, D.; Ge, X.; Yan, M.; Yang. Flocculation of kaolin particles by two typical polyelectrolytes: A comparative study on the kinetics and floc structures. Colloids and Surfaces A: Phy. and Engg. Aspects. 2006, 290, 288-294.

Yu, X.; Somasundaran, P. Role of polymer conformation in interparticle-bridging dominated flocculation. J. Colloid Interface Sci. 1997, 177, 283–287.

Zbik, M.S.; Smart R.S.; Morris G.E. Kaolinite flocculation structure. J. Colloid Interface Science. 2008, 328, 73-80.

Zeiss website, 2015.
http://www.zeiss.com/microscopy/en_us/products/scanning -electron-microscopes/sigma.html

Zhang, P.; Bogan, M. Recovery of phosphate from Florida beneficiation slimes I. Re-identifying the problem. Miner. Eng. 1995, 8, 523-534.

Zhao, Y.Q. Settling behavior of polymer flocculated water-treatment sludge II: effects of floc structure and floc packing. Sep. Purif. Technol. 2004, 35, 175–183.

Zhou, D.M.; Deng, C.F.; Cang, L. Electrokinetic remediation of a Cu contaminated red soil by conditioning catholyte pH with different enhancing chemical reagents. Chemosphere. 2004, 56, 265–273.

Zhu, Z.; Tao, L.; Jiajuan, L.; Dongsheng, W.; Chonghua, Y. Characterization of kaolin flocs formed by polyacrylamide as flocculation aids. International Journal of Mineral Processing. 2009, 91, 94–99.